

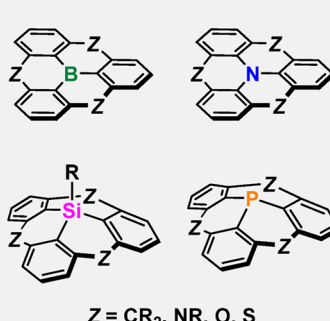
Structurally Constrained Boron-, Nitrogen-, Silicon-, and Phosphorus-Centered Polycyclic π -Conjugated Systems

Masato Hirai,[†] Naoki Tanaka,[†] Mika Sakai,[‡] and Shigehiro Yamaguchi^{*,†,‡,ID}

[†]Institute of Transformative Bio-Molecules (WPI-ITbM), Nagoya University, Furo, Chikusa, Nagoya 464-8601, Japan

[‡]Department of Chemistry, Graduate School of Science and Integrated Research Consortium on Chemical Sciences (IRCCS), Nagoya University, Furo, Chikusa, Nagoya 464-8602, Japan

ABSTRACT: Incorporation of main group elements into the π -conjugated frameworks is a sophisticated strategy to alter the fundamental nature of the parent conjugated π -systems, giving rise to attractive electronic and photophysical properties that are otherwise inaccessible with classic carbon- or metal-based materials. Out of all π -conjugated heterocycles, those that are structurally constrained by tethered aryl substituents surrounding the main group center deserve a great deal of attention because not only do they commonly possess the maximum efficiency of π -conjugation and intermolecular interaction, but they also enjoy remarkable thermal and morphological stabilities that are especially crucial for solid-state performances. In certain cases, elucidation of the behavior of such compounds may additionally provide sufficient perspective toward graphene materials doped with main group elements, which are widely considered as potential next-generation optoelectronic materials. In this review, we will specifically focus on historical developments of structurally constrained polycyclic π -electron systems particularly of those with boron, nitrogen, silicon, or phosphorus atoms annulated directly into the center of π -conjugated systems.



CONTENTS

1. Introduction	8292	3.2.2. Partially Diarylmethylene-Bridged Triarylaminies	8310
2. Boron-Centered Polycyclic Compounds	8292	3.2.3. Partially Carbonyl-Bridged Triarylaminies	8310
2.1. Boron-Centered PAHs	8293	3.2.4. Partially Oxygen-Bridged Triarylaminies	8311
2.1.1. Triarylboranes Constrained with Alkyl Bridges	8293	3.2.5. Partially Sulfur-Bridged Triarylaminies	8312
2.1.2. Fully and Partially Fused Boron-Embedded Polycyclic Systems	8296	3.3. Triarylamine Radical Cations and Bis-(triarylamine) Dications Stabilized by Structural Constraint	8313
2.2. Structurally Constrained Triarylboranes with Heteroatom Bridges	8297	3.3.1. Radicals of Dimethylmethylenes-Bridged Triarylamine Derivatives	8313
2.3. Diphenylborane-Fused Porphyrins	8299	3.3.2. Radicals of Oxygen-Bridged Triarylamine Derivatives	8313
2.4. Boron-Doped Nanographene and Graphene Nanoribbons	8299	3.3.3. Radicals of Partially Sulfur-Bridged Triarylamine Derivatives	8315
3. Nitrogen-Centered Polycyclic Compounds	8301	3.4. Diarylamine-Fused Porphyrins	8315
3.1. Nitrogen-Centered Triangulenes: N-Heterotriangulenes	8302	4. Silicon-Centered Polycyclic Compounds	8316
3.1.1. Carbonyl-Bridged N-Heterotriangulenes	8302	5. Phosphorus-Centered Polycyclic Compounds	8317
3.1.2. Arylvinylidene-Bridged N-Heterotriangulenes	8303	5.1. Phosphorus-Centered Triangulenes: P-Heterotriangulenes	8317
3.1.3. Dimethylmethylenes-Bridged N-Heterotriangulenes	8304	5.1.1. P-Heterotriangulenes with Methylenes Bridges	8317
3.1.4. Diarylmethylene-Bridged N-Heterotriangulenes	8307	5.1.2. P-Heterotriangulenes with Heteroatom Bridges	8318
3.1.5. N-Heterotriangulene-Based Oligomers, 2D Network Structures, and Polymers	8308		
3.2. Partially Bridged Triarylaminies	8309		
3.2.1. Partially Dimethylmethylenes-Bridged Triarylaminies	8309		

Special Issue: Frontiers in Main Group Chemistry

Received: October 23, 2018

Published: March 12, 2019

5.2. Partially Bridged Triarylphosphines and Their Oxidized Derivatives	8320
5.3. Diarylphosphine-Fused Porphyrins and Their Oxidized Derivatives	8321
6. Conclusion and Perspectives	8321
Author Information	8322
Corresponding Author	8322
ORCID	8322
Notes	8322
Biographies	8322
Acknowledgments	8322
Abbreviations	8322
References	8323

1. INTRODUCTION

Organic π -conjugated materials have become inherent tools in modern scientific disciplines with a rich spectrum of modern applications spanning from organic electronics, molecular sensing, and bioimaging to supramolecular chemistry.^{1–12} The most fundamental yet promising class of such compounds are polycyclic aromatic hydrocarbons, abbreviated as PAHs, owing to their predictable and controllable electronic and self-assembling properties. For instance, simple PAHs such as anthracene, phenanthrene, and pyrene have been frequently utilized as efficient chromophores and fluorophores^{13–18} as well as elementary building blocks of organic electronic devices.^{19–26} The isolation of graphene, a monocrystalline graphitic film, entering the 21st century was most definitely a turning point toward the research of PAHs with much larger sizes,^{27,28} owing to its uncommon properties that are unprecedented in smaller systems such as optical transparency, mechanical flexibility, high carrier mobility, and thermal stability.^{29–38} Regardless of these remarkable peculiarities, the advancement of graphene-based materials including semiconductors have not been living up to expectation, mostly due to (1) the underdevelopment of novel synthetic methodologies to create pure and consistent material and (2) such materials typically possessing small or no bandgaps. In turn, the research of nanographenes including graphene quantum dots and graphene nanoribbons (GNRs) have accelerated explosively in recent years because (1) precise and structurally uniform materials can be systematically prepared by bottom-up synthetic methods and (2) the bandgap can be accurately modulated by the topology of the materials, thus semiconducting character can be added.^{39–43} Indeed, nanographenes and GNRs as well as their simple derivatives have already been proven to be suitable toward numerous applications including optoelectronics,^{44–53} chemical and strain sensing,^{54–56} photocatalysis,⁵⁷ as well as medical and biological sciences.^{58–63}

An alternative powerful approach is to integrate heteroatoms, especially from those of groups 13–16, directly into the π -skeleton.^{64–66} For instance, simple displacement of one of the carbon atoms with an electron-deficient boron and an electron-rich nitrogen append n-type and p-type characters, respectively, to the parent PAH (details will be described later in the text). In principle, such a feature is especially appealing for materials based on graphene because the electronic structures can be modified pertinently to adjust the electrochemical, charge carrier, and semiconducting properties to construct integral components of electronic devices.^{67–73} Unfortunately, the precise control to introduce the hetero-

atomic dopant to a specific destination of a graphene scaffold still remains a challenge, and the frontrunning and most generic synthetic techniques such as chemical vapor deposition^{74–78} and microwave plasma method⁷⁹ quite often result in randomly doped, inconsistent structures. This limitation can be resolved by on-surface chemistry reactions. In fact, atom-precise nitrogen-doped graphene has been systematically produced through a rational bottom-up approach, utilizing appropriate precursor molecules.^{80,81} However, precedent examples only have the nitrogen atoms located at the periphery of the graphene platform, exemplifying the difficulty to generate carbon-based π -conjugated materials annulated with main group elements. This is indeed true for smaller systems, but synthetic strategies have gradually evolved over time, allowing access to polycyclic systems with the aryl rings surrounding the main-group element center aligned in a fixed orientation.

While sterically constrained polycyclic π -systems can be regarded as building blocks or subunits of heteroatom-doped graphenes, they are attractive materials on their own. First of all, the size and the shape as well as the heteroatom content can be adjusted in a controlled manner, leading to predictable yet unique electronic structures thus electrochemical and photophysical properties. Furthermore, depending on the electronic nature, heteroatoms in π -conjugated systems can play an effective role to stabilize cations,⁸² anions,⁸³ or even high-spin organic species.⁸⁴ Moreover, the physical states of polycyclic π -conjugated compounds can be vastly controlled by structural rigidity, extended π -surfaces, steric bulkiness, and dipole moments, which are particularly influential toward the self-organization behavior.⁸⁵ Owing to these momentous characteristics, sterically constrained polycyclic π -systems have sparked great interest as promising tools in material sciences. The motivation of this review is to highlight the contributions of structurally constrained π -systems embedding boron, nitrogen, silicon, or phosphorus atoms in the center of the core and their use in electronic and optical devices and other practical applications. All polycyclic systems introduced herein are composed of the central main group element surrounded by tethered hence geometrically fixed aryl substituents, which in other words function like polydentate ligands.

2. BORON-CENTERED POLYCYCLIC COMPOUNDS

While three-coordinate organoboranes are intrinsically electron-deficient and Lewis acidic owing to the vacant p orbital of the boron atom, boryl groups are regarded as σ -donors due to the low electronegativity of the boron atom. When incorporated to a π -conjugated skeleton, such moiety can also behave as efficient π -acceptors and therefore stabilizes the LUMO and alters the optoelectronic properties. Based on these features, countless boron-containing organic π -conjugated materials have been developed thus far with a broad scope of applications including anion sensing, organic electronics such as OLEDs and OFETs, nonlinear optics, two-photon optics, catalysis as well as bioimaging (refer to previously published reviews for details).^{86–97} In most cases, the inherently reactive boron center is surrounded by sterically bulky aryl groups, commonly 2,4,6-trimethylphenyl (Mes),⁹⁸ triisopropylphenyl (Tip),⁹⁹ or 2,4,6-tritert-butylphenyl¹⁰⁰ groups, which provide sufficient kinetic protection and thus stability under ambient conditions (Figure 1A). As a trade-off, however, the steric demand may also disturb the intermo-

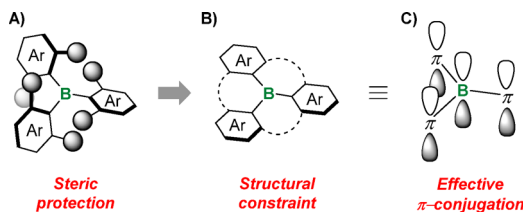


Figure 1. Illustration of (A) triarylborane stabilized by steric protection, (B) triarylborane stabilized by structural constraint, and (C) effective orbital interaction among the p orbital of the boron center and the π^* orbitals of the π -skeleton.

lecular interaction, thereby causing detrimental effects especially toward the solid-state performances such as charge carrier-transporting properties.

An alternative strategy to stabilize triarylboranes is to embed a boron atom directly into the annulated core of a π -conjugated framework to supply ample structural constraint around the tricoordinate boron moiety (Figure 1B). This gives rise to enhanced stability from two key factors: (1) the boron center energetically disfavoring the geometrical reorientation from a trigonal planar geometry to a tetrahedral geometry upon coordination of a Lewis basic species, which essentially retards the associated decomposition pathway, and (2) the three linked aryl groups behaving as a polydentate ligand toward the boron atom which prevents the B–C bond scission by chelation effect. In parallel, the orbital arrangements allow the π -skeleton to effectively conjugate through the empty p orbital of the boron atom and greatly perturb the electronic structure leading to, for instance, red-shifted absorption and emission (Figure 1C). Moreover, the removal of sterically bulky substituents is expected to strengthen the intermolecular interaction and permit the planarized triarylborane units to pack more efficiently, thus improving the charge carrier-transporting properties.

In this chapter, we will describe the development of triarylboranes featuring “a boron atom stabilized by tridentate triaryl ligand”. Such compounds possess interesting characteristics on their own but may also provide pragmatic insights

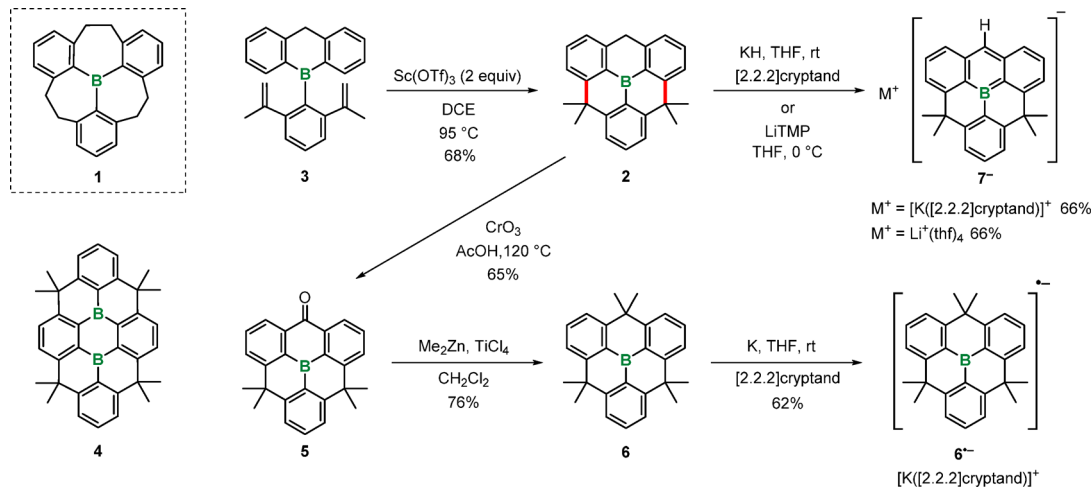
toward potential next-generation materials such as boron-doped nanographenes. In certain cases, the practical applications of planarized boron-doped polycyclic compounds in organic electronics will be introduced. We annotate that there are plentiful of intriguing examples and applications reflecting on organoboron compounds with “bidentate diaryl ligands”, but which are beyond the scope of this review. For those who are interested, we refer to other well-summarized review articles cited herein.^{92–94,97} Furthermore, research based on BN-substituted PAHs was also omitted from this review since the supposedly vacant boron p orbital is rather occupied due to effective π -donation from the nitrogen atom, leading to distinctively differing properties to those of PAHs containing BC₃ units. Interested readers should refer to the pioneering work by Piers,^{101–105} Pei,^{106–110} Liu,¹¹¹ Bettinger,^{112,113} and Hatakeyama^{114–116} as well as other associated articles^{117–119} and reviews^{40,120–124} for details.

2.1. Boron-Centered PAHs

2.1.1. Triarylboranes Constrained with Alkyl Bridges. The earliest example of a constrained triphenylborane was reported by Okada et al. in 1992.¹²⁵ In this work, they described the synthesis of triphenylborane **1** (Scheme 1), which possesses three ethylene bridges connecting the three phenyl rings, and studied its dynamics in solution. Based on the VT NMR studies, the structural interconversion to the antipode occurs rapidly even at low temperatures with an estimated energy barrier of less than 8 kcal mol⁻¹. Thus, the ethylene bridges retain a certain degree of flexibility to the structure.

It was not until 2012 when the first completely planarized triphenylborane, so-called *B*-heterotriangulene, **2** was introduced in the literature.¹²⁶ *B*-Heterotriangulene **2**, which is a boron-centered heterotriangulene bearing one methylene bridge and two dimethylmethylenes, was obtained by a 2-fold intramolecular Friedel–Crafts cyclization of precursor **3** using Sc(III) triflate as a Lewis acid additive in DCE under reflux (Scheme 1). The same synthetic approach was used to prepare the doubly boron-centered species, planarized dihydro-diboranthracene **4**, starting from 9,10-dibromo-9,10-dibora-

Scheme 1. Synthesis of *B*-Heterotriangulene Derivatives **2** and **6** As Well As Planarized Dihydro-Diboranthracene **4** Featuring Sc(OTf)₃-Mediated Intramolecular Friedel-Crafts Reaction As the Key Step^a



^aCompounds **2** and **6** were used to access anion **7**⁻ and radical anion **6**^{•-}, respectively. In the dotted box is the structure of ethylene-bridged triphenylborane **1**.

thracene as a key precursor.^{127,128} Oxidation of **2** with CrO₃ in refluxing acetic acid successfully gave the corresponding carbonyl derivative **5**, which was converted to an all-methylated *D*_{3h}-symmetric congener **6** by successive treatment with Me₂Zn and TiCl₄.

Unlike triphenylborane, both **2** and **6** were persistent toward air, moisture, amine, and heat even without possessing sterically bulky ligands, thus demonstrating the increased stability by structural constraint. Despite the remarkable inertness, both **2** and **6** retained sufficient Lewis acidity to undergo a plane-to-bowl conversion upon coordination of fluoride ions. Moreover, the structural constraint of a triphenylborane scaffold also had a major influence on the photophysical properties. Notably, the fluorescence spectrum of **6** in THF featured an emission maximum at $\lambda_{\text{em}} = 407$ nm with a distinct shoulder band appearing at $\lambda_{\text{em}} = 392$ nm, a characteristic unseen for Mes₃B, which only showed a single broad band with the maximum at $\lambda_{\text{em}} = 374$ nm.¹²⁹ Theoretical studies revealed that the two emission bands are attributed to the two minimum-energy structures, planar and bowl-shaped, found in the lowest-energy excited singlet (S_1) state.¹³⁰

Single-electron reduction of **6** with potassium metal in THF yielded the corresponding radical anion **6**^{•-} as a potassium salt, which upon diffusion of hexane in the presence of [2.2.2]-cryptand crystallized as deep blue blocks.¹³¹ Single crystal X-ray diffraction analysis exposed that radical anion **6**^{•-} adopts a shallow bowl-shaped conformation rather than the planar geometry around the boron center reported for [Li(12-crown-4)₂]⁺[Mes₃B]^{•-}.¹³² Meanwhile, EPR studies indicated that the unpaired electron in **6**^{•-} is more delocalized over the entire framework compared to the nonconstrained triphenylborane radical anion,¹³³ suggesting a rather planarized geometry of **6**^{•-}. Such trend was also observed for the neutral planarized triphenylmethyl radical analog reported by Hellwinkel.¹³⁴ In fact, DFT calculations predicted that the energy difference between the planar and bowl-shaped conformations is as small as $\Delta E_0 = +0.70$ kcal/mol and the conversion among the two likely occurs at room temperature. The methylene bridge of **2** can be deprotonated by applying KH or LiTMP as Brønsted bases to afford the corresponding *B*-phenyl-planarized borataanthracene **7**[−] as a potassium salt or a lithium salt, respectively.¹³⁵ While [2.2.2]cryptand was necessary as an additive to crystallize [K([2.2.2]cryptand)][**7**], red single crystals of both metal borataanthracene salts were obtained by slow diffusion of hexane into a THF solution. X-ray diffraction analysis of [K([2.2.2]cryptand)][**7**] and [Li(thf)₄][**7**] showed that [2.2.2]cryptand and four THF molecules were encapsulating the potassium and lithium cations, respectively, forcing the ion pairs to greatly separate. Hence, both alkali-metal salts of **7**[−] displayed identical photophysical properties in THF ($\lambda_{\text{abs}} = 568$, 531, and 500 nm; $\lambda_{\text{em}} = 584$ nm and $\Phi_F = 0.45$).

The lack of sterically bulky substituents surrounding the boron center is a formidable advantage for efficient intermolecular interaction thus improved solid-state properties such as charge carrier-transporting abilities. As prototypical examples, π -extended *B*-heterotriangulenes **8a** and **8b** with attached thiophene and 2,2'-bithiophene spacers (Figure 2A), respectively, were synthesized.¹³⁶ Both compounds showed high thermal stability, which allowed thin film preparation via vacuum vapor deposition. Thin films of compounds **8a** and **8b** were subsequently used as electron-transporting layers for OLEDs. The applied voltages required to exhibit luminance of

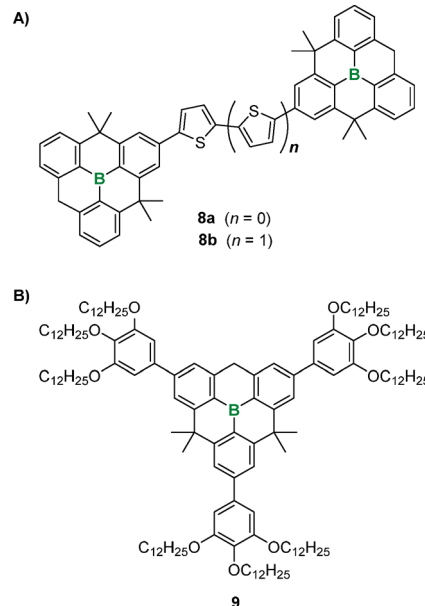


Figure 2. (A) Structures of π -extended *B*-heterotriangulenes **8a** and **8b** with electron-transporting properties and (B) structure of trigonally π -extended *B*-heterotriangulene **9** as discotic liquid crystals possessing ambipolar carrier-transporting properties.

1000 cd m^{−2} for those applied with **8a** and **8b** in the NPD/Alq₃/Liq/Al cell configurations were 9.4 and 7.6 V, respectively, the latter of which was comparable to that using a classical electron-transporting layer Alq₃ (7.2 V).

B-Heterotriangulene **2** was also transformed into air-stable discotic liquid crystals **9** (Figure 2B) in two steps: (1) iridium-catalyzed C–H borylation at the para positions of the three phenyl rings followed by (2) Suzuki–Miyaura cross-coupling reaction with 3,4,5-tridodecyloxyphenylbromide.¹³⁷ DSC and XRD measurements elucidated that **9** forms a π -stacked hexagonal columnar liquid-crystal phase with a disc-to-disc proximity of 3.6 Å at ambient temperature. The fluorescence spectrum recorded in the liquid-crystal phase was blue-shifted relative to that measured in THF ($\lambda_{\text{em}} = 427$ nm and $\Phi_F = 0.61$ in liquid-crystal phase; $\lambda_{\text{em}} = 457$ nm and $\Phi_F = 0.99$ in THF). This observation verifies that **9** in the liquid crystalline state is densely π -stacked and thus cannot freely interconvert from the planar to bowl-shaped conformations. Arising from the ordered columnar stacking and short intermolecular distances, the liquid crystal of **9** expressed electron and hole mobilities of 10^{-3} and 3×10^{-5} cm² V^{−1} s^{−1}, respectively, according to the time-of-flight measurements, confirming its ambipolar carrier-transporting nature.

A laterally π -extended derivative of **2**, planarized triarylboration **10**, as well as its structurally encumbered mesityl analog **11** were synthesized by Wagner, Yamaguchi et al. in 2016 (Figure 3).¹³⁸ For the latter compound, a series of related derivatives were extensively documented in previous literature, and the findings showed that the photophysical and electronic properties were severely affected by the degree of expansion of the π -framework.^{139,140} In this work, the two compounds, **10** and **11**, displayed analogous photophysical and electronic properties as well as air stability, despite the different modes of steric environment surrounding the boron centers. DFT calculations revealed that the atomic distribution as well as the energy levels of the HOMO and the LUMO are almost identical, thus likely resulting in such similar characteristics.

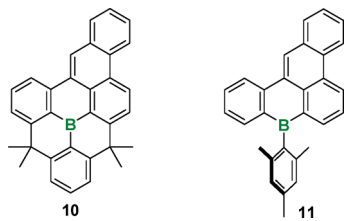


Figure 3. Structures of laterally π -extended triarylboranes **10** and **11** stabilized by structural constraint and sterically protection, respectively.

Disparity among the two compounds was observed in their Lewis acidities in which the fluoride ion binding constants estimated by UV-vis spectrophotometric titration in CHCl_3 was much greater for **11** than that of **10** ($K_F = 190 \pm 30 \text{ M}^{-1}$ for **10** and $K_F = 5300 \pm 800 \text{ M}^{-1}$ for **11**).

The fully planarized triarylborane is also a crucial scaffold to stabilize neutral π -radical species. Radical **12** (Figure 4A), in

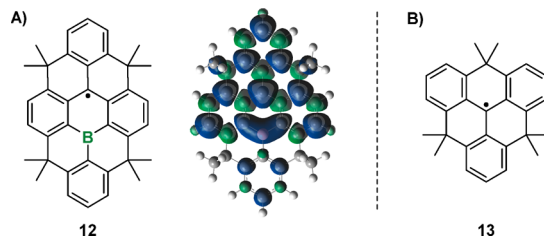


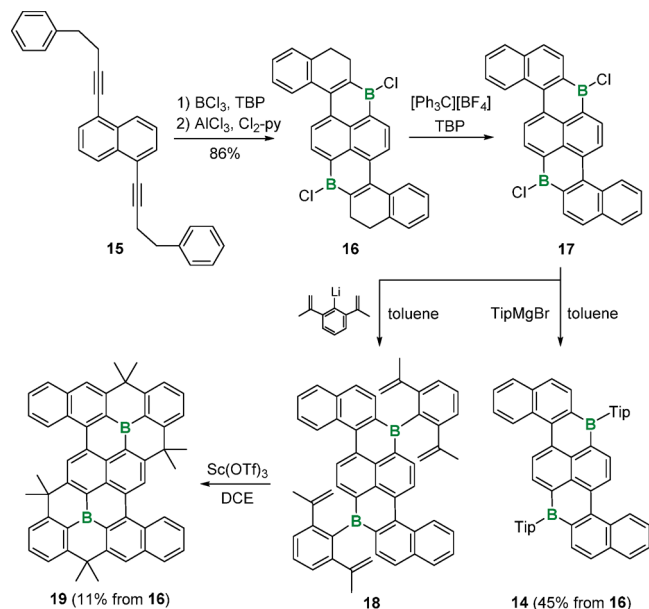
Figure 4. A) Structure of boron-stabilized planar triphenylmethyl π -radical **12** and the graphical representation of its spin density at the ground state configuration calculated at the UB3LYP/6-31+G(d) level of theory.¹²⁶ B) Structure of planar triphenylmethyl π -radical **13**.

which a boron atom is embedded directly into a planarized triphenylmethyl radical framework, is remarkably stable in air and was purified by silica gel column chromatography without special precautions.¹⁴¹ This radical also displayed a substantial thermal stability under N_2 atmosphere. EPR spectroscopy analysis along with DFT calculations unveiled that the boron atom slightly enhances the spin delocalization through the π -framework while decreasing the spin density on the triphenylmethyl moiety. The cyclic voltammogram of **12** in THF showed reversible redox waves for both the reduction and oxidation processes. The half-wave potential of reduction was much higher compared to that of planarized triphenylmethyl radical **13** (Figure 4B) reported by Hellwinkel, whereas the oxidation potential was positively shifted to a lesser extent (**12**: $E^\circ_{\text{ox}} = -0.08 \text{ V}$ and $E^\circ_{\text{red}} = -1.28 \text{ V}$; **13**: $E^\circ_{\text{ox}} = -0.36 \text{ V}$ and $E^\circ_{\text{red}} = -1.76 \text{ V}$ vs Fc/Fc^+).¹⁴² This suggested that the boron atom in **12** enhances the electron-accepting property of the radical. The authors addressed that the combination of delocalization of the spin density and the increased electron-accepting property may be relevant to the phenomenal air- and thermal-stability of radical **12**. This neutral radical compound was further applied on field effect transistors by solution-crystallized edge-cast method to evaluate its charge transport properties. Its ambipolar carrier transporting properties with well-balanced mobilities ($\mu_e = 4.5 \times 10^{-3} \text{ cm}^2 \text{ V}^{-1} \text{ s}^{-1}$ for electrons and $\mu_h = 1.1 \times 10^{-5} \text{ cm}^2 \text{ V}^{-1} \text{ s}^{-1}$ for holes) suggest the potential use of radical **12** as an organic Mott-insulator transistor operational at ambient temperature.

Ingleton et al. developed a facile yet versatile strategy to controllably synthesize boron-doped PAHs of different sizes,

shapes and number of boron atoms.¹⁴³ For instance, highly conjugated doubly boron-doped PAH **14** was synthesized via the following three steps starting from diyne precursor **15**: (1) tandem reactions of borylative cyclization¹⁴⁴ followed by intramolecular electrophilic aromatic substitution to form the corresponding *B*-chloroboracycle **16**, (2) oxidation of **16** to generate the fully conjugated *B*-chloroboracycle **17**, and (3) treatment of (2,4,6-triisopropylphenyl)magnesium bromide (Scheme 2). Compound **18** was prepared through a similar

Scheme 2. Synthesis of Doubly Boron-Doped PAHs Based on Tandem Reactions of Borylative Cyclization/ Intramolecular Electrophilic Aromatic Substitution (TBP = 2,4,6-tri-*tert*-butylpyridine, Cl₂-py = 2,6-dichloropyridine, Tip = 2,4,6-triisopropylphenyl)



procedure using (2,6-di(prop-1-en-2-yl)phenyl)lithium in the final step, but could not be cleanly isolated due to decomposition during the purification process. Instead, the impure reaction residue containing **18** was treated with $\text{Sc}(\text{OTf})_3$ in DCE to afford the desired fully planarized, doubly boron-doped PAH **19** via intramolecular Friedel–Crafts cyclization. Thorough studies on the photophysical properties demonstrated that planarization resulted in a red shift of the absorbance band along with a smaller Stokes shift, which were presumably attributed to the extension of the π -conjugated framework and the suppression of structural reorganization upon excitation.

2-Fold dimethylmethlene-bridged *B*-phenyldibenzoborepin **20** (Figure 5) was also synthesized via the intramolecular Friedel–Crafts cyclization.¹⁴⁵ While several air-stable borepin structures possessing sterically bulky aryl groups have been documented to date,¹⁴⁶ compound **20** is the first example of a borepin that is thoroughly stabilized by structural constraint. As opposed to **6** which adopts a D_{3h} symmetry, **20** in the crystalline state consists of a highly distorted structure. This, however, is contradictory to the results from DFT calculations which favored the planarized geometry above the twisted conformation. Hence, the distortion of **20** in the solid state most likely originates from packing forces. In fact, the structural flexibility provides just enough for **20** to coordinate

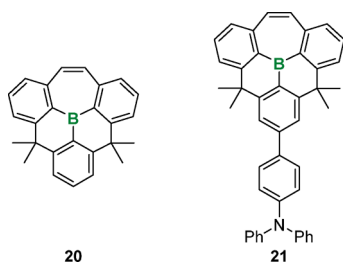
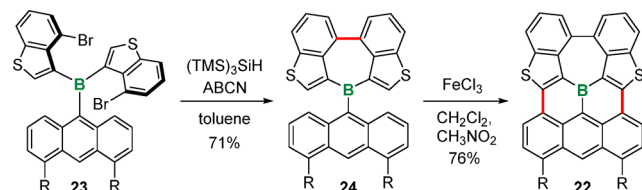


Figure 5. Structures of constrained *B*-phenyldibenzoborepin 20 and its 4-(*N,N*-diphenylamino)phenyl-substituted analog 21.

pyridine in toluene which could not be done with the more rigid **6**. The structurally constrained borepin **20** was examined as an electron-accepting building unit. Notably, D- π -A type **21** (Figure 5), which incorporates an electron-donating 4-(*N,N*-diphenylamino)phenyl group at the *B*-phenyl group, displayed a significantly large solvatochromism in fluorescence while retaining consistently high fluorescence quantum yields (cyclohexane: $\lambda_{\text{em}} = 434$ nm, $\Phi_F = 0.95$; MeCN: $\lambda_{\text{em}} = 588$ nm, $\Phi_F = 0.91$).

2.1.2. Fully and Partially Fused Boron-Embedded Polycyclic Systems. The concept of “stabilization by structural constraint” was extrapolated to much larger boron-doped polycyclic systems. One of the earliest examples is the π -extended planarized triarylborane **22** composed of fused benzothiophene and anthracene building units.¹⁴⁷ This compound was synthesized by two consecutive cyclization steps starting from precursor **23**: (1) radical-initiated fusion of the two benzothiophene groups using $(\text{TM斯})_3\text{SiH}$ and 1,1'-azobis(cyclohexanecarbonitrile) (ABCN) to afford **24** followed by (2) intramolecular oxidative cyclization via Scholl reaction employing FeCl_3 (Scheme 3). Note that the mesyloxy groups

Scheme 3. Synthesis of Boron-Containing Polycyclic π -Electron System **22 by Intramolecular Oxidative Cyclization^a**

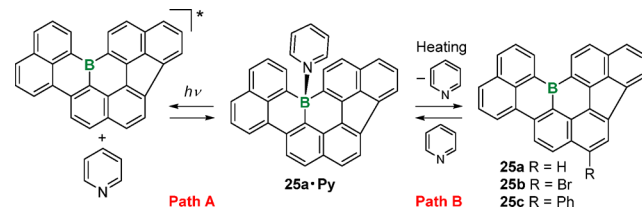


^aThe red lines denote the newly formed C–C bonds in each cyclization step. (R = OMe).

in the 4,5-positions of the anthracene unit play significant roles to facilitate the cyclization and to increase the solubility of the compound thus produced. In the crystal structure, **22** formed face-to-face dimeric π -stacks with a close intermolecular proximity of 3.53 Å. Owing to the electron-rich thiophene moieties, the absorption maxima were located in a relatively low-energy region ($\lambda_{\text{abs}} = 527, 563, 620$, and 668 nm) hence resulting in a deep purple color. Compound **22** displayed solvent-independent fluorescence and emitted light in the near-infrared region at $\lambda_{\text{em}} = 729$ nm with a low quantum yield of $\Phi_F = 0.016$. Reflecting on its structural rigidity, compound **22** is only weakly Lewis acidic but still responds to Lewis bases such as fluoride and pyridine to furnish the corresponding tetracoordinate borates.

In 2014, a partially fused trinaphthalylborane **25a** (Scheme 4) was synthesized by treatment of tris(8-bromonaphthalyl)borane

Scheme 4. Coordination/Dissociation Equilibrium of Boron-Doped PAH **25a and Pyridine, Where the Dissociation Processes Are Induced Both by Photoirradiation and Thermal Annealing^a**



^aStructures of functionalized derivatives **25b** and **25c** are shown on the right.

with $(\text{Me}_3\text{Si})_3\text{SiH}$ in the presence of ABCN as a radical initiator.¹⁴⁸ This red compound is sufficiently air, moisture, and thermally stable and can be postfunctionalized by bromination with NBS (**25b**) followed by Suzuki-Miyaura coupling without deconstruction of the tricoordinate boron moiety (e.g., using phenylboronic acid as the substrate affords compound **25c**; Scheme 4). Single crystal X-ray analysis demonstrated that **25b** forms a columnar π -stacked structure with an average plane-to-plane distance of 3.54 Å. Consequently, **25a** showed an ambipolar charge transporting behavior with a hole mobility of $\mu_h = 9.3 \times 10^{-6} \text{ cm}^2 \text{ V}^{-1} \text{ s}^{-1}$ and an electron mobility of $\mu_e = 1.7 \times 10^{-5} \text{ cm}^2 \text{ V}^{-1} \text{ s}^{-1}$.

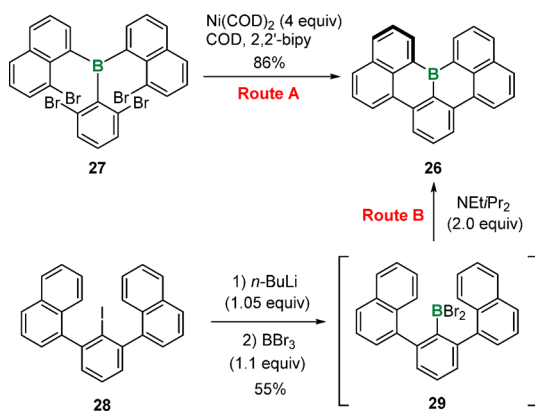
The Lewis acidity of **25a** was sufficiently high to form adducts with pyridine and its derivatives. Single crystals of the pyridine adduct **25a·Py** contained two crystallographically independent molecules in the asymmetric unit, both of which embraced a bowl-shaped geometry. The pyridine affinity of **25a** was evaluated by UV-vis spectrophotometric titration. Addition of pyridine to a toluene solution of **25a** induced decreases of the bands at $\lambda_{\text{abs}} = 429$ and 546 nm and concomitant appearance of new bands at $\lambda_{\text{abs}} = 346, 374$, and 490 nm, indicating the disruption of the π -conjugation through the boron center upon coordination of pyridine. The binding constant quantified at room temperature was $K_{\text{py}} = 5.1 \times 10^3 \text{ M}^{-1}$, which is significantly high for such a rigid structure. The titration experiment was also carried out using fluorescence spectroscopy. Compound **25a** in toluene showed a broad emission band centered at 573 nm with a low quantum yield of $\Phi_F = 0.15$. Incremental addition of pyridine led to a new emission band emerging at 500 nm but with only a slight decrease in intensity associated with **25a** at 573 nm. This observation is in virtue of the photodissociation of pyridine from the B–N Lewis pairs in the excited state, thus the dual fluorescence arising from both **25a** and **25a·Py** (Scheme 4, path A).

The coordination/dissociation dynamics of B–N Lewis adduct was particularly useful to produce semiconducting films of PAH-based materials.¹⁴⁹ Just like many other PAHs, **25a** suffers from poor solubility in most common organic solvents including chloroform, toluene, and chlorobenzene. In the presence of a small amount of pyridine, the solubility significantly improved due to the formation of the nonplanar **25a·Py**. Taking this disposition under consideration, a solution of **25a** was dissolved in chloroform containing 1 wt % of pyridine and subsequently spin coated on a glass substrate to

prepare a thin film which the absorption spectrum ($\lambda_{\text{abs}} = 360$ and 450 nm) was reminiscent to that of a toluene solution of **25a·Py**. Annealing the film at 180 °C resulted in a rapid transformation to a polycrystalline film (Scheme 4, path B). The absorption profile of the thus prepared film was similar to that of a vapor-deposited film of **25a**, confirming the successful thermal conversion of **25a·Py** to **25a** on the surface of a glass substrate. A FET device applied with **25a** as the semiconducting layer applying this method exhibited a conventional p-type characteristic with a hole-transfer mobility ($\mu_h = 2.5 \times 10^{-4} \text{ cm}^2 \text{ V}^{-1} \text{ s}^{-1}$), which is 2 orders of magnitude higher than that of the corresponding FET device prepared by the direct vapor-depositon of **25a**.

Simple π -extended PAHs quite often suffer from poor solubility in common organic solvents. One of the most effective strategies to improve solubility of PAHs is to bend or distort the structure. In 2015, Wagner and Hatakeyama groups independently reported novel strategies to synthesize benzannulated boron-doped [4]helicene **26**. Wagner et al. prepared **26** by intramolecular 2-fold C–C bond formations via Ni(0)-mediated Yamamoto dehalogenative coupling using tetrabrominated **27** as a precursor (Scheme 5, route A).¹⁵⁰ Soon after,

Scheme 5. Synthesis of the Boron-Doped [4]Helicene **26 through (A) Yamamoto Coupling Reaction on **27** and (B) Twofold Intramolecular Electrophilic Arene Borylation Reaction with a Base**

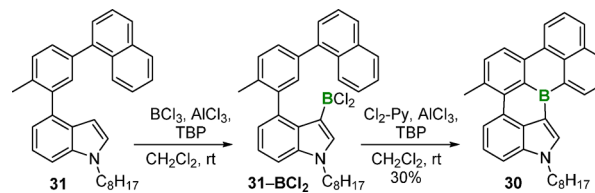


Hatakeyama et al. developed an alternative approach to furnish the same compound via one-pot synthetic sequence starting from *m*-teraryl iodide **28**: (1) lithium-halogen exchange followed by treatment with BBr_3 to produce *m*-terarylboron dibromide **29** and then (2) tandem intramolecular electrophilic arene borylation reaction in the presence of NEt_2Pr_2 as a proton scavenger (Scheme 5, route B).¹⁵¹ Single crystal X-ray diffraction analysis elucidated that **26** is forced to take up a distorted helical scaffold due to the steric repulsion between the two hydrogen atoms at the β -positions of the boron atom. Nevertheless, dilute cyclohexane solution of **26** is remarkably fluorescent with an emission maximum at 485 nm and a quantum yield of $\Phi_F = 0.81$.¹⁵⁰ While structurally related **25** is barely soluble in $\text{C}_6\text{H}_5\text{Cl}$ even at 120 °C, the distorted **26** is greatly soluble in nonpolar solvents such as hexane without bearing any solubilizing side groups. This feature becomes particularly advantageous for solution-processed fabrication. Because of the structural constraint, **26** is also air- and moisture-stable but still retains sufficient Lewis acidity to form the corresponding B–N adduct with pyridine, which

dissociates into free **26** and pyridine under high vacuum or exposure to a stream of nitrogen even in the solid state.¹⁵⁰

In 2016, Ingleson et al. prepared a fused-triarylborane containing a *N*-heterocyclic unit, compound **30**, through a one-pot synthesis of (1) intermolecular C–H borylation of **30** by reaction with BCl_3 , TBP, and AlCl_3 to afford **31-BCl**, followed by (2) double intramolecular C–H borylation by successive addition of $\text{Cl}_2\text{-Py}$, AlCl_3 , and TBP (Scheme 6).¹⁵²

Scheme 6. Synthesis of Fused Polycyclic Aromatic Compound **31 Containing Triarylborane and *N*-Heterocyclic Units by Inter-/Intramolecular Electrophilic Borylation^a**



^aTBP = 2,4,6-tri-*t*-butylpyridine, $\text{Cl}_2\text{-Py}$ = 2,6-dichloropyridine.

Using TBP as a proton acceptor in the second step is crucial to improve the yield since the strong Brønsted acid $[\text{Cl}_2\text{Py}-\text{H}]^+$ byproduct is sought to trigger formation of undesired indole oligomers via electrophilic aromatic substitution. In the crystalline state, **30** was planar and formed an infinite 1D columnar packing structure. Similar to those of other fused triarylboranes, **30** was only weakly Lewis acidic and formed B–N Lewis adducts upon addition of 50 equivalents of pyridine in dry CD_2Cl_2 , which was confirmed by NMR spectroscopy. In addition, attributed to the rigid structure, **30** exhibited a small Stokes shift of 22 nm in CH_2Cl_2 , despite the presence of an indole unit ($\lambda_{\text{abs}} = 491$ nm and $\lambda_{\text{em}} = 492$ nm). CV analysis of **30** showed a reversible redox with a half-reduction potential of $E^\circ_{\text{red}} = -2.08$ V vs Fc/Fc^+ which is significantly less negative than for nonconstraint triarylboranes such as Mes_3B ($E^\circ_{\text{red}} = -2.57$ V vs Fc/Fc^+).¹²⁹

2.2. Structurally Constrained Triarylboranes with Heteroatom Bridges

Incorporation of other main-group elements, especially those of electron rich ones such as oxygen and nitrogen, strongly influences the structural and electronic properties of the boron-doped polycyclic π -conjugated compounds. In 2016, Oi and Kitamoto et al. accomplished the first synthesis of oxygen-bridged *B*-heterotriangulene **32** (Figure 6A) via the regioselective triple lithiation–borylation and intramolecular S_{NAr} cyclization.¹⁵³ X-ray crystallography manifested that **32** adopts a fully planarized geometry with a significantly short C–B bond distances (1.459(2)–1.461(4) Å; Figure 6B). Moreover,

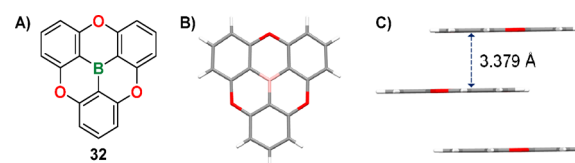
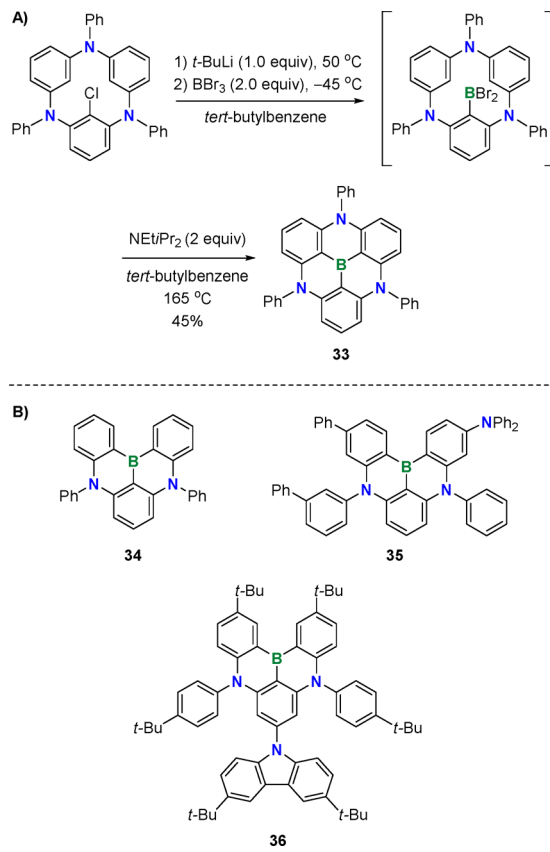


Figure 6. (A) Structure of oxygen-bridged *B*-heterotriangulene **32**, **(B)** crystal structure of **32**, and **(C)** its packing view of the cross section. The original data of the crystal structure of **32** was presented in ref 153.

32 forms a parallel offset π -stacked structure with a short interplanar distance between the adjacent stacking molecules of 3.379 Å (**Figure 6C**). This is in stark contrast to the more sterically demanding dimethylmethyleno-bridged analog **6** which embraces a face-to-edge packing structure. At 296 K in toluene, the absorption and the fluorescence maxima of **32** were obtained at $\lambda_{\text{abs}} = 338$ nm and $\lambda_{\text{em}} = 386$ nm, respectively. (For reference, the absorbance maxima and emission maxima of the carbocation analog of **32** in MeCN were $\lambda_{\text{abs}} = 450$ nm and $\lambda_{\text{em}} = 520$ nm, respectively.)^{154,155} When the temperature was lowered to 77 K, **32** exhibited a weak phosphorescence with the maxima located between $\lambda_{\text{em}} = 400$ –411 nm ($\lambda_{\text{em}} = 538$ nm in EtOH for the carbocation counterpart of **32**).

The divergent synthesis of heterotriangulenes bearing arylamino bridges was presented by Hatakeyama et al. in 2017.¹⁵⁶ The key steps for the new synthetic strategy include (1) preparation of the nitrogen-containing triarylmacrocycles followed by (2) introduction of heteroatoms into the macrocyclic framework through electrophilic C–Li and C–H substitution (see **Scheme 7A** for the synthesis of nitrogen-

Scheme 7. (A) Synthesis of Threefold Phenylamino-Bridged *B*-Heterotriangulene **33** As an Ultrapure Blue TADF Emitter and (B) Structures of Derivatives **34**–**36**



bridged *B*-heterotriangulene **33**). It is important to note that this approach can be applied not only for the boron compound but also for silicon- and phosphorus-centered heterotriangulene derivatives. Amino-bridged *B*-heterotriangulene **33** in the crystalline state was fully planarized with relatively elongated B–C bonds (1.478(7)–1.480(11) Å) compared to those in the oxygen-bridged analog **32**.¹⁵³ The UV–vis spectrum of **33** showed an absorption band corresponding to π – π^* transition

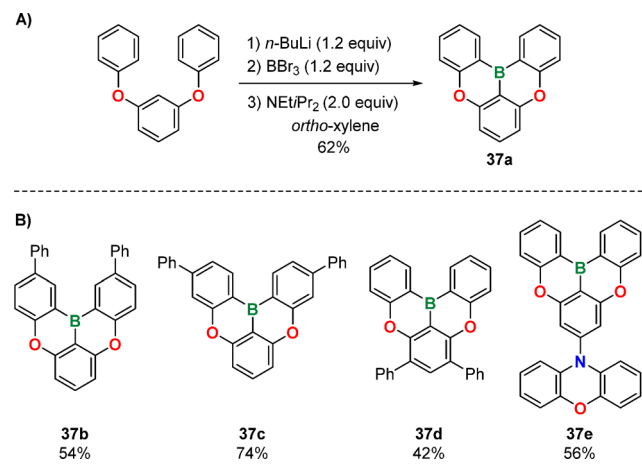
centered at $\lambda_{\text{abs}} = 385$ nm. Moreover, the fluorescence spectrum of **33** recorded at 296 K showed a sharp and intense emission band centered at $\lambda_{\text{em}} = 399$ nm with a quantum yield of $\Phi_F = 0.54$ and an astonishingly narrow fwhm of 26 nm. Phosphorescence spectrum of **33** measured at 77 K displayed a deep-blue emission at $\lambda_{\text{em}} = 427$ nm. The energy difference between the S_1 and T_1 states estimated from the two emission spectra was fairly small ($\Delta E_{\text{ST}} = 0.21$ eV), which the authors attributed to multiple resonance effect between the central boron atom and the three ancillary nitrogen atoms.

Toward the development of efficient ultrapure blue thermally activated delayed fluorescence (TADF) emitters for high performance OLEDs, Hatakeyama et al. synthesized doubly nitrogen-bridged triarylboranes **34** and **35** (**Scheme 7B**).¹⁵⁷ These compounds were obtained in multigram scales from commercially available substrates using Pd-catalyzed C–N cross coupling followed by one-pot borylation using *t*-BuLi and BBr₃. The most compelling feature of the molecular design was the efficient HOMO–LUMO separation by the multiple resonance effects mentioned previously. In fact, DFT calculations predicted that the LUMOs were mostly localized on the boron center and the relative ortho- and para-carbons, while the HOMOs predominantly involved the ancillary nitrogens and the relative ortho- and para-carbons. Along with the resonance effects, the molecular rigidity was an important factor for **34** and **35** to achieve marginal Stokes shifts and fwhm's as well as intense emission both in solution of CH₂Cl₂ and in films. Moreover, the S_1 and T_1 energy gaps estimated from the emission spectra measured at ambient temperature and 77 K were also very small ($\Delta E_{\text{ST}} = 0.15$ eV).

The above-mentioned electronic and photophysical properties are well-suited for TADF emitters. Indeed, compound **35** was employed as an emitter for OLEDs which displayed pure blue emission at 467 nm with a narrow fwhm of 28 nm as well as an IQE of approximately 100%.¹⁵⁷ Aiming at enhancement of the multiple resonance effect, Zheng et al. in 2018 developed compound **36** (**Scheme 7B**), which incorporates an electron-donating carbazole derivative at the para-position of the central phenyl anchor relative to the boron center.¹⁵⁸ This compound showed a sharp emission band at $\lambda_{\text{em}} = 470$ nm together with a small fwhm of 26 nm and an exceptional photoluminescence quantum yield of $\Phi_F = 0.97$. The ultrapure blue device utilizing **36** as an emitter exhibited superior performance with the external quantum efficiency (EQE) of up to 32.1% and a maximum luminance of more than 16×10^3 cd m⁻².

2-Fold oxygen-bridged triarylboranes have also been exploited as emitting materials. In 2015, Hatakeyama et al. developed a facile one-step borylation of 1,3-diaryloxybenzene to efficiently access a variety of doubly oxygen-bridged triarylborane derivatives.¹⁵⁹ For example, 1,3-diphenyloxybenzene was converted to 2-fold oxygen-bridged triphenylborane **37a** through a one-pot sequence of (1) direct *ortho*-lithiation applying *n*-BuLi in *ortho*-xylene at 70 °C, (2) treatment with BBr₃ to afford the dibromoboryl intermediate, and (3) successive addition of two equivalents of Hunig's base and heating at 120 °C (**Scheme 8A**). Compounds **37b**–**e** were also obtained using an analogous approach (**Scheme 8B**). Compounds **37a**–**d**, which are decorated with a pair of phenyl rings at different positions, exhibited absorbance and fluorescence maxima in the blue region ($\lambda_{\text{abs}} = 398$ –436 nm and $\lambda_{\text{em}} = 418$ –459 nm) with moderate quantum yields ($\Phi_F = 0.57$ –0.72). Intriguingly, the ΔE_{ST} values, that are, the energy

Scheme 8. (A) Synthesis of Twofold Oxygen-Bridged Triphenylborane 37a by Brønsted Base-Assisted Double Electrophilic Borylation and (B) Structures of Related Derivatives 37b–e Obtained by the Same Synthetic Procedure (Bottom)



gaps between the S_1 and T_1 states, for compounds 37b–d estimated from emission spectra recorded at 298 and 77 K were all small ($\Delta E_{\text{ST}} = 0.06\text{--}0.31$ eV). Based on these characteristics, compounds 37b and 37c were employed as the host materials for phosphorescent organic light emitting diodes (PHOLEDs) using $[\text{Ir}(\text{ppy})_3]$ as a green-emitting dopant. The devices performed superbly with the EQE exceeding 20% at 1000 cd m^{-2} and long lifetimes (1000 h with 37b and 383 h with 37c). Meanwhile, 37e (Scheme 8 bottom) bearing an electron-donating phenoxazine tether had much improved photophysical properties with an exceptionally small $S_1\text{--}T_1$ energy gap, which are suitable for TADF emissive layers ($\lambda_{\text{abs}} = 492$ nm, $\lambda_{\text{em}} = 477$ nm, $\Phi_F = 0.92$, and $\Delta E_{\text{ST}} = 0.06$ eV). Indeed, OLEDs using 37e as an emitter and 37b and 37c as host materials showed EQEs of 15.2 and 13.9%, respectively, but with short lifetimes (<1 h).

2.3. Diphenylborane-Fused Porphyrins

Doping a π -accepting tricoordinate boron moiety directly into an electron-rich porphyrin π -circuit is a simple yet highly effective method to perturb the optoelectronic properties. To this end, porphyrins fused with one or two diphenylboranes at the periphery, 38 and 39 (Figure 7), were prepared by Yorimitsu et al. from the corresponding β -(2-trimethylsilyl-

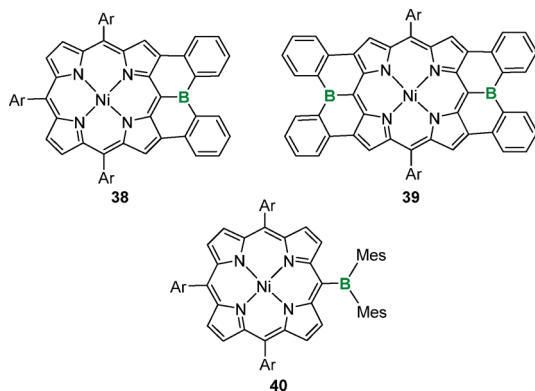


Figure 7. Structures of diphenylborane-fused porphyrins 38 and 39 and meso-dimesitylborylporphyrin 40. Ar = 3,5-di-*tert*-butylphenyl.

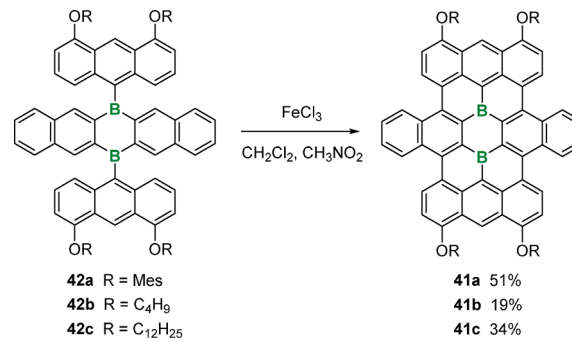
phenyl)-substituted porphyrins.¹⁶⁰ The one-pot synthesis involved Si/B exchange reactions, intramolecular bora-Friedel–Crafts reactions, and ring-closing Si/B exchange reactions. Diphenylborane-fused porphyrins 38 and 39 are remarkably air- and moisture-stable and were purified by silica gel column chromatography without any special precautions. X-ray crystallography revealed that both 38 and 39 are slightly distorted around the boron centers and adopt helical structures. The first oxidation potential of 38 (-1.23 V vs Fc/Fc⁺) was distinctly shifted to the positive direction by 0.51 V compared to the nonconstrained dimesitylboryl analog 40 (-1.74 V; Figure 7),¹⁶¹ demonstrating the importance of structural planarity for effective electronic interactions between the vacant p orbital of the boron centers and the porphyrin π -circuit. Moreover, attributed to the bespoke orbital interactions, largely red-shifted absorption maxima (38: $\lambda_{\text{abs}} = 478$, 649, 689, and 755 nm; 39: $\lambda_{\text{abs}} = 499$, 706, 845, and 956 nm) and stabilized LUMOs (38: $E_{\text{LUMO}} = -2.78$ eV; 39: $E_{\text{LUMO}} = -3.18$ eV) were achieved. Subsequently, the Lewis acidity of 38 was evaluated by UV-vis spectrophotometric titration using pyridine as the Lewis base. New absorption bands gradually appeared at the shorter wavelength upon incremental addition of pyridine to a CH_2Cl_2 solution of 38, suggesting the formation of B–N adducts.

2.4. Boron-Doped Nanographene and Graphene Nanoribbons

Graphene on its own has an intrinsic zero-band gap character which impedes its application in nanoscale transistors.^{27,162} Toward the development of attractive 2D materials based on graphene, doping electron-deficient tricoordinate boron moiety directly into the sp²-hybridized carbon-atom network adds an electron-accepting character and endows the graphene with semiconducting properties.⁷¹ We specifically listed examples of structurally well-defined boron-doped nanographenes herein.

Honeycomb-shaped nanographene containing two boron atoms arranged in opposition within the same six-membered ring, compounds 41a–c, was reported by Yamaguchi and co-workers (Scheme 9).^{163,164} Owing to the greatly extended π -

Scheme 9. Synthesis of Doubly Boron-Doped Nanographenes 41 via Oxidative Cyclodehydrogenation of 6,13-Dihydro-6,13-diborapentacene Precursors 42



systems, these compounds can be viewed as compact models of boron-doped nanographenes. Purple-colored 41a–c were prepared by Scholl reaction of 6,13-dihydro-6,13-diborapentacene precursors 42a–c (Scheme 9). X-ray crystallographic analysis enlightened that 41a is composed of 15 fused benzene rings aligned like a micrographene sheet with four cove regions and two zigzag structures. The overall structure was deviated

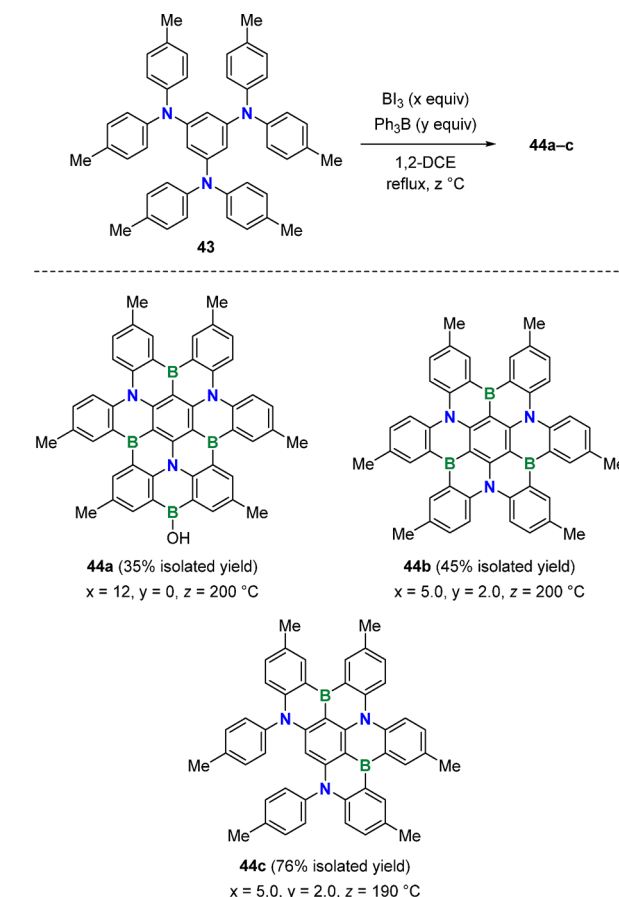
from perfect planarity ascribed to the steric repulsion among the hydrogen atoms within the cove regions. In addition, the crystals of compounds **41b** and **41c** tethering long alkyl chains were more densely packed than **41a** consisting of sterically demanding mesityl rings. The UV-vis absorption spectrum of **41a** recorded in toluene displayed a broad absorption band from 400 to 700 nm with maxima at $\lambda_{\text{abs}} = 640, 564$, and 487 nm, which were assigned to electronic transitions $\text{HOMO} \rightarrow \text{LUMO}$, $\text{HOMO-1} \rightarrow \text{LUMO+1}$, and $\text{HOMO-2} \rightarrow \text{LUMO}$, respectively, based on TD DFT calculations. Notably, all transitions involved HOMO-1 or LUMO have significant contributions from the p orbitals of the boron atoms.

The Lewis acidity of **41b** was examined by UV-vis spectrophotometric titration.¹⁶⁴ Incremental addition of TBAF to a THF solution of **41b** was concomitant with a gradual color change from purple to yellow, suggesting the corresponding B–F adduct formation. In the UV-vis spectrum, the fluoride coordination event was accompanied by a suppression of absorption bands around 390 and 580 nm and a simultaneous appearance of a new band around 470 nm. This spectral change continued until two equivalents of fluoride ions were introduced whereupon the Lewis acidic boron centers were all saturated. The same survey was also conducted using weaker Lewis bases, namely, pyridine, 4-methylpyridine (MePy), and 4-dimethylaminopyridine (DMAP), and the binding constants for the first (K_1) and second coordination (K_2) steps were $K_1 = 23 \text{ M}^{-1}$ and $K_2 = 19 \text{ M}^{-1}$ for pyridine, $K_1 = 150 \text{ M}^{-1}$ and $K_2 = 16 \text{ M}^{-1}$ for MePy, and $K_1 = 3.8 \times 10^4 \text{ M}^{-1}$ and $K_2 = 2.3 \times 10^4 \text{ M}^{-1}$ for DMAP. The crystal structure of the complex of **41b** and two molecules of MePy was determined by X-ray diffraction analysis. The two MePy molecules were coordinated to the boron atoms on the same side of the nanographene sheet, resulting in a cis-orientation. The cyclic voltammetric measurement of **41b** showed two reversible redox waves for the reduction processes at $E_{1/2} = -1.45 \text{ V}$ and $-1.66 \text{ (vs Fc/Fc⁺)}$. Thus, two-electron chemical reduction of **41b** by two equivalents of CoCp_2^* furnished the corresponding diradical species $[\textbf{41b}]^{2-}$ possessing a triplet ground state.

The use of boron-doped nanographenes as gas sensors were previously proposed by theoretical studies.¹⁶⁵ As a preliminary work, a THF solution of **41b** was exposed to NH₃ gas for a few seconds in which the solution color changed from dark purple to yellow and began to emit bright yellow greenish light under a UV lamp. Boron-doped nanographenes **41b** and **41c** were also utilized as active materials for Li battery electrodes. Stable charge/discharge performances in the 1.5–4.0 V voltage range were exhibited without any significant degradation even after 10 cycles.

In 2018, Hatakeyama et al. succeeded in the two-step synthesis of BN-doped nanographenes composed of multiple boron and nitrogen atoms within the same π -conjugated framework.¹⁶⁶ The synthesis includes intra- and intermolecular bora-Friedel–Crafts-type reactions from commercially available starting materials such as 1,3,5-tribromobenzene and di(4-tolyl)amine and using appropriate amount of Bi_3 and Ph_3B . For instance, treatment of **43** with 5 equiv of Bi_3 and 2 equiv of Ph_3B in 1,2,4-trichlorobenzene at 200 °C produced **44b** in 45% yield (**Scheme 10**). Single-crystal X-ray diffraction analysis of **44b** revealed a triple helical structure with a near D_3 conformation. The NICS calculations demonstrated that the BNC_4 rings have nonaromatic character ($\text{NICS}(0) = 0.9\text{--}1.1$), while the central C_6 ring has moderate aromatic character.

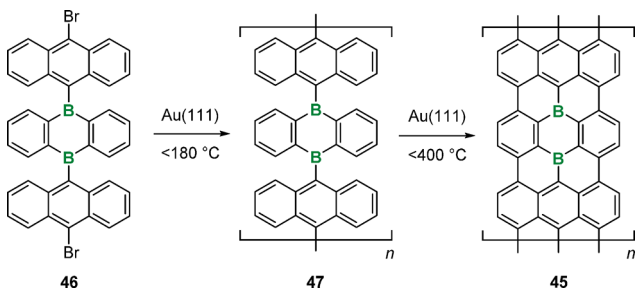
Scheme 10. Synthesis of BN-Doped Nanographenes 44 by One-Pot Multiple Electrophilic Borylation



(NICS(0) = -4.8). Interestingly, the UV-vis spectrum of **44b** displayed an absorption band centered at $\lambda_{\text{abs}} = 396$ nm, which was significantly blue-shifted compared to those of **44a** ($\lambda_{\text{abs}} = 438$ nm) and **44c** ($\lambda_{\text{abs}} = 440$ nm). TD DFT calculations predicted that the S_0-S_1 and S_0-S_2 transitions in **44b** were forbidden, and the absorption band is assignable to the combination of S_0-S_3 and S_0-S_4 transitions. Compounds **44a–c** displayed moderately intense, deep blue emission bands at 455, 441, and 450 nm, respectively, with significantly small fwhm values (**44a**: $\Phi_F = 0.53$, fwhm = 32 nm; **44b**: $\Phi_F = 0.33$, fwhm = 34 nm; **44c**: $\Phi_F = 0.57$, fwhm = 38 nm). A blue TADF OLED using **44b** as an emitter recorded strikingly high EQEs of 18.3% at 1 cd m⁻² and 12.6% at 100 cd m⁻².

In 2015, Kawai et al. developed a bottom-up synthesis of defect-free, monodispersed boron-doped graphene nanoribbon (B-GNR) via solvent-free on-surface approach (**Scheme 11**).¹⁶⁷ The preparation of B-GNR 45 was achieved through two major steps starting from precursor **46**, which is 9,10-di(9-anthryl)-9,10-dihydro-9,10-diboraanthracene. First, precursor **46** was deposited on a Au(111) surface under ultrahigh vacuum and was subsequently annealed at 180 °C to afford linear polymer **47** via surface-catalyzed dehalogenative polymerization. In turn, the elevation of annealing temperature to 400 °C triggered surface-assisted cyclodehydrogenation to cleanly produce B-GNR **45**. Around the same time, Crommie, Fischer et al. also reported the synthesis of B-GNR using a similar strategy.¹⁶⁸ The chemical structures of B-GNR **45** was directly resolved by high-resolution AFM equipped with a CO-functionalized tip. The boron atoms were indeed observed in

Scheme 11. On-Surface Ullmann-Type Dehalogenative Polymerization to Form 47^a



^aFurther elevation of temperature induced surface-assisted cyclo-dehydrogenation to give B-GNR 45.

the center of the graphene sheet, which corresponds to 4.8 atom %. Despite the rigid architecture, B-GNR 45 was found to efficiently adsorb NO at the Lewis acidic boron centers, which was verified by STM topography as well as stimulated STM image with optimized adsorption model. This property may be useful to develop B-GNR-based gas sensors. A more detailed studies on the electronic structures and properties were conducted by Garcia-Lekue, Corso, Pascual et al. in 2018.¹⁶⁹ One crucial finding from this work was that the B-GNR band structure can be precisely tuned by varying the separation between the diboron ring moieties.

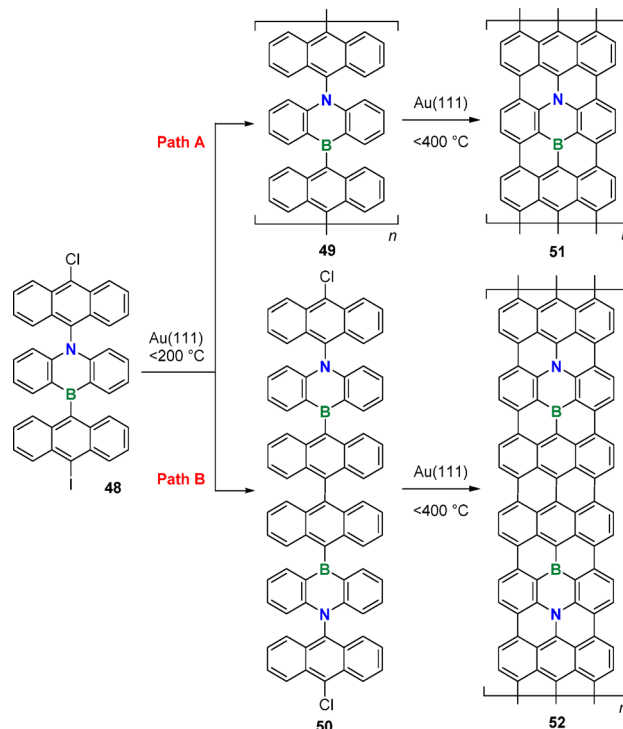
In 2018, Kawai, Hatakeyama, and Foster et al. reported the synthesis and characterization of a well-ordered graphene nanoribbon embedded with both boron and nitrogen atoms (BN-GNR).¹⁷⁰ For the preparation, precursor **48**, composed of three anthracene units with the central unit possessing a C₄BN ring and adjacent units tethering either iodine or chlorine substituents, was first annealed on a Au(111) surface at 200 °C to produce 1D polymer **49** and dimer **50** through Cl–I coupling (Path A) and I–I coupling (Path B) reactions, respectively (Scheme 12). Note that two different dehalogenative coupling reactions can occur under the same condition. Upon elevation of the annealing temperature to 400 °C, both 1D polymer **49** and dimer **50** were converted to atom-precise BN-GNRs **51** and **52**, respectively. Although AFM possessing a CO-functionalized tip was able to directly resolve the elemental difference in the obtained BN-GNRs **51** and **52**, the properties still remain unclear.

3. NITROGEN-CENTERED POLYCYCLIC COMPOUNDS

Tricoordinate nitrogen carries a lone pair of electrons and is a natural complement of a tricoordinate boron that consists of a vacant p orbital. Thus, compounds possessing such moiety are generally electron rich and triarylaminies in particular have been readily employed as hole-transporting and hole-injection materials for OLEDs and perovskite solar cells.^{171–174}

The molecular configurations and electronic properties of triarylaminies greatly impact their aggregation states and charge carrier-transporting properties. For instance, triphenylamine possesses a trigonal planar geometry with the three phenyl rings forming a propeller-shaped structure, and its ionization potential is as low as 6.80 eV, which makes it an exceptional electron donor (Figure 8A).^{175–177} Other related derivatives also have comparable geometrical and electronic characteristics. Unfortunately, conventional triarylamine derivatives tend to have low thermal and morphological stabilities, and the lifetime of the charge-separated states are rather short owing to

Scheme 12. Annealing 48 on a Au(111) Surface at 200 °C Induces Ullmann-Type Dehalogenative Coupling Reactions to Form 1D Polymer 49 (Path A; Cl–I Coupling) and Dimer 50 (Path B; I–I Coupling)^a



^aFurther elevation of the annealing temperature over 400 °C led to the formation of atom-precise BN-GNRs **51** and **52**.

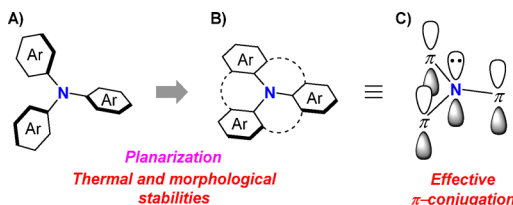


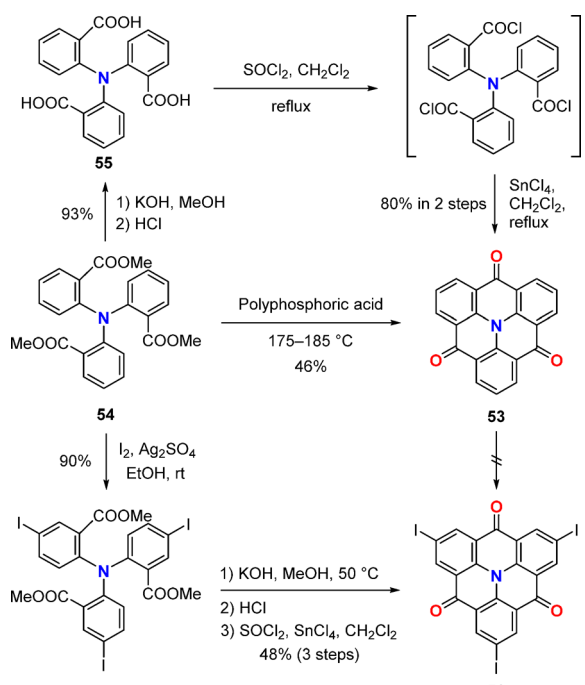
Figure 8. Illustrations of (A) a nonconstrained triarylamine, (B) a structurally constrained triarylamine, and (C) effective orbital interaction among the nitrogen lone pair and the π -skeleton.

the lack of efficient π -conjugation necessary to delocalize the generated cation. These are all critical drawbacks for practical applications. In this context, structural constraint of the triarylamine moiety is an effective approach to overcome the bespoke issues while retaining the strengths of nonconstrained derivatives (Figure 8B).¹⁷⁸ In addition, the structural planarity is also advantageous because of (1) the increased interaction between nitrogen lone pair and the π -skeleton for improved photophysical properties including red-shifted absorption and fluorescence as well as larger TPA cross-section (Figure 8C) and (2) the enhanced π – π stacking efficiency leading to higher hole mobility. With these benefits in mind, this chapter will specifically shed light on the diverse yet important investigations on planarized triarylamine derivatives with a focus on their structural and optoelectronic properties.

3.1. Nitrogen-Centered Triangulenes: *N*-Heterotriangulenes

3.1.1. Carbonyl-Bridged *N*-Heterotriangulenes. Triphenylamines that are locked in a planar conformation by bridging moieties are a compound class known as *N*-heterotriangulenes.¹⁷⁹ The very first synthesis of such compound was presented by Hellwinkel and Melan in 1971.¹⁸⁰ *N*-Heterotriangulene **53**, which bears three carbonyl bridges, was obtained via intermolecular Friedel–Crafts acylation of tribenzoate precursor **54** in the presence of polyphosphoric acid and heating at 175–185 °C (Scheme 13).

Scheme 13. Synthesis of Tricarbonyl-Bridged *N*-Heterotriangulene **53** and Its Iodide Derivative **56**



The low yield is associated with the formation of partially cyclized byproducts. It took until 2002 when Field and Venkataraman revisited this chemistry and introduced an improved synthetic strategy involving 3-fold intramolecular Friedel–Crafts acylation of the tricarbonyl chloride intermediate species generated in situ from tricarboxylic acid **55**.¹⁸¹ In the crystalline state, **53** formed densely packed columnar π -stacks with a plane-to-plane distance of 3.46 Å. Because of this aggregation tendency, **53** is poorly soluble in CHCl_3 but just enough to record a UV–vis spectrum in which the absorption maximum appeared at 411 nm. Electrochemical measurements, however, could not be done.

There are no reports regarding the direct halogenation of the three para-positions of **53**. This could be ascribed to the strong electron-withdrawing effect of the carbonyl bridges, which reduces the electron density at the periphery thereby prohibits the electrophilic aromatic substitutions. Instead, Du et al. successfully obtained triiodo derivative **56** by first carrying out iodination of the tribenzoate precursor **54** prior to intramolecular cyclization (Scheme 13).¹⁸² In the same work, **56** was utilized as a key precursor to introduce carbazole units via Ullmann coupling to afford donor–acceptor type dendrimers **57a** and **57b** (Scheme 14). The UV–vis spectra of the two

dendrimers in CHCl_3 displayed weak absorption bands centered at 370 and 420 nm, respectively, which were attributed to intramolecular charge-transfer transitions among the terminal carbazole moiety and the electron-deficient heterotriangulene core. Thin films of **57a** and **57b** were weakly fluorescent with emission maxima at 600 and 630 nm, respectively ($\Phi_F = 0.15$ for **57a** and $\Phi_F = 0.08$ for **57b**).

Triiodo derivative **56** is a useful starting material for decoration of the carbonyl-bridged *N*-heterotriangulene core by various transition-metal-mediated reactions.^{183,184} This system was especially convenient to embed solubilizing groups or other side chains to study the behavior of compounds built upon a carbonyl-bridged *N*-heterotriangulene scaffold both in solution and liquid-crystal phase. As one of the representative examples, Chen et al. synthesized compound **58a** through a Pd-catalyzed Sonogashira cross-coupling reaction between triido species **56** and three equivalents of 1-dodecyl-4-ethynylbenzene (Scheme 14).¹⁸³ In a binary solvent of $\text{MeOH}/\text{CH}_2\text{Cl}_2$, compound **58a** was found to undergo two-level self-assembly process from straight nanowires to well-organized microrods. The authors addressed that the driving force of this behavior is ascribed to the strong π – π stacking interaction among the heterotriangulene cores and the hydrophobic interactions between the alkyl chains and solvent molecules.

In 2013, Kivala et al. described the synthesis of a series of carbonyl-bridged *N*-heterotriangulene derivatives decorated with flexible *n*-dodecyl chains linked through various spacers and to assess their self-assembly behavior.¹⁸⁵ Conveniently, all compounds were obtained by cross-coupling reactions starting from triiodide **56**. In short, ethynylated derivatives **58b–e**, arylated derivative **59a**, and alkylated derivative **60a** were synthesized by Sonogashira coupling, Suzuki–Miyaura coupling, and Negishi coupling, respectively (Scheme 14). While all compounds were soluble in most of the common solvents, the self-assembly behaviors greatly depended on the nature of the lateral substituents, their steric bulkiness, and the conditions for solution processing. For instance, arylated derivative **59** self-assembled into columnar discs both in solution and in the bulk state, whereas ethynylated derivative **58b** and **58d** showed a similar behavior in the solid state but not in solution. Meanwhile, *N*-heterotriangulene derivatives possessing linked phenylene-ethynylene spacers, **58b** and **58c**, produced thermotropic liquid crystals. The alkylated derivative **59a** displayed the lowest self-association in solution but produced well-aligned fibers upon dip coating a chloroform solution.^{185,186} The high crystallinity, which was confirmed by its electron diffraction pattern, suggested that the fibers were composed of columnar stacks of molecules of **59a** similar to that of **53**. In the same year, Inagi et al. used a simple derivative of **58d**, compound **58e**, to mediate electrocatalytic reduction of *meso*-1,2-dibromo-1,2-diphenylethane to give *trans*-stilbene.¹⁸⁷

In 2014, Hildner et al. reported two novel multichromophoric compounds based on carbonyl-bridged *N*-heterotriangulene **61a** and **61b** (Figure 9), which tether naphthalimides and 4-(5-hexyl-2,2'-bithiophene)naphthalimides, respectively, as peripheral chromophores.¹⁸⁸ The two compounds were obtained by simply reacting triamino-substituted *N*-heterotriangulene with appropriate acyl chlorides.¹⁸⁹ It became evident from steady-state and time-resolved spectroscopic analysis of these compounds that intramolecular energy transfer only occurs for multichromophoric systems. The

Scheme 14. Trigonal Functionalization of Tricarbonyl-Bridged N-Heterotriangulene Scaffold by Diverse Cross-Coupling Reactions Starting from Triiodinated Precursor **56**

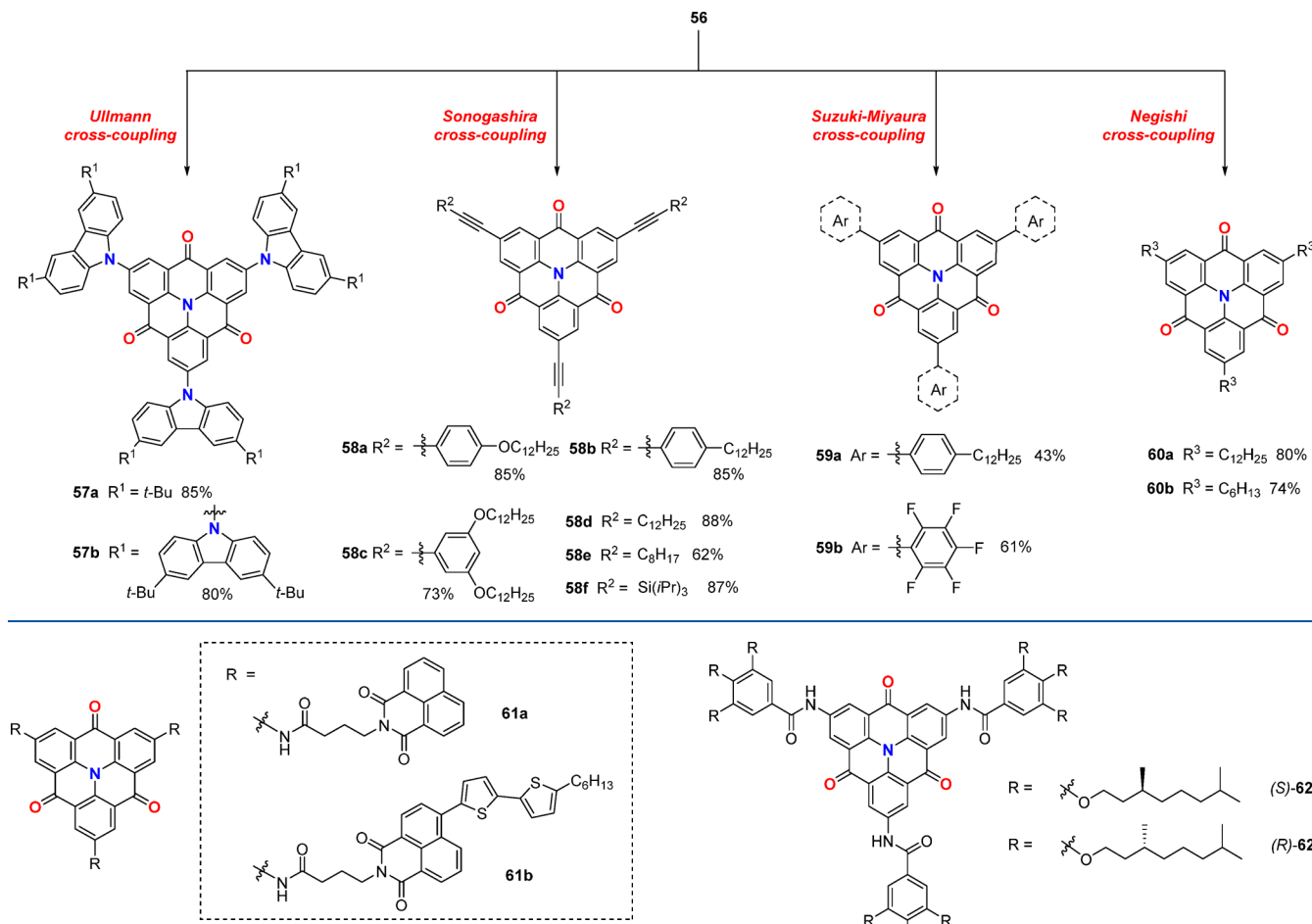


Figure 9. Structures of naphthalimide-substituted N-heterotriangulene derivatives **61a** and **61b** possessing multichromophoric behavior.

direction of the energy transfer depended on the nature of the naphthalimide-based chromophores. For compound **61a**, the energy was delivered from the peripheral naphthalimides to the N-heterotriangulene core. The donor/acceptor roles were reversed in **61b**, therefore the energy flew in the opposite direction. Furthermore, compound **61b** formed orange-colored fluorescent gel in *ortho*-dichlorobenzene at a low concentration of 0.7 mM. It is noteworthy that the energy-transfer and photoluminescent properties were retained in this gel state. Most importantly, both **61a** and **61b** can self-assemble to form supramolecular fibers that are capable of transporting excitation energies over micrometer distances at room temperature.¹⁹⁰

Two years later, Schmidt and Meijers et al. presented a seminal study on the complex enantioselective self-assembly process utilizing chiral derivatives of carbonyl-bridged triarylamine trisamides.¹⁹¹ The two enantiomers (*S*)–**62** and (*R*)–**62** (Figure 10) were discovered to self-assemble via two different pathways depending on the thermal profile. Upon continuous cooling at 7 °C, a kinetically trapped state was obtained via a proposed isodesmic process. On the other hand, a thermodynamically stable state was favorably obtained via a nucleation-elongation mechanism by initially undercooling at –5 °C prior to warming up to 7 °C. Mixing the two different states of the same enantiomers triggered a supramolecular

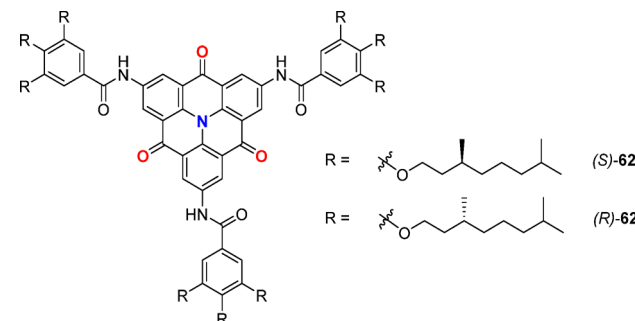


Figure 10. Structures of chiral carbonyl-bridged triarylamine trisamides (*S*)-**62** and (*R*)-**62** which exhibit two-pathway self-assembly behavior in solution.

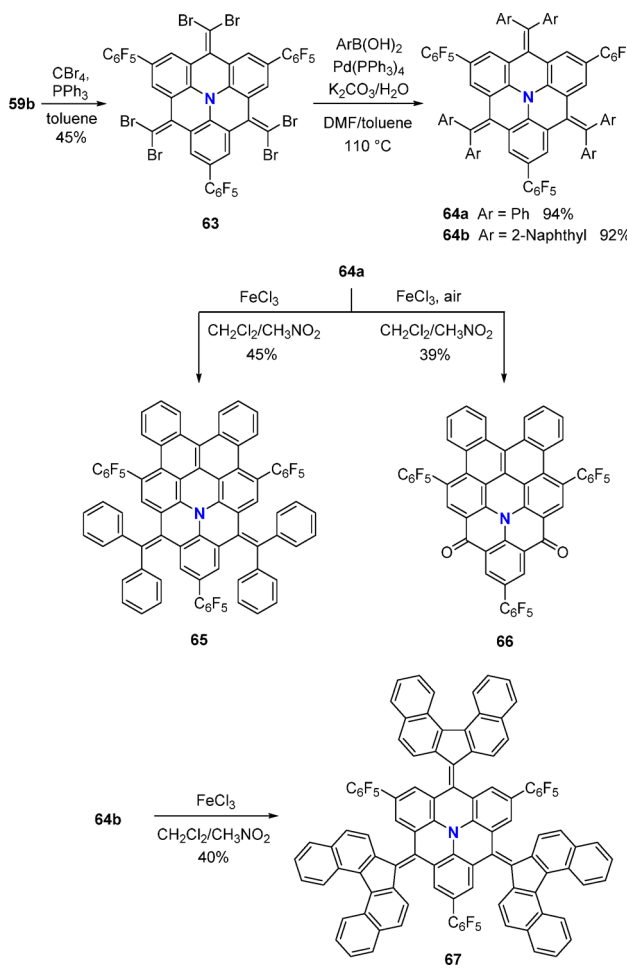
polymerization in a controlled manner, which essentially induced a complete conversion of the kinetically trapped state to the thermally stable state.

3.1.2. Arylvinylidene-Bridged N-Heterotriangulenes.

One of the first attempts to functionalize a carbonyl-bridged N-heterotriangulene scaffold involved the Pd-catalyzed Kumada cross-coupling reaction of the triiodo species **56** with *n*-dodecylmagnesium bromide.¹⁸⁵ Owing to the high nucleophilicity, however, the Grignard reagent was found to attack the bridging carbonyls instead, resulting in multiple undesired products. This finding was rather encouraging in the sense that further functionalization can be achieved in the bridging positions.

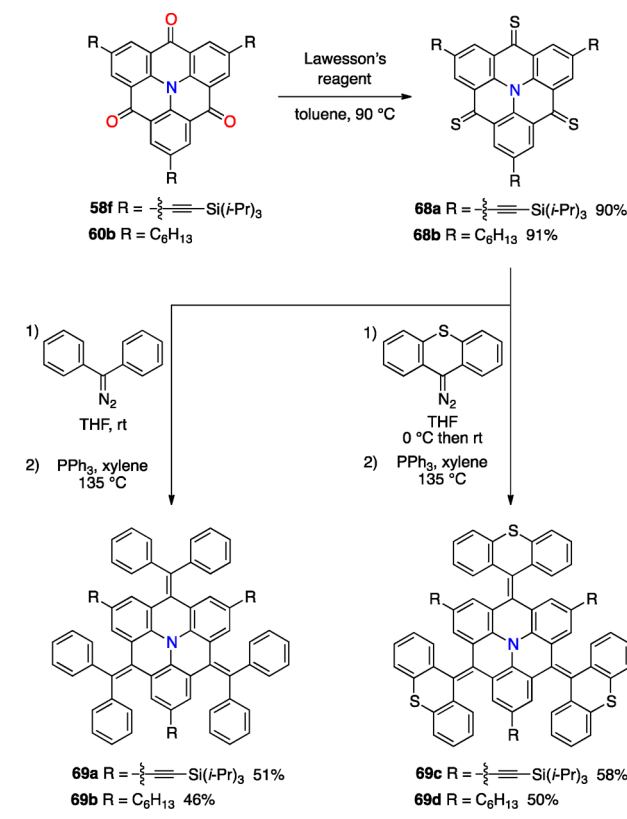
Indeed, the expansion of N-heterotriangulene at the bridging position was achieved in 2014.¹⁹² Initially, carbonyl-bridged N-heterotriangulene **59b** was transformed to the hexabrominated derivative **63** via Corey-Fuchs reaction (Scheme 15). Then, **63** was subjected to Suzuki-Miyaura cross-coupling reactions with phenylboronic acid or 2-naphthylboronic acid to furnish the corresponding 6-fold coupling products **64a** and **64b**, respectively. Subsequent Scholl reaction converted **64a** into 10-ring fused compound **65** and dicarbonyl-substituted 10-ring-fused compound **66** under degassed and aerated

Scheme 15. Synthesis of a Series of *N*-Heterotriangulenes Expanded at the Bridging Positions with a Fused Polycyclic Skeleton 65–67



conditions, respectively. In the case of hexanaphthyl derivative **64b**, Scholl reaction under an argon atmosphere induced dehydrogenative coupling of the terminal naphthyl groups instead, producing dibenzo[*cg*]-fluorenylidene-substituted *N*-heterotriangulene **67** as the main product. X-ray crystallographic analysis confirmed that **67** has a highly twisted conformation, attributed to the steric crowdedness around the alkene moieties. DFT calculations verified that the unfavorable structural conformation of the bridging vinylidene moieties led to a drastic stabilization of the LUMO, thus adding electron-accepting character to the electron-rich heterotriangulene core. Indeed, the unusual electronic structure was responsible for **67** to absorb radiation all the way in the NIR region ($\lambda_{\text{abs}} = 797$ nm) and to undergo multiredox processes for both oxidation and reduction. The half redox potential for the first reduction of **67** was as low as -1.13 V vs Fc/Fc^+ , which is comparable to that of C_{60} (-1.0 V).¹⁹³ A year later, Kivala et al. introduced an efficient method to access arylvinylidene-bridged *N*-heterotriangulene (Scheme 16).¹⁹⁴ First, triketone species **58f** and **60b** were heated with Lawesson's reagent in toluene to quantitatively yield thioketones **68a** and **68b**, respectively, as stable purple solids.¹⁹⁵ These thioketones were then subjected to the 3-fold Barton-Kellogg olefination reaction with either diphenyldiazomethane or 9-diazo-9*H*-thioxanthane. The resulting intermediate thioepoxides were used without purification to successively react with appropriate diaryldiazomethane

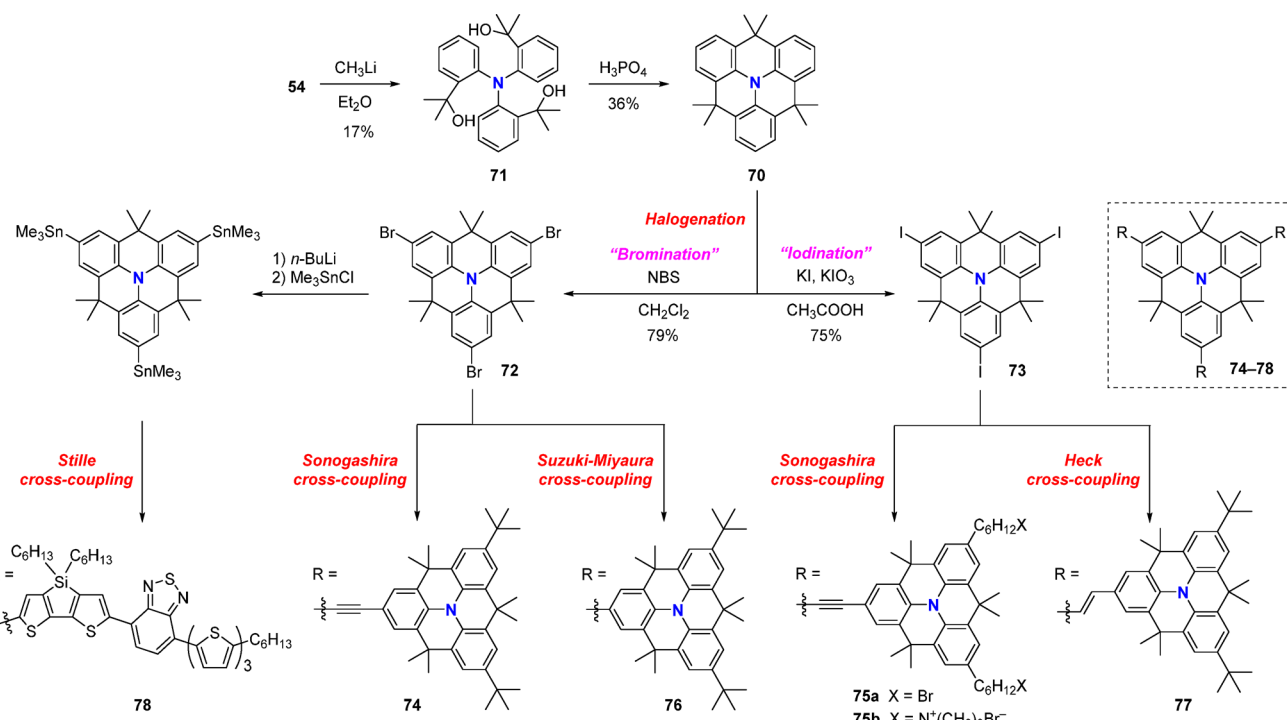
Scheme 16. Synthesis of Diphenylvinylidene-Bridged *N*-Heterotriangulenes **69 from Carbonyl-Bridged Derivatives via Thionation Followed by Barton-Kellogg Olefination**



derivatives in the presence of triphenylphosphine to afford the desired olefinated *N*-heterotriangulenes **69a**–**d**. X-ray crystallography exposed that all of these compounds adopt a shallow bowl-shaped structure in contrary to a perfectly planarized conformation found in carbonyl-bridged analog **53**.¹⁸¹ The authors addressed that the distortion of the overall structure was likely caused by the steric demand surrounding the exocyclic $\text{C}=\text{C}$ bonds, which thereby were forced to bend away from the polycyclic plane.¹⁹⁶ Nevertheless, sulfur-tethered **69c** and **69d** were highly fluorescent with emission maxima at $\lambda_{\text{em}} = 498$ and 511 nm and quantum yields of $\Phi_F = 0.57$ and 0.46, respectively. In addition, compounds **69a**–**d** were all relatively strong electron-donors competent of multiple reversible oxidation processes. The potential of the first oxidation of diphenylvinylidene-bridged **69b** ($E^\circ_{\text{ox}} = +0.05$ V vs Fc/Fc^+) in specific was comparable to that of ferrocene.

3.1.3. Dimethylmethylene-Bridged *N*-Heterotriangulenes. Three years after the first appearance of carbonyl-bridged *N*-heterotriangulene **53** in the literature, Hellwinkel and Melan synthesized the dimethylmethylene-bridged derivative **70** via Brønsted-acid-catalyzed intramolecular cyclization employing tricarbinol **71** as a precursor.^{179,197} While the dimethylmethylene bridges ensue structural constraint to the *N*-heterotriangulene framework, **70** retains a certain extent of flexibility and the structure in the crystalline state determined by X-ray crystallography was a shallow bowl shape.¹⁹⁸ Furthermore, the sp^3 -hybridized methylene bridging units possess a tetrahedral geometry with the methyl groups pointing away from the *N*-heterotriangulene plane. This out-of-plane steric effect is enough to prevent the $\pi-\pi$ interaction especially in the solid state. Compound **70** therefore enjoys

Scheme 17. Strategies to Functionalize and Expand the Dimethylmethylenes-Bridged N-Heterotriangulenes Scaffold at the Periphery^a



^aUpon halogenation, various transition-metal-mediated cross-coupling reactions can be applied.

superb solubility in most common organic solvents, which is in marked contrast to insoluble carbonyl-bridged analog 53. Moreover, the cyclic voltammetric studies exposed that 70 undergoes a single reversible one-electron oxidation with $E^\circ_{\text{ox}} = 0.34$ V vs Fc/Fc⁺¹⁹⁹ which is more cathodically shifted by 0.1 V compared to the parent triphenylamine ($E^\circ_{\text{ox}} = 0.43$ V).²⁰⁰

In the dimethylmethylenes-bridged triarylamine, the central nitrogen atom should facilitate electrophilic aromatic substitutions on the para-positions of the phenyl groups. Nevertheless, it was not until 2009 when Samoc et al. described the first postmodification of dimethylmethylenes-bridged N-heterotriangulene 70 by bromination of the three para-positions using NBS in CHCl₃ to produce the corresponding tribrominated species 72.^{198,201} Lai, Liu et al. soon after showed that the same positions can be iodinated by reacting 70 with excess KI and KIO₃ in glacial acetic acid to furnish the triiodinated species 73.^{198,200}

Both trihalogenated compounds 72 and 73 are highly versatile precursors for transition-mediated cross-coupling reactions and thus numerous trigonally extended dimethylmethylenes-bridged N-heterotriangulene core have been synthesized. For example, Lai et al. prepared star-shaped acetylene-linked tetramer 74 by the Sonogashira coupling reaction of 72 with ethynyl N-heterotriangulene precursors.²⁰⁰ Such rigid dendrimer-like compound was designed to possess high fluorescence quantum yield and TPA cross-section, which are both consequential parameters for applications in, for example, two-photon fluorescence microscopic bioimaging.^{202,203} Indeed, 74 possessed an emission maximum at $\lambda_{\text{em}} = 438$ nm with an efficient quantum yield of $\Phi_F = 0.53$ in CHCl₃ as well as a large TPA cross section of $\delta = 4800$ GM. In turn, Liu et al. obtained the hexabrominated 75a and water-

soluble hexacationic 75b also by Sonogashira coupling reactions starting from triiodinated 73.¹⁹⁸ Similar to that of 74, both neutral 75a and cationic 75b emitted intense blue fluorescence and demonstrated large TPA cross sections (75a in toluene: $\lambda_{\text{em}} = 429$ nm, $\Phi_F = 0.89$, $\delta = 4340$ GM; 75b in MeOH: $\lambda_{\text{em}} = 433$ nm, $\Phi_F = 0.70$, $\delta = 4150$ GM). For compound 75b, the TPA measurement was also conducted in water but showed an acute suppression in δ value (148 GM), relative to that in MeOH. This decrease was ascribed to the aggregation of 75b in water.

Lai et al. in 2012 accomplished the synthesis of arylated tetramer 76 by Suzuki-Miyaura cross-coupling reaction from tribrominated 72 and vinylated tetramer 77 by Heck reaction from triiodinated 73.²⁰⁴ Both 76 and 77 have low first oxidation potentials of $E^\circ_{\text{ox}} = 0.06$ and 0.035 V (vs Fc/Fc⁺), respectively. In order to test the performance as hole-transporting materials in OLEDs, double-layer devices with the ITO/HTL/Alq₃/Al configuration were constructed with spin-coated tetramers 76 and 77 employed as HTLs. The devices employing 76 produced high brightness (1800 cd m⁻²) even with an operating voltage much less than 10 V, while those utilizing 77 had a significantly lower brightness at the same voltage. The difference in performance is likely ascribed to the more rigid structure of the direct-linked 76 over the vinyl-linked 77 (Scheme 17).

In 2012, Ko et al. synthesized a starburst organic semiconductor 78²⁰⁵ as a p-type hole-transfer material in solution-processed OFETs²⁰⁵ and CH₃NH₃PbI₃ (perovskite) solar cells.^{206–209} Compound 78 was obtained by Stille coupling reaction of tristanny N-heterotriangulene and three equiv of the appropriate bromide precursor with Pd(PPh₃)₄ as the catalyst. The flattened triarylamine core donor and the three π -conjugated motifs containing terthiophene and

benzothiadiazole play roles (1) to obtain increased lifetime of the charge-separated state, (2) to adjust the HOMO and LUMO energy levels and lower the energy gap, and (3) to induce charge-transfer transitions within the molecule. A perovskite solar-cell device based on **78** as a hole-transporting layer enjoyed high PCE of $\eta = 12.8\%$ under the illumination of 98.8 mW, which is much better than that without it. More importantly, in comparison with the well-established spiro-OMeTAD,²¹⁰ this new device can be utilized without any additives while exhibiting competitive photovoltaic performance. Out of all transition-metal-mediated coupling reactions listed above, Suzuki-Miyaura cross-coupling reaction has been the most frequently utilized approach owing to its versatility. For instance, such reaction was effectual to construct electron-rich *N*-heterotriangulenes as shown by the work of Ko et al., who synthesized **79a** and **79b** that implement electron-donating 4-methoxyphenyl groups attached through vinyl and aniline spacers, respectively, to the triarylamine core.^{211,212} Both compounds were found to be competent hole conductors in fabricating organic/inorganic hybrid solar cells. In particular, the perovskite-based solar cell using the latter compound **79b** yielded a high PCE of $\eta = 13.6\%$. In addition, the solar-cell device displayed ample stability and retained its photovoltaic performance even after continuous irradiation under AM 1.5 sunlight for 500 h. The derivative of **79b** with an unconstrained triarylamine core was less efficient and persistent, thus proving the significance of planarization. The same group continued to develop hole-transporting materials based on star-shaped *N*-heterotriangulene with that possessing bulkier bis(dimethylfluorenyl)amino moieties,²¹³ which are responsible to prevent aggregation and to facilitate the formation of durable amorphous glass to build resistance toward degradation.^{172,214} Compound **80** has an appropriate HOMO level (-5.21 eV) commensurable to that of spiro-OMeTAD (-5.22 eV) and matched well with that of $\text{CH}_3\text{NH}_3\text{PbI}_3$ perovskite (-5.43 eV). Indeed, perovskite solar cell using **80** achieved a PCE of $\eta = 14.2\%$ under one sun illumination which is comparable to the spiro-OMeTAD-based cell ($\eta = 14.7\%$).

Ko et al. also showed that *N*-heterotriangulenes decorated with thiophene derivatives can be used as organic sensitizers for solar-cell devices. As prototypical examples, organic dyes **81a** and **81b** containing planarized *N*-heterotriangulene unit as the electron donor and cyanoacrylic acid as the electron acceptor with thiophene-derived spacers were prepared via Suzuki-Miyaura cross-coupling reactions followed by Knoevenagel condensation.²¹⁵ Among the two solar cell devices implementing **81a** or **81b** as photosensitizers, the one with **81b** was more efficient, achieving a PCE of $\eta = 7.86\%$ under AM 1.5 sunlight. Moreover, exposure of the device containing **81b** under light for 1000 h at 60 °C only led to a marginal decrease of the efficiency to 7.45%, validating the high photostability of **81b**. In a follow up work, the performance of the solar cells was shown to improve upon incorporation of long alkyl chains, which helps spatial separation of the charges, to the backbone of the *N*-heterotriangulene core.²¹⁶ A solar cell device using nonyl-substituted **82** as a sensitizer instead exhibited PCE of over 8.71% (Figure 11). In a related study, Grätzel et al. in 2013, showed that expanding the π -conjugated framework with an ethenyl linkage between the *N*-heterotriangulene core and the terthiophene-derivative arm induce a bathochromic shift of the absorption maximum without suppressing the electron-donating ability²¹⁷ *N*-Heterotriangulene is an intrinsic

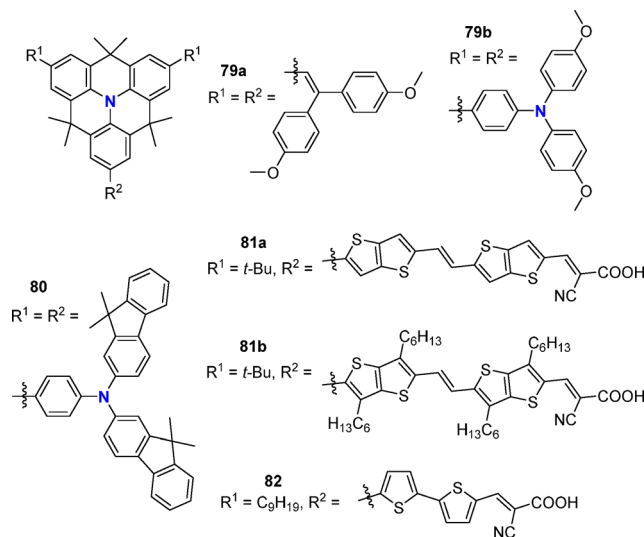


Figure 11. Examples of functionalized dimethylmethyleno-bridged *N*-heteratriangulenes synthesized through Suzuki-Miyaura cross-coupling reactions.

electron-donating building unit that upon coupling with a pertinent electron-accepting moiety forms an efficient donor–acceptor (D–A) type scaffold. Perry, Müllen et al. in 2012 prepared a series of D–A type compounds combining a *N*-heterotriangulene core and one to three lateral dimesitylboryl²¹⁸ moieties, and investigated their two-photon properties. Compounds 83a–c were obtained by treatment of mono-, di-, and tribrominated *N*-heterotriangulenes with an appropriate amount of *n*-BuLi and subsequently adding an excess of Mes₂BF (Figure 12). The work highlighted that increasing the number of diarylboryl groups from one to two or three results in an overall increase of the TPA cross sections.

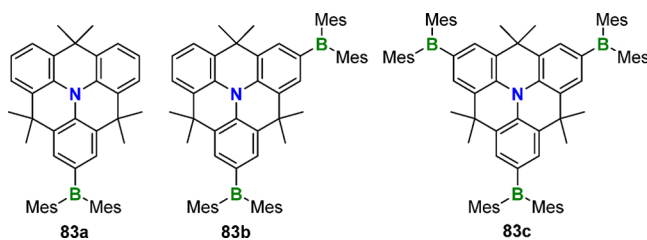


Figure 12. Structures of dimethylmethyleno-bridged *N*-heterotriangulenes **83a–c** featuring one, two, or three dimesitylboryl groups at the periphery.

In 2016, Guldⁱ et al. documented a series of *N*-heterotriangulenes bearing one, two, and three electron-withdrawing 4-pyridyl moieties, which were designed to serve as anchors to attach the *N*-heterotriangulene units onto the TiO₂ and ZnO surfaces and investigated their ability as dye-sensitizers.²¹⁹ The three compounds, mono-, di-, and tri(4-pyridyl)-substituted *N*-heterotriangulenes, 84a–c, were prepared by Pd-catalyzed Suzuki-Miyaura cross-coupling reactions with 4-pyridylboronic acid and *N*-heterotriangulene derivatives with appropriate number of bromo substituents (Figure 13). DFT calculations predicted that all three compounds consist of D–A type characteristics with the *N*-heterotriangulene core and peripheral 4-pyridyl groups contributing as electron donors and acceptors, respectively. Increasing the number of pyridyl groups stabilizes both the LUMO and the HOMO, the

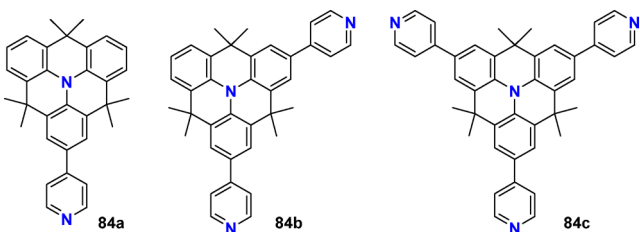
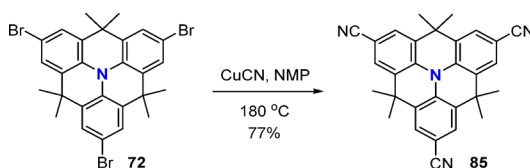


Figure 13. Structures of mono, di, and tri(4-pyridyl)-substituted dimethylmethylened-bridged *N*-heterotriangulenes **84**. The 4-pyridyl groups are necessary to stick the *N*-heterotriangulene units onto the TiO₂ and ZnO surface.

latter of which was perturbed to a lesser extent. Furthermore, both absorption and emission bands experienced pronounced solvatochromism and bathochromic shifts upon protonation, which make compounds **84** potential candidates as pH-responsive fluorescent sensors. Alluringly, TiO₂-based dye-sensitized solar cells employing dipyridyl-substituted **84b** performed the best compared to those of mono- and trisubstituted relatives ($\eta = 0.26\%$ for **84a**, 0.98% for **84b**, and 0.75% for **84c**). The difference in efficiency may be because monopyridyl species **84a** is not strong enough to remain attached to the electrode surface and tripyridyl species **84c** has the tendency to self-aggregate, thus dipyridyl species **84b** is the most balanced.

Owing to the unsymmetric charge distribution and the negatively polarized terminal nitrogen atom, cyano groups coordinate to metals in different forms including clusters²²⁰ and 2D surfaces.^{221,222} Based on this characteristic, Müller, Kivala, and Stöhr in 2016 synthesized cyano-substituted *N*-heterotriangulene **85** to study its self-assembly behavior on coinage metal surfaces.²²³ Compound **85** was obtained by the reaction of tribrominated precursor **72** with CuCN in anhydrous NMP.²²⁴ The type of intermolecular interactions and the bonding motifs of **85** depended on the type of coinage metal used to create the layers (Scheme 18). On Ag(111), only

Scheme 18. Synthesis of Tricyano-Substituted Dimethylmethylene-Bridged N-Heterotriangulene 85^a



^aThis compound was used to study its self-assembly behavior on the three coinage metal surfaces.

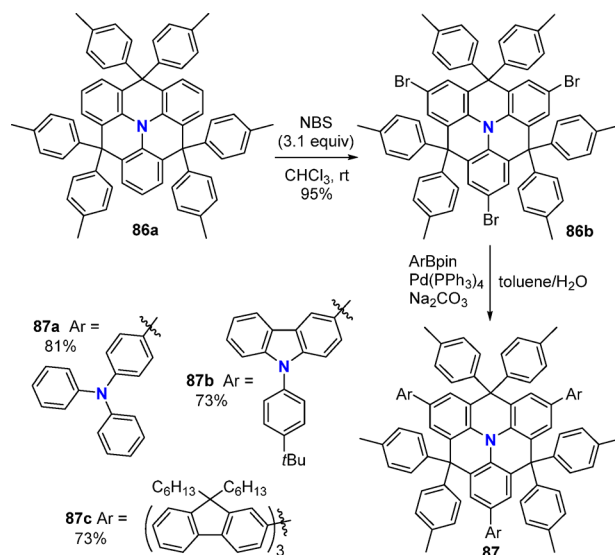
a single hexagonally closed-packed phase stabilized through hydrogen bonding existed, whereas on Au(111), two distinct, well-ordered phases stabilized by dipolar coupling, hydrogen bonding, and metal coordination were observed. The self-assembly patterns on Ag(111) and Au(111) were in stark contrast to that on Cu(111), where only small patches of molecules stabilized by metal coordination were obtained along with discorded molecules predominantly interacting with each other by dipolar coupling. The different motifs found on the coinage metal surfaces are due to the varying molecular mobility and the combination of intermolecular and intra-molecular molecule–substrate interactions.

3.1.4. Diarylmethylene-Bridged *N*-Heterotriangular-

3,4,4,5-Tetramethylmethylene-bridged N-heterotriangulenes. As described in the previous section, the electronic structures, thermal stabilities, diverse and facile functionalization, and good hole-transporting abilities of planarized dimethylmethylenes-bridged *N*-heterotriangulene derivatives are relevant to extensive applications toward organic-based materials and devices such as OLEDs as well as organic and organic/inorganic-hybrid solar cells. Despite the extraordinary peculiarities, however, the steric demand provided by the out-of-plane methyl groups may not be satisfactory to afford morphologically stable and uniform amorphous films.^{225,226} In this context, simply displacing the methyl groups with sterically bulkier aryl groups, for instance, may be an effective solution. It is noteworthy that sterically hindered structures of host materials are also advantageous to segregate the triplet emitters.²²⁷

The earliest example of a diarylmethylene-bridged *N*-heterotriangulene was reported by Ma et al. in 2009 (Scheme 19).²²⁸ Compound 86a, which possesses 4-tolyl groups

Scheme 19. Synthesis of Trigonally Extended Derivatives of Di(4-tolyl)methylene-Bridged triphenylamine 87



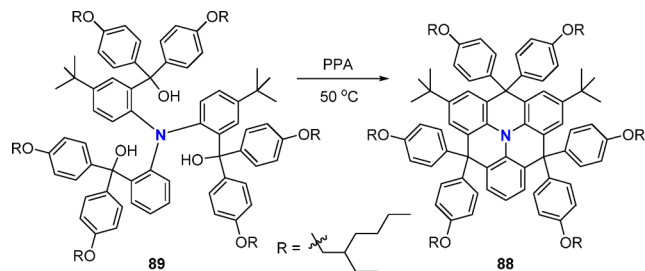
attached to the methylene bridges, was synthesized relying on the same approach as the dimethylmethylene-bridged analog **70**. X-ray crystallographic analysis determined that the geometry of the *N*-heterotriangulene core of **86a** is shallow bowl shape, analogous to that of **70**. The potential of the first oxidation process was $E^\circ_{\text{ox}} = 0.42$ V (vs Fc/Fc⁺) which is fairly close to those of the parent triphenylamine ($E^\circ_{\text{ox}} = 0.43$ V) and dimethylmethylene-bridged analog **70** ($E^\circ_{\text{ox}} = 0.34$ V). This observation indicates that the low hole-injection retained regardless of structural planarity and steric effect of the substituents on the bridges. Moreover, the high triplet energy of **86a** was also conserved (ca. 2.78 eV). OLEDs with **86a** as a host material and Ir(ppy)₃ as the triplet emitter exhibited maximum current efficiency of 83.5 cd/A (an equivalent to EQE of 23.4%) and maximum power efficiency of 71.4 lm/W for green electrophosphorescence, which are considerably higher than conventional CBP- or TAZ-hosted devices.^{229,230}

The π -conjugated framework of the 4-tolyl-bridged derivative **86a** can be extended in the three lateral directions similar to that of dimethylmethylenediphenyl-analog **70**. For example,

86a was first triply brominated by treatment with NBS in CHCl_3 to afford **86b**, and subsequent Suzuki-Miyaura cross-coupling reactions with appropriate arylboronic acid pinacol esters furnished trigonally extended derivatives **87a**, **87b**,²³¹ and **87c**²³² which are decorated with triphenylamine, carbazole, and oligofluorene moieties, respectively (**Scheme 19**). The potentials of the first oxidation processes of these derivatives were all within the range of 0.29–0.40 V (vs Fc/Fc^+), indicating that efficient hole injections are conserved regardless of the modification. One conspicuous advantage of compounds **87a–c** that is worth highlighting is the facile solution processabilities. Fine thin films of these compounds were all easily prepared by spin-coating followed by annealing under an N_2 atmosphere. In turn, compounds **87a** and **87b** were utilized as hole-transporting materials in three-layer Alq_3 emitting OLEDs, while the most elongated starburst oligofluorene **87c** was applied as an emitter in deep-blue double-layered OLEDs.

Surface wettability of the hole-transporting layer is known to significantly affect the device performance.^{233,234} To create a water-free surface, Jin et al. in 2018 designed and synthesized *N*-heterotriangulene derivative **88** possessing hydrophobic aryloxy groups at the bridging positions (**Scheme 20**).²³⁵

Scheme 20. Synthesis of Triphenylamine-Based Hole-Transporting Materials **88 from Triol Precursor **89**^a**

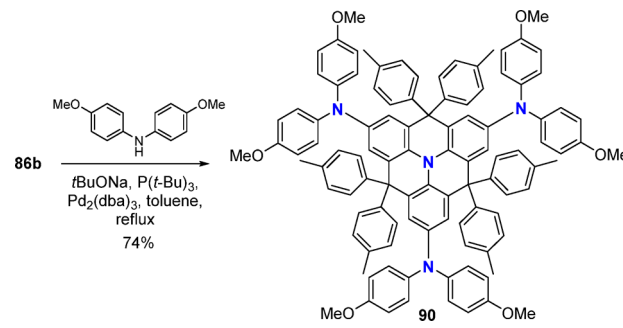


^aThe substitution with hydrophobic alkyl tails helps to produce a water-free surface.

The aryloxy groups with a long alkyl chain, namely, 4-(2-ethylhexyloxy)phenyl groups, help repel water contents on the perovskite surface and modulate the surface energy of the hole-transporting material. This compound was synthesized by treating the triol precursor **89** with PPA. Compound **88** was evaluated as a dopant-free hole-transporting material for bulk heterojunction inverted organic solar cells and gave rise to a PCE of 7.04%.

In 2017, Zhang et al. synthesized compound **90** which tethers electron-donating bis(4-methoxyphenyl)amine groups at the periphery through Buchwald-Hartwig amination starting from tribrominated **86b** (**Scheme 21**).²³⁶ Owing to the effective conjugation among the *N*-heterotriangulene core and the pendent amino-donor groups, compound **90** has an excellent balance of hole mobility and energy levels sufficient for its use as hole-transporting materials in perovskite solar cells. In fact, **90** has a higher T_g value and a better hole mobility as well as a bathochromic-shifted emission band in CH_2Cl_2 compared to those of spiro-OMeTAD (**90**: $T_g = 169^\circ\text{C}$, $\mu_h = 1.4 \times 10^{-4} \text{ cm}^2 \text{ V}^{-1} \text{ s}^{-1}$, $\lambda_{\text{em}} = 452 \text{ nm}$; spiro-OMeTAD: $T_g = 122^\circ\text{C}$, $\mu_h = 9.1 \times 10^{-5} \text{ cm}^2 \text{ V}^{-1} \text{ s}^{-1}$, $\lambda_{\text{em}} = 409 \text{ nm}$). Moreover, the first oxidation potential was $E^\circ_{\text{ox}} = 0.68 \text{ V}$ against Ag/Ag^+ couple (0.1 M TBAPF₆ in DMF) which is slightly elevated from the parent di(4-tolyl)methylene-

Scheme 21. Synthesis of Di(4-tolyl)methylene-Bridged *N*-Heterotriangulene **90 Conjugated with Three Bis(4-methoxyphenyl)amine Groups via Buchwald-Hartwig Amination**



bridged congener **86** ($E^\circ_{\text{ox}} = 0.42 \text{ V}$). The perovskite solar cell applied with compound **90** exhibited a PCE of 16.4%, which outperformed the device constructed with spiro-OMeTAD under the same conditions (PCE = 14.8%).

3.1.5. *N*-Heterotriangulene-Based Oligomers, 2D Network Structures, and Polymers. The 3-fold-symmetrical and flattened architecture makes *N*-heterotriangulene derivatives as versatile building blocks toward precise synthesis of π -expanded and covalently bonded macrosystems using a bottom-up approach. In 2011, Fasel et al. obtained 2D covalent networks of *N*-heterotriangulene units on a $\text{Ag}(111)$ surface using tribrominated **72** as the key precursor.²³⁷ Depending on the fabrication temperatures, different composition of *N*-heterotriangulene-based 2D networks were obtained. For instance, when the annealing temperature was set at 300°C , a one-molecule thin film of dimethylmethylenedibridged *N*-heterotriangulene covalently linked at the periphery was formed.

Elevation of the temperature to 400°C triggered demethylation without destructing the 2D architecture to afford **91** (**Figure 14**). STM topography showed that the resulting sheet consists of an ultraflat covalent framework with regular size and shaped pores. Kan et al. estimated using computational methods that the porous sheet **91** has a ferromagnetic half-metal characteristic with a bandgap of approximately 1 eV, which is a feature suitable for spin-selective conductors.²³⁸

In the following year, Fasel et al. carried out comparative analysis of solution-based and surface-mediated one-pot synthesis of *N*-heterotriangulene macrocycles starting from the same building unit, dibrominated *N*-heterotriangulene **92**.¹⁹⁹ In solution, Yamamoto homocoupling of **92** in DMF at 85°C furnished complex mixtures of acyclic oligomers with different lengths along with a small amount of the hexameric macrocycle **93a** (**Figure 15**). In stark contrast, sublimation followed by thermal annealing of **92** on a $\text{Au}(111)$ surface preferentially furnished *N*-heterotriangulene macrocycles over zigzag conformational oligomers **94** (**Figure 15**). Alternatively, macrocycle **93a** can be selectively isolated in a few hundred milligram scale by stepwise protocol in solution. The expansion of the macrocyclic core toward branched architectures was achieved by first brominating the six peripheral positions of heterotriangulene boronic acid pinacol ester derivatives. Expanded macrocycles **93b** and **93c** were isolated in 26% and 12% yields, respectively, relative to the amount of **92** used. Solutions of *N*-heterocycle macrocycles all displayed deep-blue

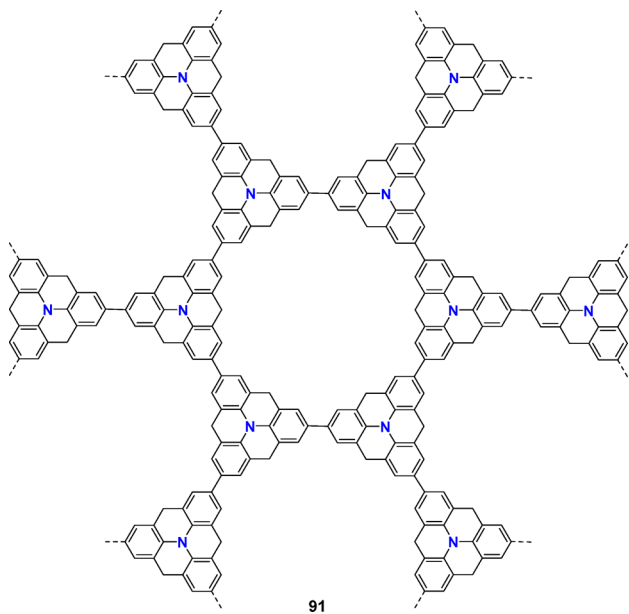
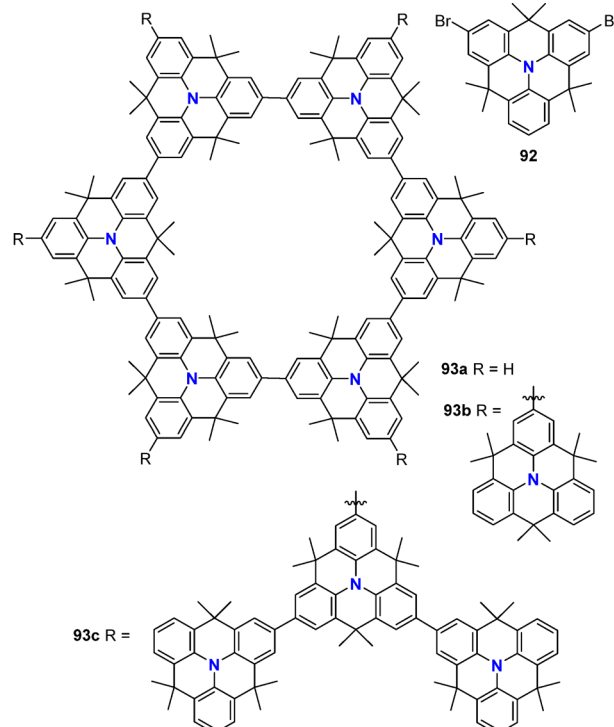


Figure 14. Ultraflat and porous 2D covalent network **91** composed of repetitive units of methylene-bridged *N*-heterotriangulenes. The dotted lines represent C–C bonds connecting neighboring units.



fluorescence together with significant improvement of quantum yields (**93a**: $\lambda_{\text{em}} = 430$ nm and $\Phi_F = 0.89$; **93b**: $\lambda_{\text{em}} = 436$ nm and $\Phi_F = 0.79$; **93c**: $\lambda_{\text{em}} = 436$ nm and $\Phi_F = 0.53$) compared to that of the parent *N*-heterotriangulene **70** ($\lambda_{\text{em}} = 416$ nm and $\Phi_F = 0.02$), which was partly attributed to the expansion of the π -framework. DFT calculations confirmed that the HOMO and LUMO of **93** were delocalized over the entire molecular skeleton, verifying effective conjugation between all *N*-heterotriangulene units.

Polymer of *N*-heterotriangulene sequence, **95** (Figure 15), was introduced by List et al. in 2013 as an amorphous organic p-type semiconductor.²³⁹ Synthesis of polymer **95** was accomplished by Ni(0)-mediated Yamamoto homocoupling of dibrominated **92** in a 2:1 toluene:DMF mixture in the dark. The polymer **95** was employed as hole-transporting materials in bottom-gate/bottom contact OFETs, which showed a saturation mobility of 4.2×10^{-5} cm² V⁻¹ s⁻¹ and an on/off current ratio of 10^5 .

In 2017, Maier et al. accomplished the on-surface synthesis of defect-free macrocycles, 1D polymer chains, and 2D covalent networks with carbonyl-functionalized pores on Au(111) using halogenated carbonyl-bridged *N*-heterotriangulene derivatives **96a** or **96b** as key precursors (Scheme 22).²⁴⁰ The growth mechanism of 2D polymer **97** on a metal surface was investigated by STM in combination with DFT calculations. In short, the 2-fold symmetric halogenated *N*-heterotriangulene precursors were first converted to hexameric macrocycle **98** and 1D polymer chain **99** by annealing on a Au(111) surface at temperatures ranging from 420 to 540 K, which were subsequently interlinked by Ullmann coupling reactions, which produced structurally well-defined 2D polymer **97**. The electronic bandgap became narrower with increased dimensionality going from the monomer to the planar 1D chain and the 2D network comprised of the same building block. This shows interplay between dimensionality and decreased bandgap upon effective conjugation in organic polymeric systems applied in a bottom-up approach.

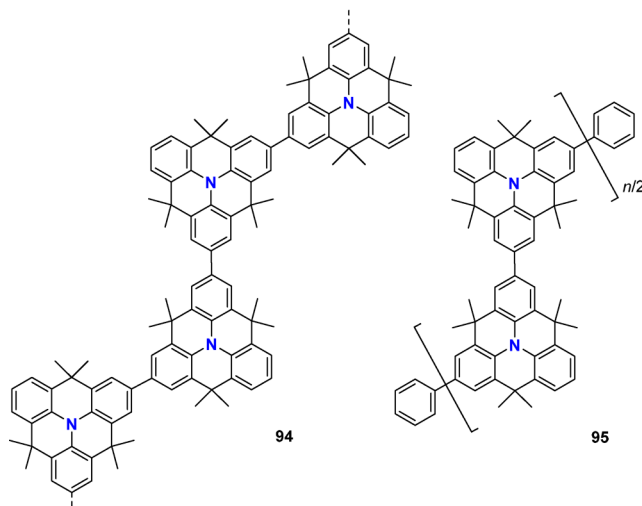


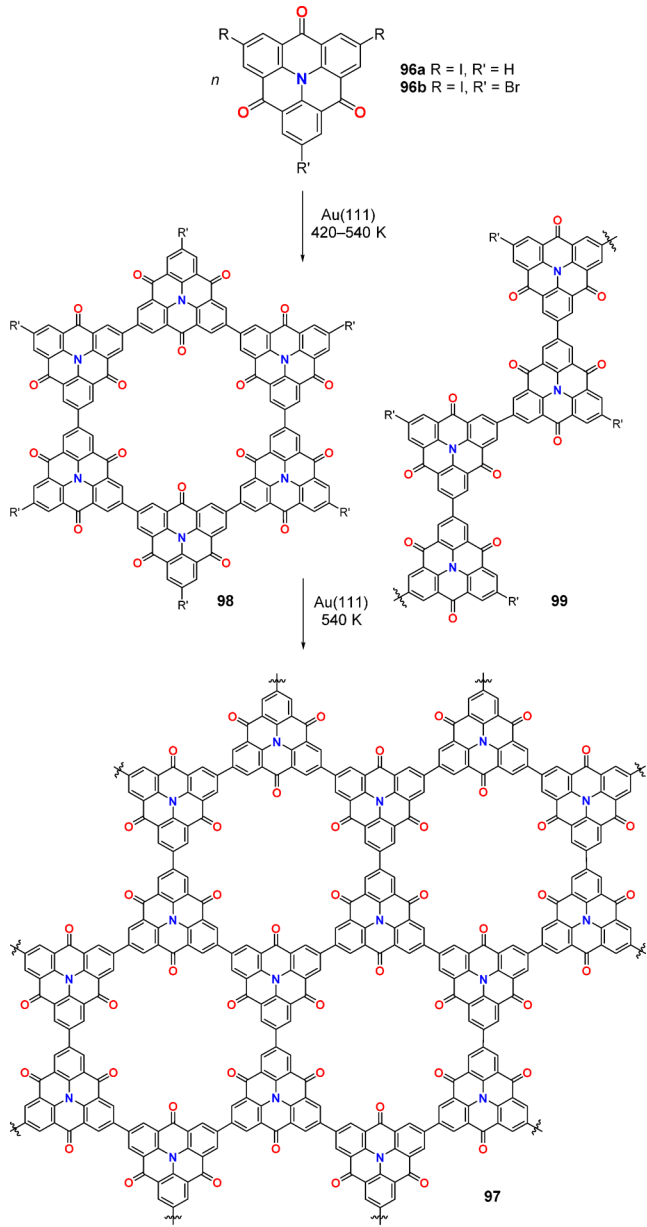
Figure 15. Structures of hexameric macrocycle **93a** and its derivatives **93b** and **93c**, zigzag conformational oligomer **94**, and 1D polymer **95** capped with phenyl rings.

3.2. Partially Bridged Triarylamines

Unlike the fully planarized *N*-heterotriangulenes, partially bridged triarylamines have helical or pseudo planar conformations due to the steric repulsion of the hydrogen atoms at the β -positions of the nitrogen center. The geometric intermediacy of the partially bridged triarylamines between conventional propeller-like triarylamines and planarized triarylamines gives rise to intriguing photophysical and electronic properties as well as distinct intermolecular interaction which in some occasions are more attractive than the fully planarized π -systems.

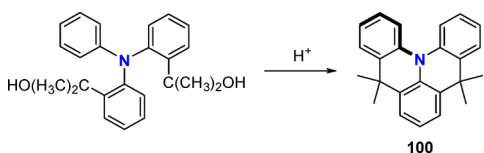
3.2.1. Partially Dimethylmethylen-Bridged Triarylamines. Compared to *N*-heterotriangulene, examples of 2-fold dimethylmethylen-bridged triphenylamine derivatives are

Scheme 22. On-Surface Synthesis of Nitrogen-Doped Macrocycles 98, 1D Chains 99, and 2D Polymers 97 with Carbonyl-Functionalized Pores



rather scarce. The first doubly dimethylmethylened-bridged triphenylamine **100** was prepared by Hellwinkel and Schmidt in 1980 through the essentially same approach as the 3-fold bridged analog **70**, i.e., proton-catalyzed intramolecular Friedel–Crafts cyclization reactions (Scheme 23).¹⁷⁹ While the crystal structure of **100** has yet to appear in the literature,

Scheme 23. Synthesis of Doubly Dimethylmethylened-Bridged Triphenylamine **100** by Proton-Catalyzed Intramolecular Friedel–Crafts Cyclization



¹H NMR studies suggested that the structure is slightly distorted with a racemization barrier of 24 kcal mol⁻¹. Direct functionalization of **100** at one, two, or three of the para-positions by bromination, amination, and nitration have been achieved thus far.¹⁷⁹

3.2.2. Partially Diarylmethylene-Bridged Triarylamines. Analogous to those of *N*-heterotriangulenes, partially bridged triarylamines bearing sterically bulky diarylmethylene bridges have also been investigated. One of the earliest examples of such compounds was reported by Yang et al. in 2009. Di(4-tolyl)methylene-bridged triarylamine–triphenylsilane hybrid compound **101** (Figure 16A) was synthesized and

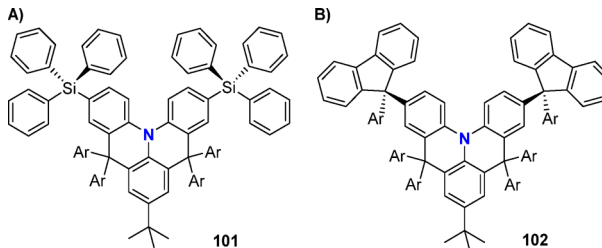


Figure 16. (A) Structures of diarylmethylene-bridged triphenylamine–triphenylsilane hybrid **101** and (B) triphenylamine–fluorene hybrid **102**. Ar = 4-tolyl.

applied as host materials to PHOLEDs.²⁴¹ The triphenylsilyl groups were introduced to the partially bridged triarylamine scaffold by bromination, Li–Br exchange, followed by treatment with Ph₃SiCl. Compound **101** has two major features to achieve a large HOMO–LUMO energy gap and molecular size: (1) introduction of triphenylsilyl groups to block the para-positions relative to the central nitrogen atom, which are the electrochemically active sites and (2) incorporation of bulky di(4-tolyl)methylene bridges together with triphenylsilyl groups to effectively segregate the triplet guest molecules and prohibit aggregation. X-ray crystallography revealed that **101** has a 3D scissor-like structure, which should be beneficial to achieving the latter issue described above. Furthermore, TGA demonstrated that **101** is thermally stable with a high *T_d* value of 491 °C. A PHOLED device employing **101** as a host material achieved the maximum external quantum efficiency of 15.4% for blue and 19.7% for green electrophosphorescence. The same group also synthesized a similar compound **102** (Figure 16B), but this time with terminal 9-aryl-9H-fluorene derivatives.²⁴² This compound enjoyed remarkable thermal, morphological, and electrochemical stabilities. The performance of the PHOLED devices employing **102** had the maximum quantum efficiencies of blue and green electrophosphorescence of 9.4% and 19.5%, respectively.

3.2.3. Partially Carbonyl-Bridged Triarylamines. The first 2-fold carbonyl-bridged triphenylamine **103** was documented in the same literature as the *N*-heterotriangulene analog **53** by Hellwinkel and Melan in 1971.¹⁸⁰ Field and Venkataraman reinvestigated this chemistry in 2002 and obtained the X-ray crystal structure of **103**, which revealed the C₂-symmetric geometry with a helical distortion (Figure 17).¹⁸¹ In a continuing work, a series of related derivatives, **104a–c**, were synthesized via intramolecular Friedel–Crafts acylation, similar to that of the *N*-heterotriangulene analog **53**.²⁴³ These compounds all consist of helically chiral, twisted conformations in the crystalline state. Their racemization

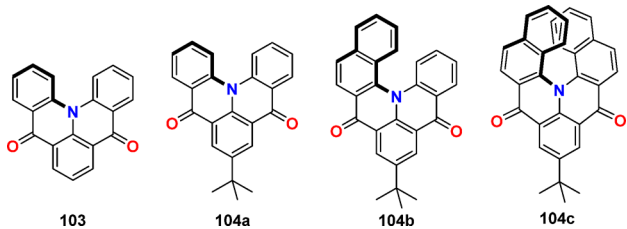


Figure 17. Structures of 2-fold carbonyl-bridged triarylamines **103** and **104a–c**. Only one of the two enantiomers is depicted for each compound.

energy barriers were not determined, however, and the behavior in solution is not clearly described. In CHCl_3 , the emission maxima of **104a–c** were observed at 460, 468, and 486 nm, respectively.

In 2003, Venkataraman et al. synthesized compounds **105a** and **105b** (Figure 18), and discovered that these two were able

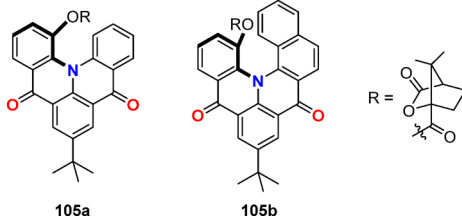


Figure 18. Structures of triaryamine-based helicenes **105** capable of emitting CPL. Only one of the two enantiomers is depicted for each compound.

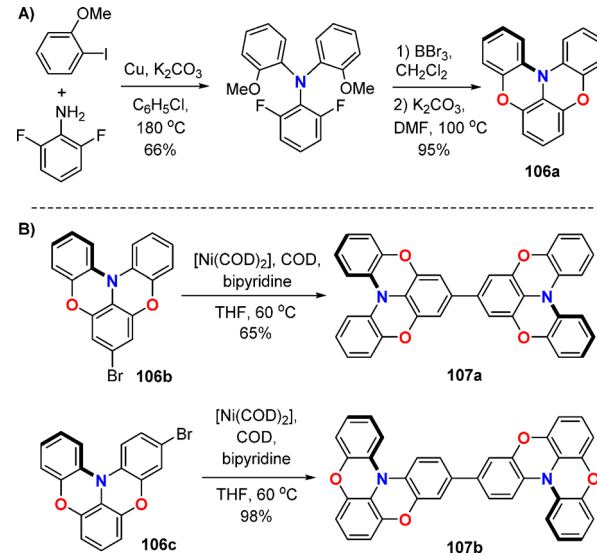
to emit CPL with differing signs.²⁴⁴ The pendent bulky camphanate substituents play a pivotal role to stabilize the absolute configuration. The emission spectra of the enantiomers *P*-**105a** and *M*-**105a** were virtually identical with the maximum at 453 nm. The same applied for enantiomers *P*-**105b** and *M*-**105b**, which displayed an emission maximum at 478 nm. Based on the fluorescence spectra, the g_{em} values, which defines the degree of the CPL, were +0.0009 and -0.0011 at 453 nm for *P*- and *M*-**105a** and +0.0008 and -0.0007 at 478 nm for *P*- and *M*-**105b**, respectively. It should be noted that Barnes et al. in 2006 directly observed FDOD from a single molecule of **105b**, which the technique was only applicable for bulk samples.²⁴⁵ This technique later became available in polymer-supported thin films²⁴⁶ as well as dimeric systems.²⁴⁷

3.2.4. Partially Oxygen-Bridged Triarylamines. Okada et al. established the synthetic method to prepare doubly oxygen-bridged triphenylamine **106**, which involves (1) aromatic nucleophilic substitution reaction of 2,6-dichloronitrobenzene with two equivalents of *ortho*-bromophenol, (2) reduction of the nitro group into an amino group, followed by (3) ring closure by 2-fold intramolecular amination.²⁴⁸ X-ray diffraction analysis unveiled that this compound adopts a C_2 -like quasi-planar structure, which can be described as an intermediate between planarized and propeller-shaped triarylamines. Although the structure was marginally twisted, **106** forms a densely packed π -stacks in the crystalline state.

An alternative strategy to prepare doubly oxygen-bridged triarylamine derivatives was reported by Wakamiya et al. in 2014, which utilizes a 2-fold intramolecular nucleophilic aromatic substitution for the final cyclization step.²⁴⁹ Compound **106a** was obtained by (1) Ullmann reactions of

ortho-iodoanisole and 2,6-difluoroaniline, (2) deprotection of the methoxy groups by BBr_3 , and finally (3) treatment with K_2CO_3 in DMF (Scheme 24A). The overall yield of this route

Scheme 24. (A) Synthesis of Doubly Oxygen-Bridged Triphenylamine **106** and (B) Structural Isomers of Its Dimers **107a** and **107b** via Ni(0)-Mediated Yamamoto Coupling Reactions Starting from Brominated Precursors **106b** and **106c**



was 63% which is approximately a three-time improvement from the original method reported by Okada group. The monobrominated derivatives **106b** and **106c** were prepared by the same route but by starting with appropriate brominated precursors prior to cyclization instead.

The authors continued to synthesize a series of dimers **107a** and **107b** through Ni(0)-mediated Yamamoto coupling reactions of brominated precursors **106b** and **106c** and examined their efficiencies as hole-transporting or hole-injection layers in OLEDs (Scheme 24B). Structurally isomeric dimers **107a** and **107b** formed needle-like single crystals upon recrystallization from toluene. X-ray crystallographic analysis revealed that both compounds have quasi-planar structures and composes on-top π -stacks with intermolecular distances of 3.79 and 3.75 Å, respectively. Together with the delocalized HOMOs, these structural arrangements led to high and anisotropic carrier mobilities in the direction of the π -stacks. Notably, a significant anisotropy of the carrier mobility was also observed in vacuum-deposited films of both **107a** and **107b**, and the mobility in the perpendicular direction to the substrate (**107a**: $\Sigma \mu_{\text{per}} = 0.98 \text{ cm}^2 \text{ V}^{-1} \text{ s}^{-1}$; **107b**: $\Sigma \mu_{\text{per}} = 0.57 \text{ cm}^2 \text{ V}^{-1} \text{ s}^{-1}$) was about three times larger than that in the parallel direction (**107a**: $\Sigma \mu_{\text{par}} = 0.38 \text{ cm}^2 \text{ V}^{-1} \text{ s}^{-1}$; **107b**: $\Sigma \mu_{\text{par}} = 0.19 \text{ cm}^2 \text{ V}^{-1} \text{ s}^{-1}$). In fact, X-ray diffraction studies of the films verified that the two dimers seem to maintain the face-on π -stacks even in amorphous films, thereby facilitating out-of-plane charge transport.

The charge carrier transporting properties in vapor-deposited films of **107a** and **107b** were evaluated using TOF measurements. Their hole mobilities were strongly correlated with the applied electric field.²⁵⁰ At high electric fields ($E^{1/2} > 600 \text{ V}^{1/2} \text{ cm}^{-1/2}$) suitable for OLED devices, the hole mobilities of **107a** and **107b** were $\mu_h = 8.1 \times 10^{-4} \text{ cm}^2 \text{ V}^{-1}$

s^{-1} and $1.7 \times 10^{-5} \text{ cm}^2 \text{ V}^{-1} \text{ s}^{-1}$, respectively.²²⁹ While OLEDs utilizing **107a** as a hole transporting layer was rather defective only exhibiting EQE of 0.32%, OLEDs using **107a** or **107b** as hole injection layers in combination with α -NPD performed much improved EQEs of 1.23% and 1.11%, respectively, under the same conditions.

A two-dimensionally expanded π -system composed of azulene core with four doubly oxygen-bridged triarylamine moieties **108** (Figure 19) was synthesized by Wakamiya et al.

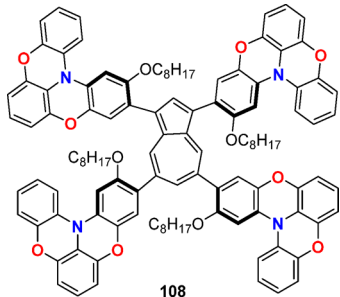


Figure 19. Two-dimensionally π -expanded compound **108** that possesses four dioxy-bridged triarylamine moieties directly connected to an azulene core.

in 2015.²⁵¹ Azulene, which is a nonbenzenoid aromatic hydrocarbon, can be regarded as a fused product of a 6π -electron cyclopentadienyl anion and a 6π -electron tropylum cation which therefore has an unusual electron-donating and -accepting character. Compound **108** was synthesized by Suzuki-Miyaura cross-coupling reactions of 1,3,5,7-tetra(Bpin)-azulene with monobrominated oxygen-bridged triarylamine. DFT calculations showed that the HOMO is delocalized over the entire molecule (-4.23 eV) and the LUMO is predominantly localized on the azulene core. Moreover, cyclic voltammetric investigation showed that **108** undergoes four reversible oxidation events with a first oxidation potential of $E^\circ_{\text{ox}} = 0.00 \text{ V}$ vs Fc/Fc^+ , which corresponds to a HOMO energy level of -5.04 eV . DFT calculations together with the electrochemical analysis suggested the high electron-donating ability of the cyclopentadienyl ring of the azulene core. Compound **108** was exploited as a hole-transport layer in perovskite solar cells, which exhibited superior performance especially when the layer was prepared using a one-step solution method (toluene dropping)²⁵² and Co(III)-based oxidizing agent, FK209,²⁵³ was employed as an additive (EQE = 16.5%).

In a continuing work, Wakamiya, Murata et al. synthesized derivatives of *meta*-phenylene-linked doubly oxygen-bridged triphenylamine, **109a** and **109b**, as transparent hole transporting materials (Figure 20A).²⁵⁴ The two compounds have comparable electronic structures and properties to each other based on DFT calculations and electrochemical analysis (**109a**: $E_{\text{HOMO}} = -4.73 \text{ eV}$, $E_{\text{LUMO}} = -1.04 \text{ eV}$, $E^\circ_{\text{ox}} = +0.31 \text{ V}$ vs Fc/Fc^+ ; **109b**: $E_{\text{HOMO}} = -4.73 \text{ eV}$, $E_{\text{LUMO}} = -1.03 \text{ eV}$, $E^\circ_{\text{ox}} = +0.31 \text{ V}$ vs Fc/Fc^+). Notably, the central benzene ring does not strongly contribute to the HOMOs of both **109a** and **109b**, indicating the ineffective π -conjugation among the triarylamine skeletons. Vacuum deposited films of **109a** and **109b** displayed hole mobilities of $\mu_h = 2.2 \times 10^{-4}$ and $1.6 \times 10^{-5} \text{ cm}^2 \text{ V}^{-1} \text{ s}^{-1}$, respectively. Furthermore, the absorption bands of **109a** and **109b** in the UV-vis spectra recorded both in CH_2Cl_2 and in film were mostly occupying the regions outside of visible light,

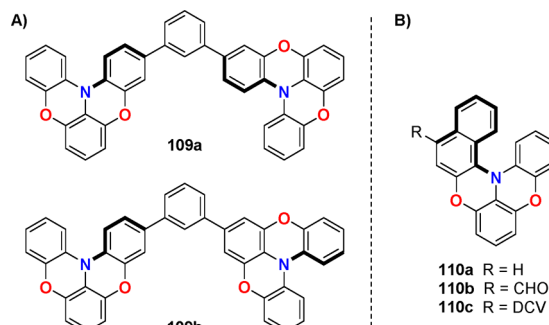


Figure 20. (A) *Meta*-phenylene-linked dioxy-bridged triphenylamine dimers **109a** and **109b** as transparent organic hole-transporting materials. (B) Dioxy-bridged diphenylnaphthylamine derivatives **110a–c** as CPL materials (DCV = 2,2-dicyanovinyl).

suggesting that these compounds are viable candidates for transparent materials which are significant for OLEDs and OFETs to inhibit the decrease of light-extraction efficiency. Most importantly, both compounds exhibited ample amorphous stability and no signs of crystallization was observed even upon annealing at 160°C .

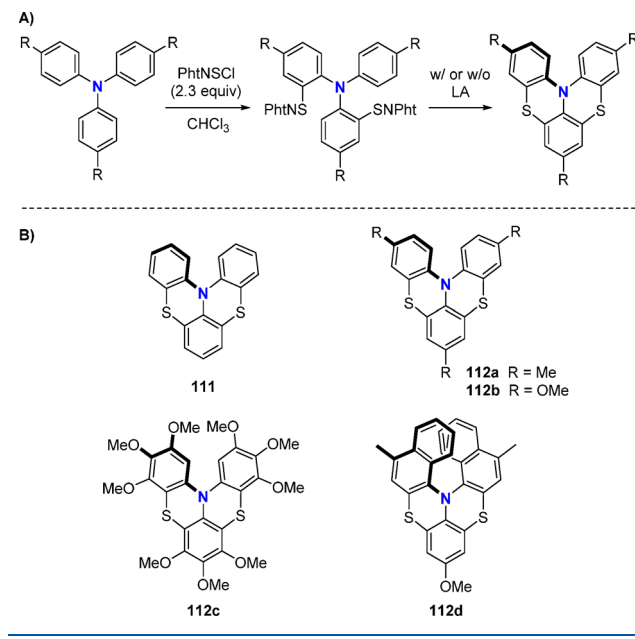
In 2017, Wakamiya et al. developed 2-fold oxygen-bridged diphenylnaphthylamine **110a** and its formyl- and 2,2-dicyanovinyl-substituted derivatives, **110b** and **110c**, respectively, toward CPL materials (Figure 20B).²⁵⁵ The synthesis of **110a** followed a similar procedure to the triphenylamine analog **106**. By simply replacing one of the ancillary phenyl rings of **106** with a more sterically demanding naphthyl group enhances the inversion energy estimated by DFT calculations from 9.1 to 29.3 kcal mol⁻¹. Therefore, **110a** was isolated as a racemic mixture at ambient temperature. The treatment of **110a** with POCl_3 in DMF led to monoformyl derivative **110b**, which was subsequently converted to mono-2,2-dicyanovinyl derivative **110c** by treatment with malononitrile and TEA. As both formyl and 2,2-dicyanovinyl groups are strong electron-withdrawing groups, compounds **110b** and **110c** possess ICT characters in the excited state. The photophysical properties of all three compounds were evaluated in solution with different polarity. While **110a** only showed slight polarity-dependent fluorescence with blue to blue-greenish emission ($\lambda_{\text{em}} = 459$ –500 nm; $\Phi_F = 0.68$ –0.81), both **110b** and **110c** experienced pronounced solvent-dependent fluorescence with quantum yields gradually decreasing upon elevated polarity (**110b**: $\lambda_{\text{em}} = 520$ –603 nm, $\Phi_F = 0.96$ –0.11; **110c**: $\lambda_{\text{em}} = 608$ –706 nm; $\Phi_F = 0.63$ –0.02 ongoing from cyclohexane to MeCN). Moreover, enantiomers of compounds **110a–c** all showed CPL signals with sufficient g_{em} values around 10^{-3} . The CPL properties were also retained in the crystalline state.

3.2.5. Partially Sulfur-Bridged Triarylamines. Although the sulfur-bridged triphenylamine was briefly mentioned in 1944,²⁵⁶ its synthesis was not accomplished until 2014 when Okada et al. obtained compound **111** using a similar procedure to prepare the oxygen-bridged analog **106**.²⁴⁸ Because of the longer C–S bonds compared to C–N bonds, the constrained triarylamine moiety is slightly more twisted in **111** than that of **106**. Furthermore, unlike **106** that undergoes a reversible oxidation event, the cyclic voltammetric investigation of **111** showed irreversible oxidation peak with $E_{\text{ox}} = +1.14 \text{ V}$, indicating instability of the corresponding radical cation under the measurement conditions. Decomposition of the radical cation likely occurred at the para-positions relative to the

nitrogen atom which are the electrophilic reactive sites. The details on the radical cations will be discussed in the next section.

A practical approach to synthesize the sulfur-bridged triarylamine hetero[4]- and [6]-helicenes was developed by Menichetti et al. in 2008 (Scheme 25A).²⁵⁷ Depending on the

Scheme 25. (A) Synthesis of Dithia-Bridged Triarylamines and (B) Structures of Dithia-Bridged Triarylamines 111 and 112a–d



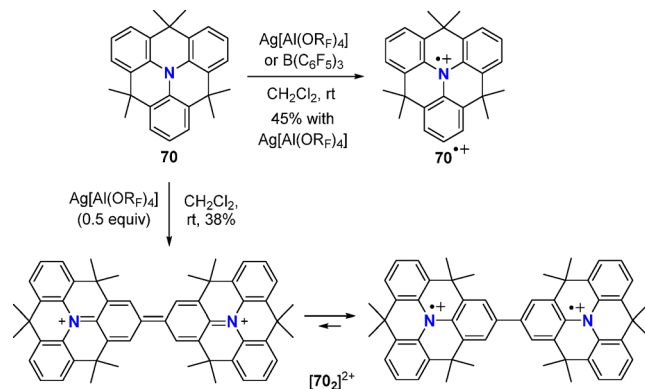
aryl groups of the amines, a series of [4]- and [6]-heterohelicenes such as 112a–d were obtained by treatment of PhNSCl with or without a Lewis acid (Scheme 25B). During the synthesis of 112c, the four tandem electrophilic aromatic substitution reactions were facilitated by the electron-donating trimethoxy-substituted phenyl groups. Since the racemization barriers for all compounds were sufficiently high, the enantiomers were separated by HPLC using a chiral phase column. DFT calculations indicated that the hyperpolarizability of the sulfur-bridged triarylamine helicenes increases with extension of π -conjugation and incorporation of electron-donating groups.²⁵⁸

3.3. Triarylamine Radical Cations and Bis(triarylamine) Dications Stabilized by Structural Constraint

As highlighted in the previous two sections, fully and partially planarized triarylamine derivatives have a broad scope of applications including OLEDs, OFETs, and solar cells. Meanwhile, their oxidized counterparts, especially radical cations as well as dications, are attractive on their own because of their unique electronic and magnetic properties.²⁵⁹ While numerous examples of such compounds have been reported thus far, only a handful are stable without substituents on the para-positions where spin densities are largely accumulated.^{260–263} In this section, examples of triarylamine radical cations and their derivatives “stabilized by structural constraint” will be listed. The idea is that the structural constraint in a planar fashion enhances the efficiency of π -conjugation and spin delocalization, thus burkes the reactivity at the para-positions.

3.3.1. Radicals of Dimethylmethylen-Bridged Triarylamine Derivatives. Bamberger et al. successfully prepared a triarylamine radical cation without para-substituents in 1975.²⁶⁴ They obtained such species by treating the parent dimethylmethylen-bridged N-heterotriangulene 70 with concentrated sulfuric acid or trifluoroacetic acid; however, its existence was only identified in situ and its crystal structure was not determined. It was not until a few decades later when Wang et al. in 2013 revisited this chemistry by using $B(C_6F_5)_3$ and silver salts as oxidants.²⁶⁵ The reactions of 70 with equimolar of $B(C_6F_5)_3$ or $Ag[Al(OR_F)_4]$ ($OR_F = OC(CF_3)_3$)²⁶⁶ resulted in deep blue solutions of the corresponding ionic pairs of radical cation $70^{\bullet+}$, which the formation was confirmed by EPR spectroscopy (Scheme 26). The absorption

Scheme 26. Oxidation of Dimethylmethylen-Bridged N-Heterotriangulene 70 with 1 equiv of $Ag[Al(OR_F)_4]$ or $B(C_6F_5)_3$ and 0.5 equiv of $Ag[Al(OR_F)_4]$ ($OR_F = OC(CF_3)_3$)^a



^aThe bottom illustration shows the resonance structures of the dication $[70_2]^{2+}$ which was revealed to have a singlet diradical character (stronger contribution from the structure on the righthand side).

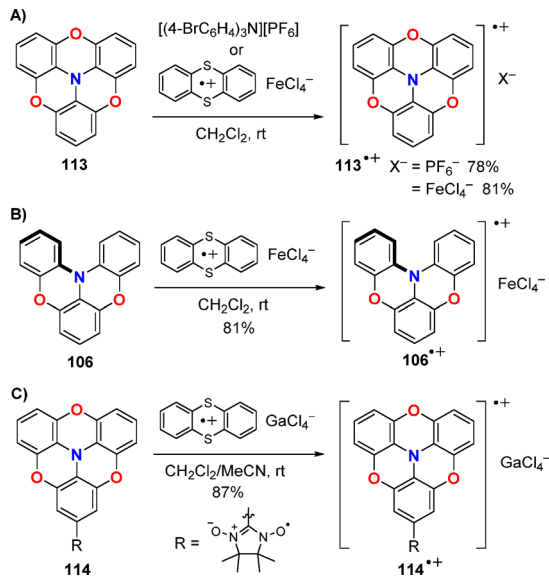
maximum of $70^{\bullet+}$ was found in the visible region around 600 nm. Single crystals of this radical cation suitable for X-ray diffraction analysis was obtained as aluminate salts. In the crystal structure, $70^{\bullet+}$ embraced a fully planarized geometry and no elongation of the N–C bonds from the neutral counterpart 70 was observed. Further reaction of $70^{\bullet+}[Al(OR_F)_4]^-$ with a trace amount of $Ag[Al(OR_F)_4]$ furnished the dimeric dication salt $[70_2]^{2+} \cdot 2[Al(OR_F)_4]^-$ (Scheme 26). DFT calculations determined that the $[70_2]^{2+}$ possesses a small singlet–triplet energy gap and the most stable electronic state is the open-shell singlet. In fact, the estimated diradical character of $[70_2]^{2+}$ was $y = 0.770$, which is higher than that of the previously reported bis(acridine) dimer tetracation ($y = 0.615$).²⁶⁷

3.3.2. Radicals of Oxygen-Bridged Triarylamine Derivatives. The dimethylmethylen bridges certainly contribute toward the stabilization of N-heterotriangulene derivative $70^{\bullet+}$ via structural constraint and spin delocalization. However, their out-of-plane steric hindrance was sought to disrupt the intermolecular interaction that is necessary for electronic and magnetic materials. To counter this problem, displacement of the bridges with oxygen atoms was considered.

In 2005, along with its neutral counterpart, Okada et al. isolated an oxygen-bridged N-heterotriangulene radical cation $113^{\bullet+}$.^{248,268} The neutral parent compound 113 was prepared

from 2,6-difluoronitrobenzene in a six-step sequence, which involves intramolecular cyclization by Pd(0)-catalyzed cross-coupling reaction and intramolecular nucleophilic substitutions as pivotal bond-formation steps. Compound **113** showed a reversible oxidation process with $E^\circ_{\text{ox}} = +0.12$ V. Hence, treatment of **113** with tris(*para*-bromophenyl)ammoniumyl hexafluorophosphate ($[(4\text{-BrC}_6\text{H}_4)_3\text{N}][\text{PF}_6]$) in CH_2Cl_2 afforded the corresponding radical cation salt $\text{113}^{\bullet+}[\text{PF}_6]^-$ which was recrystallized from MeCN and Et_2O (Scheme 27A).

Scheme 27. Synthesis of (A) Air-Stable Radical Cations $\text{113}^{\bullet+}$ as PF_6^- and FeCl_4^- Salts, (B) $\text{106}^{\bullet+}$ as an FeCl_4^- Salt, and (C) $\text{114}^{\bullet+}$ as an GaCl_4^- Salt



In comparison with the parent neutral compound **113** that has a shallow bowl-shaped structure, radical cation $\text{113}^{\bullet+}$ had a fully planarized structure. DFT calculations predicted that the spin density of the radical cation was delocalized throughout the molecule with noticeable contributions from the central nitrogen atom and para-carbon atoms as well as the bridging oxygen atoms.

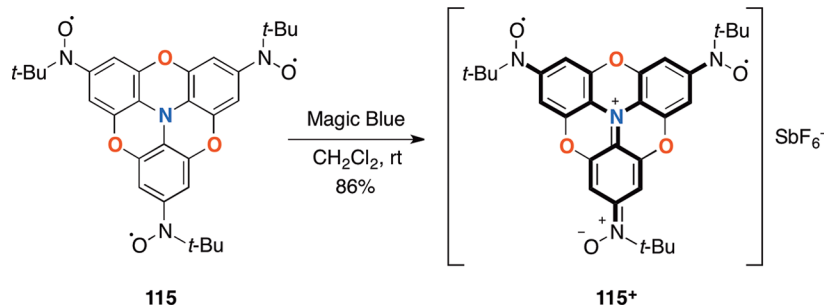
In 2007, Shiomi et al. treated both trioxy-*N*-heterotriangulene **113** and dioxytriphenylamine **106** with thianthrenium tetrachloroferrate, a single-electron cationic oxidant, to produce the corresponding radical cations $\text{113}^{\bullet+}$ and $\text{106}^{\bullet+}$ (Scheme 27B).²⁶⁹ Radical cation $\text{113}^{\bullet+}$ in the crystals of FeCl_4^- salt adopted a fully planarized structure analogous to

that in PF_6^- salt and was packed as slightly offset $\pi-\pi$ stacked dimers which were surrounded by FeCl_4^- counteranions. On the other hand, $\text{106}^{\bullet+}$ had a similarly distorted structure to that of the neutral parent compound **106** and showed no signs of dimer formation. Most intriguingly, FeCl_4^- salts of radical cations $\text{113}^{\bullet+}$ and $\text{106}^{\bullet+}$ were persistent under aerated conditions both in solution and in solid state. The same group similarly treated mono(nitronyl nitroxide)-substituted trioxyphenylamine **114** with thianthrenium tetrachlorogallate to afford the corresponding radical cation $\text{114}^{\bullet+}$ (Scheme 27C), which was comparably as stable as $\text{113}^{\bullet+}$.²⁷⁰

In 2012, Okada et al. decorated the three para-pzpositions of trioxy-*N*-heterotriangulene **113** with *N*-*tert*-butylnitroxide groups to afford triradical (Scheme 28).²⁷¹ This compound was synthesized from oxygen-bridged *N*-heterotriangulene **113** in a three-step sequence: (1) bromination of the three para-positions, (2) trilithiation followed by treatment with 2-methyl-2-nitrosopropane to furnish the corresponding trihydroxylamine derivative, and (3) oxidation with an excess of Ag_2O . Triradical **115** in the crystalline state had a shallow bowl-shaped structure similar to that of a neutral trioxy-*N*-heterotriangulene **113**. Meanwhile, the first oxidation potential of the triradical was $E^\circ_{\text{ox}} = -0.29$ V, which is significantly smaller than that of **113** ($E^\circ_{\text{ox}} = +0.12$ V). Notably, triradical **115** has a low-spin preference with a sizable antiferromagnetic exchange coupling, and therefore has a doublet ground state. Moreover, the corresponding diradical cation $\text{115}^{\bullet+}$, obtained by one-electron oxidation of **115** using Magic Blue in CH_2Cl_2 , takes a triplet ground state (Scheme 28). In fact, this spin state is crucial to stabilize radical cation $\text{115}^{\bullet+}$ because it has a partial quinoidal character which can be drawn in three different resonance structures (only one of the resonance structures is depicted in Scheme 28). It is noteworthy that the radical cation of the nonconstrained tris(4-nitroxylphenyl)-amine derivative could not be isolated, exemplifying the importance of structural planarity for the spin delocalization.²⁷²

In 2017, Suzuki et al. reported a series of trioxy-*N*-heterotriangulene dimers attached at different positions of the *N*-heterotriangulene units directly through C–C bonds.²⁷³ Dimers **116a–c** (Figure 21), prepared by either Yamamoto homocoupling or Suzuki-Miyaura cross-coupling reactions, all underwent two-electron oxidation using tris(4-bromophenyl)-ammoniumyl hexafluoroantimonate ($[(4\text{-BrC}_6\text{H}_4)_3\text{N}][\text{SbF}_6]$) as the oxidant. Just like the monomeric systems, all dimeric dications 116a^{2+} – 116c^{2+} were remarkably persistent in air and each triarylamine moiety adopted a completely planarized

Scheme 28. Trinitroxide-trioxy-*N*-heterotriangulene **115** and Its One-Electron Oxidized Derivative $\text{115}^{\bullet+}$ ^a



^aCompound **115** is in a doublet ground state, whereas cation $\text{115}^{\bullet+}$ takes a triplet ground state. The thick black lines denote the π -conjugation in the cationic system.

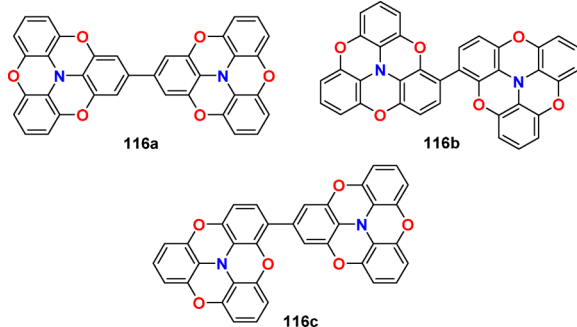


Figure 21. Structures of trioxy-N-heterotriangulene dimers **116a–c**. Each N-heterotriangulene unit can undergo one-electron oxidation resulting in the formation of the corresponding dications.

structure. The connection pattern of the dimers greatly impacted the electronic structures. Most notably, results based on EPR spectroscopy and magnetic susceptibility measurements concluded that **116a**²⁺, **116b**²⁺, and **116c**²⁺ have a singlet ground state with a large singlet–triplet (S–T) energy gap, a singlet ground state with a small S–T energy gap and a triplet ground state, respectively.

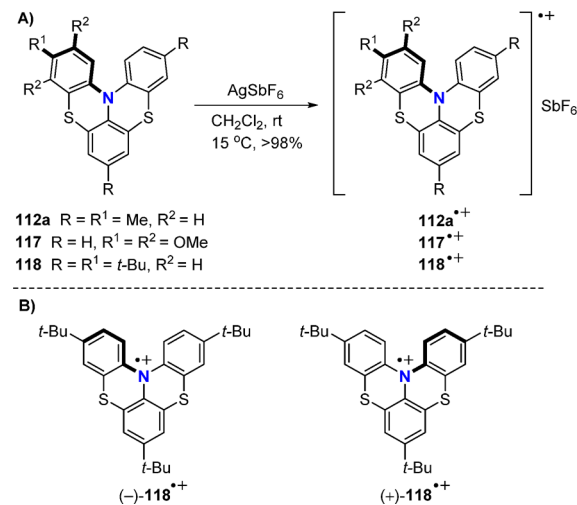
3.3.3. Radicals of Partially Sulfur-Bridged Triarylamine Derivatives. In 2015, Menichetti et al. reported one-electron oxidation of 2-fold sulfur-bridged triarylamine derivatives, **112a** and **117**, which led to the corresponding radical cations, **112a**^{•+} and **117**^{•+}, respectively.²⁷⁴ Hetero[4]-helicene **117** was obtained using a similar synthetic sequence from an earlier report.²⁵⁷ Cyclic voltammetry measurements of **112a** and **117** displayed reversible oxidation processes with potentials of $E^\circ_{\text{ox}} = 0.25$ and 0.26 V, respectively (in CH_2Cl_2 using TBAPF_6 vs Fc/Fc^+). In turn, the reactions of **112a** and **117** with AgSbF_6 resulted in immediate deepening of the solution color and precipitation of solid Ag, indicating the successful one-electron oxidation to furnish the corresponding radical cations **112a**^{•+} and **117**^{•+} as SbF_6^- salts. Based on EPR spectroscopy and DFT calculations, the unpaired electron in both radical cations were found to delocalize throughout the whole molecule, in which the highest spin density values were measured at the nitrogen centers. X-ray crystallographic analysis of **112a**^{•+} and **117**^{•+} unveiled an improved planarity compared to the parent neutral congeners (**Scheme 29**).

Similarly, Berova et al. in 2017 synthesized chiral doubly sulfur-bridged triarylamine radical cations **(−)-118**^{•+} and **(+)-118**^{•+} as SbF_6^- salts.²⁷⁵ The parent neutral species was obtained as a racemic mixture and the enantiomers were separated by preparative HPLC on a chiral stationary phase column prior to oxidation. Chiroptical methods involving ECD, ORD, and VCD as well as DFT calculations showed that the radical cations **(−)-118**^{•+} and **(+)-118**^{•+} conserve the absolute configuration of the parent neutral counterparts while undergoing an overall flattening of the helical structures.

3.4. Diarylamine-Fused Porphyrins

Meso-diarylaminoporphyrins have been extensively studied as a potential scaffold for next-generation devices such as dye-sensitized solar cells.²⁷⁶ The diarylamine groups serve as electron-donating groups, which give rise to elevated HOMO level of the porphyrin core. However, the effect is only moderate because the twisted conformation disturbs the efficiency of π -conjugation between the diarylamine moiety and the porphyrin circuit. To overcome this issue, Kim et al. synthesized diarylamine-fused porphyrins, where the triaryl-

Scheme 29. (A) Generation of Doubly Thia-Bridged Triarylamine Radical Cations **112a**^{•+}, **117**^{•+}, and **118**^{•+} and (B) Superimposed Images of Configurationally Stable Chiral Dithia-Bridged Triphenylamine Radical Cations **(−)-118**^{•+} and **(+)-118**^{•+}

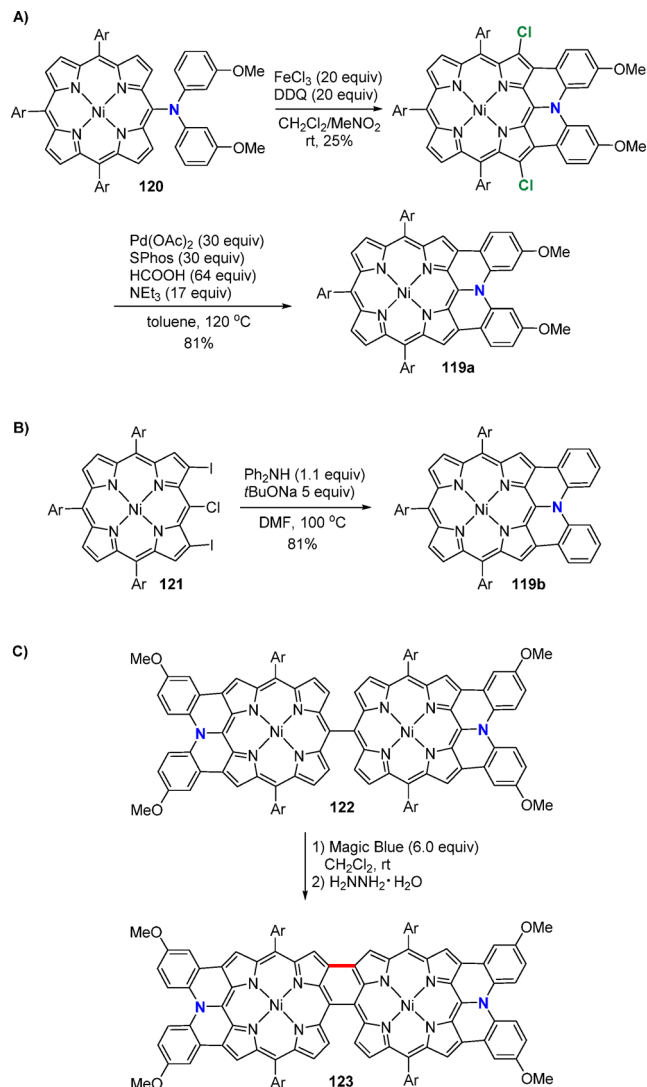


amine moieties adopt a quasi-planar geometry.²⁷⁷ Ni(II)-centered diarylamine-fused porphyrin **119a** was prepared by (1) Buchwald-Hartwig amination of *meso*-brominated Ni(II)-porphyrin with bis(3-methoxyphenyl)amine, (2) oxidative fusion of the corresponding *meso*-(diarylamo)porphyrin derivative **120** using FeCl_3 and DDQ , followed by (3) dechlorination by Pd-catalyzed reduction with HCOOH and TEA (**Scheme 30A**). The electrochemical properties of *meso*-diarylaminoporphyrin **120** and its doubly fused product **119a** were examined by CV. Compared to that of **120**, partially planarized **119a** has (1) a lower first oxidation potential ($E^{1/2}_{\text{ox1}} = 0.36$ V for **120** and 0.15 V for **119a**) and (2) a larger energy gap between the half-wave potentials of the first and second oxidation processes ($\Delta E_{\text{ox}} = 0.22$ V for **120** and 0.56 V for **119a**), suggesting an enhanced electron donation from the fused amino moiety. In 2015, Yorimitsu et al. established a convenient synthetic strategy to access doubly diphenylamine-fused porphyrin **119b**, that is, the $\text{S}_\text{N}\text{Ar}$ reaction of *meso*-chloro-diiodoporphyrin **121** with diphenylamine using *t*BuONa as an additive (**Scheme 30B**).²⁷⁸

This synthetic method was also applicable to prepare *meso*-*meso* linked diphenylamine-fused porphyrin dimer **122**, which was subsequently converted to *meso*-*meso* β - β doubly linked dimer **123** upon treatment with Magic Blue (**Scheme 30C**).²⁷⁹ X-ray crystallographic analysis of **119b** revealed that the amino group and the porphyrin plane were nearly coplanar while the two phenylene units were locked in a skewed conformation.

Subsequently in 2017, Furukawa et al. accomplished the synthesis of doubly phenoxazine-fused porphyrin **124**, a more planarized analog of **119b**.²⁸⁰ X-ray crystallographic cyclic voltammetry analysis of **124** showed that the half-wave potential of the first oxidation process ($E^{1/2}_{\text{ox1}} = 0.03$ V) was smaller than that of **119a**, suggesting an increased electron-donating ability of the peripheral amino group. Moreover, **124** underwent a one-electron oxidation by treatment with Magic Blue to generate the corresponding radical cation **124**^{•+} as a SbF_6^- salt, which, however, gradually chlorinated in the β -position to furnish **125** under air (**Scheme 31A**). Conversion of **124** to the corresponding β,β' -dichloroporphyrin **126** by

Scheme 30. (A) Synthesis of Diarylamine-Fused Porphyrin 119a by Oxidative Cyclization Followed by Dehalogenation, (B) Synthesis of Doubly Diphenylamine-Fused Porphyrin 119b via S_NAr Reaction, and (C) Cyclization Reaction of Porphyrin Dimer 122 with Magic Blue to Give *meso*-*meso* β - β Doubly Linked Dimer 123^a



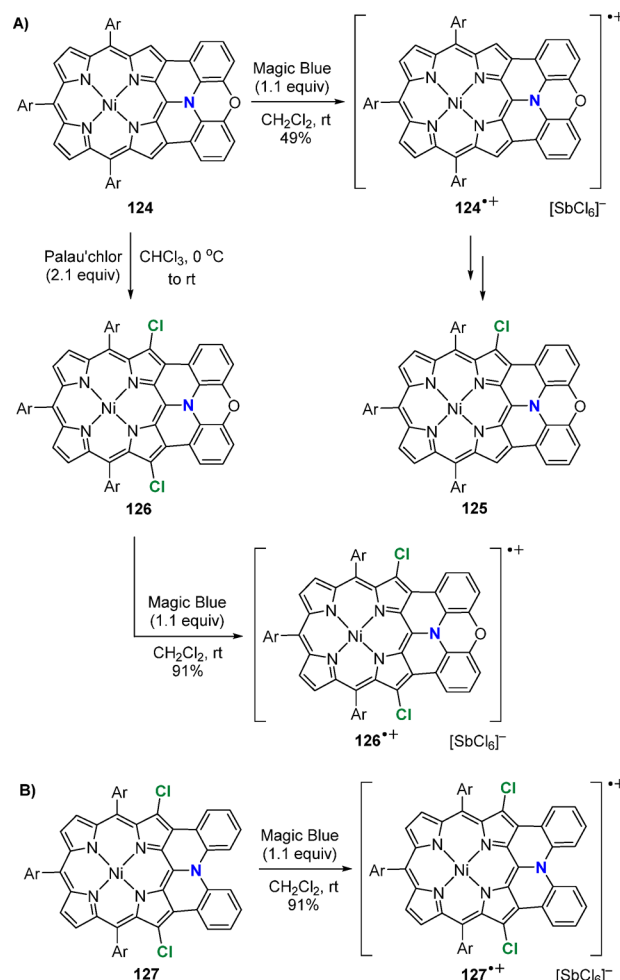
^aThe red line is assigned to the newly formed C–C bond. Ar = 3,5-di-*tert*-butylphenyl.

chlorination with Palau'chlor²⁸¹ prior to oxidation was therefore necessary to cleanly access radical cation 126^{•+}. Strikingly, this radical cation was perfectly durable under aerobic conditions and was purified by silica gel column chromatography. Likewise, porphyrin 119b was also converted to the corresponding β,β' -dichloroporphyrin 127 and successively oxidized with Magic Blue to furnish radical cation 127^{•+}, which was equally stable to that of 126^{•+} (Scheme 31B).

4. SILICON-CENTERED POLYCYCLIC COMPOUNDS

While a large variety of triangulene derivatives with neutral tetracoordinate, cationic tricoordinate, and neutral radical tricoordinate carbon-centers have been studied, examples of those of heavier congeners, such as silicon, are far less documented in literature. It is reasonable to consider that the

Scheme 31. (A) Synthesis of SbF₆[–] Salt of Phenoxazine-Fused Porphyrin Radical Cation 124^{•+} and Its Decomposition Product 125 As Well As Radical Cation 126^{•+} and (B) Synthesis of Radical Cation 127^{•+}^a



^aAr = 3,5-di-*tert*-butylphenyl.

underdevelopment of such compounds is associated with the ongoing challenge of facile formation of Si–C bonds, especially via C–H activation. In fact, there have only been two examples of silicon atom-centered triangulenes analogs. In 2016, the synthesis of silicon-embedded porphyrin 128 (Figure 22) was accomplished by Yorimitsu et al. via an intramolecular silyl-Friedel–Crafts reaction.²⁸² The crystal structure of 128 revealed that the nonfused phenyl ring on the silicon center was oriented close to a perpendicular fashion to the marginally distorted π -conjugated plane. The σ^* orbital of the Si–Ph

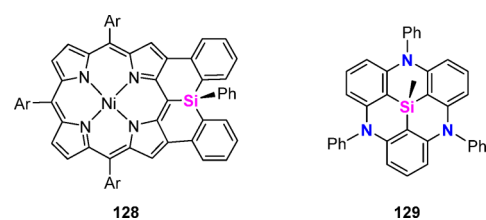


Figure 22. Structures of silicon-embedded porphyrin 128 and 3-fold nitrogen-bridged Si-heterotriangulene 129. Ar = 3,5-di-*tert*-butylphenyl.

bond was therefore directly engaged with the porphyrin π -circuit, thereby stabilizing the LUMO energy level. Hatakeyama et al. in 2017 obtained the silicon-centered 4,8,12-triazatriangulene **129** (Figure 22), which can also be viewed as triply nitrogen-bridged *Si*-heterotriangulene, using a similar approach to access the boron-centered analog **33**.¹⁵⁶ X-ray crystallographic analysis of **129** unveiled a bowl-shaped structure.

5. PHOSPHORUS-CENTERED POLYCYCLIC COMPOUNDS

While some commonalities do exist, phosphorus-embedded polycyclic π -conjugated compounds have intriguing structural and electronic properties relative to those of nitrogen analogs because (1) the covalent radius of a phosphorus atom is significantly larger compared to those of carbon and nitrogen atoms (P: 1.07(3) Å, C: 0.73(2) Å, N: 0.72(1) Å),²⁸³ which essentially forces the phosphorus atom to stay out of the plane when incorporated directly into the π -system, (2) the energy barrier of pyramidal inversion is large ($\Delta G_{403}^{\ddagger} \cong 30\text{--}35$ kcal mol⁻¹) thus the structural configuration is rather stable,²⁸⁴ and (3) phosphorus, while being a third-row element, is more electropositive than carbon and nitrogen, thereby does not readily hybridize (Bent's Rule).²⁸⁵ Because of these features, structurally constrained phosphorus-embedded polycyclic π -systems commonly adopt permanent bowl-shaped or helical structures depending on the connectivity of the three aryl groups. This is in stark contrast to those of nitrogen-centered analogs, which embrace fully- or quasi-planarized structures. As illustrated in Figure 23B, the bowl-shaped compound typically

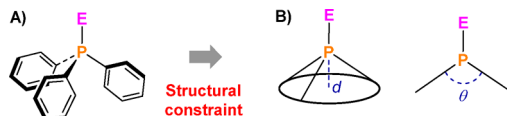


Figure 23. (A) Structures of triphenylphosphine and its axially occupied derivatives; (B) illustration defining the bowl depth (d) and the cone angle (θ) upon structural constraint of triarylphosphine skeletons.

has a concave shape, which the dimension is defined by the bowl depth d and the cone angle θ , which are relevant to capturing guest molecules with suitable size. What is also worth mentioning is that the structural and electronic factors are highly dependent on the oxidation state of the phosphorus center. Trivalent phosphorus atom formally has an electron-donating character attributed to its localized electron lone pair, whereas the corresponding pentavalent phosphoryl is an electron-accepting group due to the increased electronegativity. While related species, namely, phospholes, phosphinine, and phosphaphenalenes are useful building units toward functional organic materials,^{286–289} this section will specifically highlight the synthesis, properties, and applications of trivalent and pentavalent phosphorus directly annulated into π -systems.

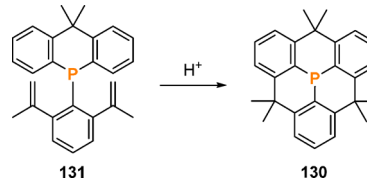
5.1. Phosphorus-Centered Triangulenes: *P*-Heterotriangulenes

5.1.1. *P*-Heterotriangulenes with Methylene Bridges.

The very first example of a phosphorus-centered triangulene derivative, so-called *P*-heterotriangulene, was reported in 1990 by Hellwinkel et al.²⁹⁰ In this work, structurally constrained *P*-heterotriangulene possessing three dimethylmethylene bridges,

130, was prepared by 2-fold Brønsted acid-catalyzed Friedel–Crafts cyclization of triphenylphosphine precursor **131** (Scheme 32). The arsenic analog was also prepared by the

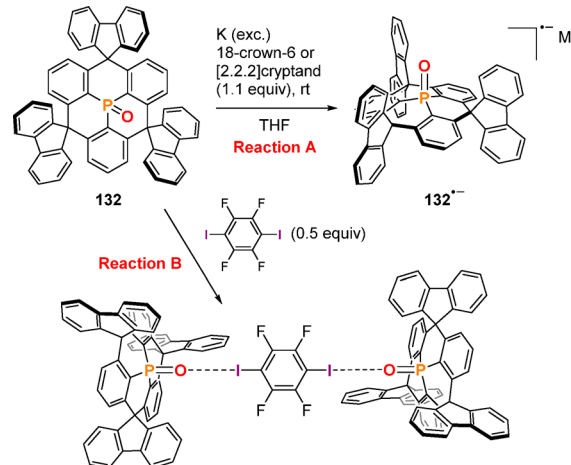
Scheme 32. Synthesis of *P*-Heterotriangulene **130 via Proton-Catalyzed Intramolecular Friedel-Crafts Cyclization of **131****



same synthetic route. X-ray crystallographic analysis verified that **130** embraces a C_{3v} symmetric bowl-shaped structure as opposed to the planarized nitrogen congener **70**. The $\text{P}-\text{C}_{\text{ipso}}$ bonds in **130** (approximately 1.81 Å) were only marginally shorter than those in Ph_3P (1.83 Å).²⁹¹ A more distinct deviation appeared in the sum of the $\text{C}_{\text{ipso}}-\text{P}-\text{C}_{\text{ipso}}$ angles, where the value for **130** was about 15° smaller than that in Ph_3P ($\Sigma(\angle_{\text{C}_{\text{ipso}}} \text{P} \text{---} \text{C}_{\text{ipso}}) = 293.7^\circ$ for **130** and 309° for Ph_3P).

It was not until just over a quarter century later when Kivala et al. revisited the chemistry and successfully replaced the dimethylmethylene bridges with more sterically demanding spirofluorenylmethylene bridges but with an oxidized phosphorus center (phosphine oxide **132**; Scheme 33).²⁹² Cyclic

Scheme 33. Structure of **132 and Its Reactivity^a**



^a(A) One-electron reduction of **132** with K in the presence of 18-crown-6 or [2.2.2]cryptand in THF and (B) the 2:1 complex formation between **132** and 1,4-diiodotetrafluorobenzene ($\text{M}^+ = [\text{K}\cdot\text{18-crown-6}]^+$ or $[\text{K}\cdot[2.2.2]\text{cryptand}]^+$).

voltammetry showed that **132** undergoes a reversible reduction process at -2.85 V vs Fc/Fc^+ . Treatment of **132** with an excess amount of potassium metal in the presence of 18-crown-6 or [2.2.2]cryptand in THF led to a deep red coloring of the mixture, suggesting the successful conversion to radical anion **132^{•-}** (Scheme 33, reaction A). The absorption profile of the reaction mixture remained unchanged for 3 days, exemplifying the high stability of **132^{•-}** even in solution ($\lambda_{\text{abs}} = 378$ and 485 nm). EPR studies unveiled that the unpaired electron is delocalized over the phosphoryl center and the three phenyl

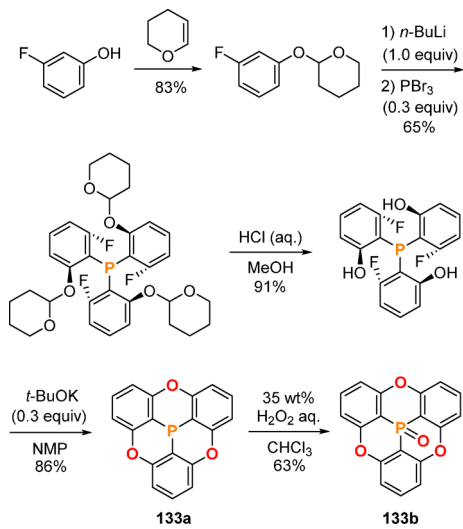
rings bonded to the phosphorus center. Along with the steric protection from the bulky fluorenyl groups, the distribution of the spin density may be responsible for the persistence of the radical anion $132^{\bullet-}$. X-ray crystallographic analysis of $132^{\bullet-}[\text{K}\cdot\text{18-crown-6}]^+$ elucidated that the radical anion and the polyether-encapsulated potassium cation were well separated and an increased pyramidalization about the phosphorus center was observed compared to that of the neutral parent compound 132 . The authors noted that this work was the first to characterize the crystal structure of a triarylphosphine oxide radical anion.

In a later work by the same group, the Lewis basicity of the $\text{P}=\text{O}$ moiety of 132 was analyzed.²⁹³ The Mayer's bond order of the $\text{P}-\text{O}$ bond determined by DFT calculations was largely reduced in 132 compared to triphenylphosphine oxide (Ph_3PO) regardless of the level of theory used, thereby illustrating that the electron density is greatly polarized toward the oxygen atom (132 : 1.59–1.76 and Ph_3PO : 2.05–2.10). In the presence of an electron-deficient aryl iodide, namely, 1,4-diiodotetrafluorobenzene, compound 132 formed colorless single crystals suitable for X-ray crystallographic analysis (Scheme 33, reaction B). The unit cell of the cocrystals was composed of one molecule of the aryl iodide directly surrounded by a total of six molecules of 132 , two of which were strongly bound with the aryl iodide through a short $\text{P}=\text{O}\cdots\text{I}$ halogen bond of $2.683(5)$ Å. The remaining four molecules were involved in the $\pi\cdots\pi$ stacking and hydrogen bonds with fluorine, which DFT calculations determined to be as equally as important to $\text{O}\cdots\text{I}$ interactions for the cocrystallization.

5.1.2. *P*-Heterotriangulenes with Heteroatom Bridges.

The triply oxygen-bridged *P*-heterotriangulene was reported before its nitrogen-centered analog. Krebs et al. in 1997 described the synthesis of fully oxygen-bridged *P*-heterotriangulene 133a (Scheme 34).²⁹⁴ This compound was obtained by a straightforward four-step synthetic sequence

Scheme 34. Four-Step Synthetic Sequence to Prepare Threecold Oxygen-Bridged *P*-Heterotriangulene 133a Featuring Aromatic Nucleophilic Substitution for the Intramolecular Cyclization Reaction^a



^aThe resulting phosphine was oxidized using 35 wt % aq. H_2O_2 to afford phosphine oxide 133b .

starting from commercially available 3-fluorophenol with the final step involving a 3-fold intramolecular cyclization through aromatic nucleophilic substitutions. The corresponding phosphine oxide derivative 133b (Scheme 34) was prepared by treating of the parent *P*-heterotriangulene 133a with H_2O_2 in CHCl_3 . Despite the high molecular symmetry, compound 133a does not exhibit strong intermolecular interactions as proven by a low sublimation temperature. In the crystalline state, however, compound 133a was determined by X-ray crystallography to adopt a locked bowl-shaped structure and forms π -stacks, hence the presence of a permanent dipole moment. Later in 2000, Madsen et al. applied multipolar modeling on 133a and evaluated the dipole moment in the solid state as 4.7 D.²⁹⁵ This study translates to a 42% enhancement of the dipole moment going from a CHCl_3 solution to the crystalline state. Lin et al. in 2001 recorded atomic-scale images of 133a on a $\text{Ag}(111)$ surface by STM and discovered three characteristic types of binding configurations which depended on the orientation of the molecules against the metal surface.²⁹⁶

In 2014, Yamamura prepared compound 134a (Figure 24A), a π -extended phenylethyne-substituted derivative of phos-

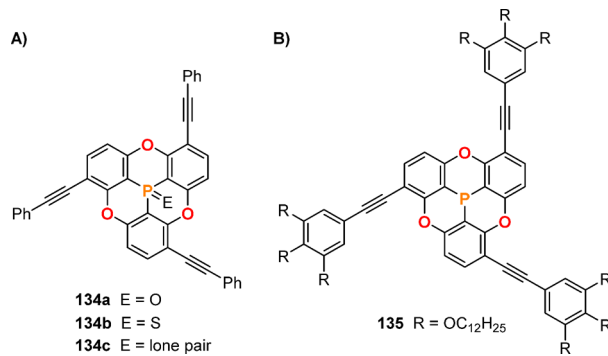


Figure 24. (A) Structures of C_3 symmetric *P*-heterotriangulenes $134\text{a}\text{--c}$ bearing three phenylethyne groups and (B) structure of liquid crystal of a chiral bowl-shaped *P*-heterotriangulene 135 featuring long alkyl chains.

phine oxide 133b and used it as a host molecule toward C_{60} .²⁹⁷ Compound 134a (Figure 24A) was first obtained as a racemic mixture by Sonogashira cross-coupling reactions of the tribrominated derivative of 133a with phenylacetylene, which was then purified into each enantiomer by chiral HPLC. Compound 134a adopted a C_3 -symmetric chiral concave structure determined by X-ray crystallography and exhibited chiroptical properties with a noticeable anisotropy. In the cocrystal with C_{60} , four molecules of 134a were found to perfectly encapsulate and cover the surface of C_{60} . This type of $\pi\cdots\pi$ stacking tendency is also seen with other bowl-shaped host compounds, such as corannulene and pentabenzoazacorannulene.⁸⁵ In the MALDI-TOF spectrum of the cocrystal, an ion peak assigned to a 1:1 complex of the oxygen-bridged *P*-heterotriangulene 134a and a C_{60} molecule was observed, indicating that the concave/convex interaction was strong enough to hold the host and guest molecules together even upon ionization. The ^1H NMR analysis of a mixture containing 134a with C_{60} functionalized with solubilizing groups confirmed that the two also exist as a 1:1 complex in solution. The induced CD signal of a fullerene was also observed,

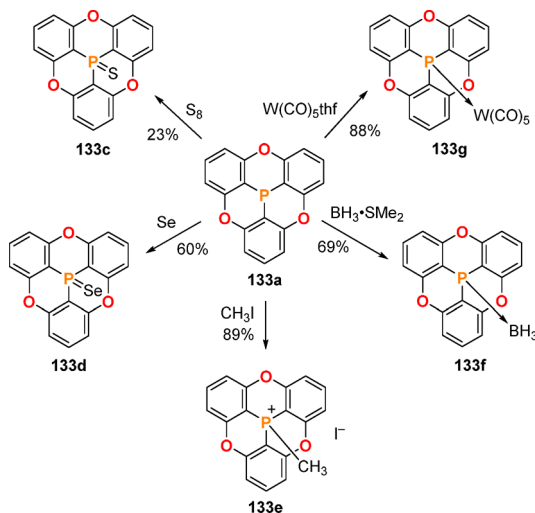
demonstrating the transfer of the chiroptical properties from the host compound **134a** to the guest C_{60} .

In the following year, Yamamura et al. prepared a phosphine sulfide derivative **134b** and a trivalent derivative **134c** to evaluate the effect of axial substituents toward encapsulating capabilities (Figure 24A).²⁹⁸ X-ray crystallographic analysis together with DFT calculations predicted that the environment of the axial position of the phosphorus center dictated the bowl depth and the cone angle of the *P*-heterotriangulene core. For instance, quantum-chemical calculations estimated that the cone angle of the phosphine derivative **134c** ($\theta = 115^\circ$) is smaller than those of the oxide and sulfide derivatives ($\theta \cong 121^\circ$), which in turn led to a deeper bowl depth in the former species ($d = 2.46 \text{ \AA}$) over the latter two ($d \cong 2.23 \text{ \AA}$). These trends demonstrated that simple modification of the axial substituent allows tuning of the bowl geometry. Moreover, the three phosphorus-containing bowl-shaped molecules cocrystallized with C_{60} as a guest molecule. Both **134a** and **134b**, with shallow bowl depths, led to chiral cavities composed of four host molecules, whereas the phosphine counterpart **134c**, with a much deeper concave, formed an achiral cavity comprised of two host molecules.

Introduction of multiple terminal alkoxy chains to **134c** produced liquid-crystalline compound **135** (Figure 24B).²⁹⁹ DSC and XRD analyses unveiled that the enantiomeric pure *M*-isomer of liquid crystal formed hexagonal columns between 29 and 94 °C. The racemic mixture also had a similar self-assembly behavior; however, the stacked columns were less ordered compared to enantiomerically pure **135**. The CD signal of **135** can be switched by a reversible phase transition between the crystalline and liquid crystalline phases, which can potentially be applied to new polarization-responsive chiral multifunctional materials.

A more detailed investigation of the relationship between the bowl geometry of oxygen-bridged *P*-heterotriangulene and the axial groups on the phosphorus atom was conducted by Yamamura et al. in 2016.³⁰⁰ In this study, the authors, in addition to previously reported **133a** and **133b**, newly synthesized *P*-heterotriangulenes bearing S, Se, CH_3 , BH_3 , and $\text{W}(\text{CO})_5$ as axial substituents (**133c–g**; Scheme 35).

Scheme 35. Synthesis of Bowl-Shaped *P*-heterotriangulene **133c–g Possessing Various Axial Substituents on the Phosphorus Atom**



Based on the crystal structures, the bowl depths d were in the order of **133a** > **133g** > **133f** > **133c** ≈ **133d** > **133b** > **133e**, which the trend was approximately reversed in the cone angles θ . The NBO analysis suggested that the increased s orbital character of the phosphorus in P-E bonds is responsible for wider cone angles and deeper bowl concaves. It was also recorded that the oxidation potential of **133a** was 1.55 V which is significantly higher than that of a simple triphenylphosphine (1.05 V). This implied that structural constraint of triarylphosphines lower the HOMO energy level hence the electron affinity.

Altering the bridging atoms also vastly affected the bowl geometry of *P*-heterotriangulenes. Yamamura et al. also prepared a series of *P*-heterotriangulenes with differing numbers of oxygen and sulfur atoms in the three bridging positions, i.e., compounds **136a–c** (Figure 25), and

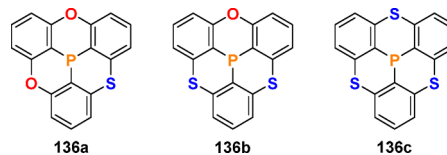


Figure 25. Bowl-shaped *P*-heterotriangulenes **136** possessing different combinations of oxygen and sulfur bridges.

determined their solid-state structures by X-ray diffraction analysis.³⁰¹ By virtue of the larger size of sulfur atom over oxygen atom, the bowl geometries as well as the packing structures heavily depended on the bridging atoms. Notably, increasing the number of sulfur bridges resulted in increased cone angles and decreased bowl depths. In brief, the bowl depths of 3-fold oxygen- and sulfur-bridged derivatives **133a** and **136c** were $d = 2.43$ and 2.03 \AA , respectively, differing by nearly 20%. Furthermore, C_{3v} symmetric **133a** and **136c** aligned perfectly to form one-dimensional concave/convex stacks, whereas C_s symmetric **136a** and **136b** constructed zigzag noncolumnar structures. Suzuki et al. later utilized sulfur-bridged *P*-heterotriangulene **136c** as a neutral donor ligand to complex a $\text{Au}(\text{I})$ -(nitronyl nitroxide)-2-ide fragment to produce an air-stable organometallic radical.³⁰²

The syntheses of 3-fold phenylamino-bridged *P*-heterotriangulene **137a** and its phosphine oxide and sulfide analogs **137b** and **137c**, respectively, were reported by Hatakeyama et al. in 2017 (Figure 26).¹⁵⁶ The key step to embed a

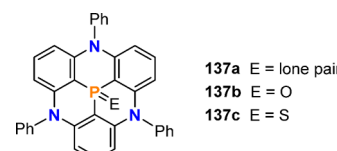


Figure 26. Structures of 3-fold phenylamino-bridged *P*-heterotriangulene (**137a**) and its oxide (**137b**) and sulfide derivatives (**137c**).

phosphorus atom to the center of a triaryl framework involved an intramolecular C–H phosphorylation, similar to those of boron- and silicon-analogs. The bowl-shaped architecture of trivalent *P*-heterotriangulene **137a** was verified by X-ray crystallography. Compared to those of sulfur- and oxygen-bridged analogs **133a** and **136c**, the concave of nitrogen-bridged **137a** was much shallower, which DFT calculations determined was due to crystal packing force. Owing to the

distorted structure, **137a** was only weakly fluorescent with an emission maximum at $\lambda_{\text{em}} = 383$ nm and a low quantum yield of $\Phi_F = 0.05$. In a continuing work, Hatakeyama et al. found that sulfur-capped *P*-heterotriangulene **137c** consists of an electronic structure and thermal stability suitable for an exciton blocking layer (EBL) in PHOLEDs.³⁰³ Indeed, an Ir(ppy)₃-based green PHOLED applied with **137c** as the EBL displayed a pronounced external quantum efficiency value of 20% at 1000 cd m⁻², which is approximately twice as high as PHOLEDs without **137c**.

5.2. Partially Bridged Triarylphosphines and Their Oxidized Derivatives

Partially bridged triarylphosphines have been documented in literature for over 30 years. In 1985, Chen et al. reported the two examples of doubly dimethylmethylene-bridged π -systems containing phosphorus centers.³⁰⁴ Although in poor yield of 4%, structurally constrained phosphine oxide **138a** (Figure 27A) was synthesized through two successive Brønsted-acid-

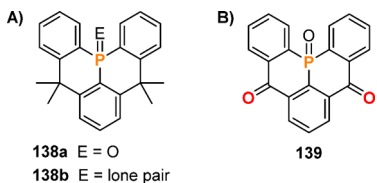


Figure 27. (A) Structures of 2-fold dimethylmethylene-bridged triphenylphosphine oxide **138a** and its reduced triphenylphosphine derivative **138b** and (B) 2-fold carbonyl-bridged triphenylphosphine oxide **139**.

mediated intramolecular Friedel–Crafts cyclization reactions. Subsequent treatment with trichlorosilane cleanly converted phosphine oxide **138a** to the corresponding phosphorus(III) derivative **138b** in nearly quantitative yield. X-ray crystallographic analysis revealed that **138b** has a C_s symmetry and the geometry about the phosphorus center is highly pyramidalized leading to an overall bowl-shaped structure (the sum of three $C_{\text{ipso}}-\text{P}-C_{\text{ipso}}$ angles = 305.8°, $d = 0.81$ Å). Owing to the single bond character of $\text{P}-C_{\text{ipso}}$ bonds, no appreciable interaction of the phosphorus lone pair with the adjacent aromatic rings were detected. The cyclic voltammetry measurement of **138b** exposed a single irreversible oxidation wave at 1.18 V vs Fc/Fc⁺. The oxidation potential was higher compared to the nitrogen congener **106** (0.95 V), thereby implying that the HOMO energy level was stabilized upon replacing the nitrogen center in the π -system with a phosphorus atom. Notably, changing from $\text{C}(\text{sp}^3)$ -hybridized dimethylmethylene bridges to $\text{C}(\text{sp}^2)$ -hybridized carbonyl bridges (**139**) only had a marginal effect on the geometry in both the P(III) and the P(V) oxidation states (Figure 27B).³⁰⁵

In 2011, Hatakeyama et al. invented a versatile tandem phospha-Friedel–Crafts reactions to prepare a series of 2-fold bridged triarylphosphine derivatives composed of waved π -conjugated frameworks.³⁰⁶ In this study, a series of structurally constrained triarylphosphines (**140a**, **141a**, and **142a**) as well as their oxide (**140b**, **141b**, and **142b**) and sulfide (**140c**, **141c**, and **142c**) derivatives were synthesized (Figure 28). The crystal structures of phosphine **141a**, phosphine oxide **141b**, and phosphine sulfides **140–142c** were determined by X-ray crystallography. The overall geometries of the phosphine sulfide derivatives were helical for **140c**, bowl-shaped for **141c**, and quasi-planar for **142c**. These results indicated that the

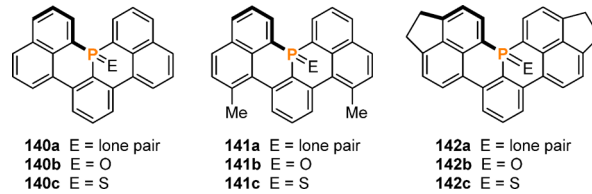


Figure 28. Structures of phosphaperylene derivatives **140a–c**, **141a–c**, and **142a–c**.

structural properties of the doubly bridged triarylphosphine derivatives largely depended on the peripheral substituents. Moreover, both phosphine **141a** and phosphine oxide **141b** also take up bowl-shaped structures just like **141c**, revealing that the substituents on the phosphorus atoms also impact the shape of the molecules. DFT calculations evaluated that the HOMOs and the LUMOs of **140a** and **140b** were delocalized over the entire molecular skeletons. This delocalization is relevant to the relatively narrow HOMO–LUMO gap of **140a** (3.68 eV), which is only slightly larger than that of anthracene (3.59 eV). It was also noted that the HOMO and LUMO energies of **140b** were lower than those of **140a** due to the electron-withdrawing character of the $\text{P}=\text{O}$ moiety. In addition, phosphine **140a** in CH_2Cl_2 exhibited a fluorescence with two distinct bands, one intense emission at 436 nm, and a broader excimer-type emission at 540 nm. A similar emission profile was observed for the phosphine analog **141a**. On the other hand, phosphine oxides **140–142b** displayed strong blue fluorescence with emission maxima (λ_{em}) at 418, 415, and 468 nm, respectively ($\Phi_F = 0.68$, 0.83, and 0.20). It is worth annotating that phosphaperylene derivatives all have exceptional thermal stabilities and showed no signs of decomposition even upon heating at 600 K.

In an extended study, Hatakeyama et al. in 2014 prepared double helicenes containing two doubly bridged triarylphosphine moieties using the same tandem phospha-Friedel–Crafts reactions described above.³⁰⁷ Double helicene **143a** (Figure 29A) implementing axial sulfide substituents on the two

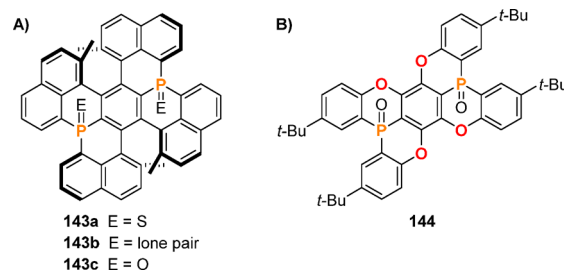


Figure 29. (A) Structures of double helical phosphine and its oxidized derivatives **143** and (B) extended host **144** containing two concave phosphorus-containing oxygen-bridged systems.

phosphorus centers was obtained in four steps starting from hexabromobenzene. X-ray crystallographic analysis unveiled that **143a** has a C_2 symmetry with the two [5]helicene-like units positioned in the same helicity (M,M' -isomer). Concomitantly, the two sulfur atoms were oriented in a *cis* conformation. Notably, the central benzene ring sandwiched between the two phosphorus atoms was heavily distorted with a large bending angle of 23°, which is only marginally smaller than that in [1.1]paracyclophane (24.9°).³⁰⁸ Nonetheless, DFT calculations predicted that the π -conjugation in **143a** was

not entirely disrupted, as the HOMO and LUMO were delocalized over the whole structure. In fact, the NICS(0) value of the central benzene ring was -4.3 ppm, suggesting a weak but subsistent aromatic character. Thus, **143a** still had a reasonably narrow HOMO–LUMO gap of 2.96 eV, which is comparable to that of tetracene (2.78 eV). Despite the reduced aromaticity, compound **143a** exhibited remarkable thermal persistence with no detectable decomposition even at 600 K. Treatment of **143a** with Et_3P and *m*-CPBA afforded the corresponding bis(phosphine) **143b** and bis(phosphine oxide) **143c**, respectively. The authors suggested the potential application of **143b** as a C_2 -symmetric bis(phosphine) ligand. The photophysical properties of **143a–c**, however, were not discussed within the text.

In 2015, Yamamura et al. synthesized π -extended concave compound containing two phosphorus centers, **144** (Figure 29B), in three steps via intramolecular C–O cyclization as the key step.³⁰⁹ Single crystal X-ray diffraction analysis revealed an overall bowl-shaped structure of **144**, where the two phosphorus atoms were positioned right above the plane of the central benzene ring. The depth of the bowl, which is the distance measured from centroid of the central benzene ring and the plane of the terminal methyl groups, was as deep as 3.56 Å. These structural features were well-suited for **144** to encapsulate fullerene C_{60} and C_{70} . Indeed, compound **144** and guest molecules were found to form 2:1 host–guest sandwich complexes in the black-colored cocrystals regardless of solvent combination for recrystallization. Furthermore, the MALDI-TOF mass spectra of these complexes exhibited two intense peaks as $m/z = 1478.3$ and 1598.3 verify the existence of 1:1 host–guest complexes of **144** even in the vapor phase. This also supported the fact that the first interaction among the host–guest pair was stronger than that of the second one. The formation of the 1:1 complex of **144** and $\text{C}_{60}/\text{C}_{70}$ in solution was also confirmed by NMR and UV-vis absorption spectroscopies.

5.3. Diarylphosphine-Fused Porphyrins and Their Oxidized Derivatives

As a continuing interest in chemistry of main-group-doped porphyrin derivatives, Osuka et al. in 2017 synthesized a Ni(II)-centered porphyrin with a diarylphosphine oxide moiety fused in the meso position as well as its reduced counterpart, **145a** and **145b**, respectively (Figure 30).³¹⁰ Compound **145a** was prepared through a three-step synthetic sequence of (1) nucleophilic aromatic substitution with lithium diphenylphosphide, (2) oxidation with H_2O_2 , and (3) Pd(0)-catalyzed intramolecular cyclization. Reduction of **145a** by trichlorosilane yielded the corresponding phosphine product **145b**. In the crystalline state, compound **145a** consisted of a waved π -conjugated structure arising from the tetrahedral diarylphosphine-oxide-unit, which forcefully distorts the framework. Furthermore, **145a** formed π -stacked dimers that were arranged in an antiparallel and offset orientation with an averaged interplanar distance of 3.79 Å. Meanwhile, the (diarylphosphino)porphyrin derivative **145b** possessed a planar structure as opposed to the expected trigonal pyramidal geometry. In fact, **145b** has an averaged $\text{C}_{\text{ipso}}-\text{P}-\text{C}_{\text{ipso}}$ angle of 107.4° and a bottom depth of 0.66 Å, suggesting that the P(III) center is much closer to a planar conformation compared to that of triphenylphosphine. In addition, compound **145b** in the crystal formed face-to-face dimers but with a short contact of 2.35 Å between P(III) and

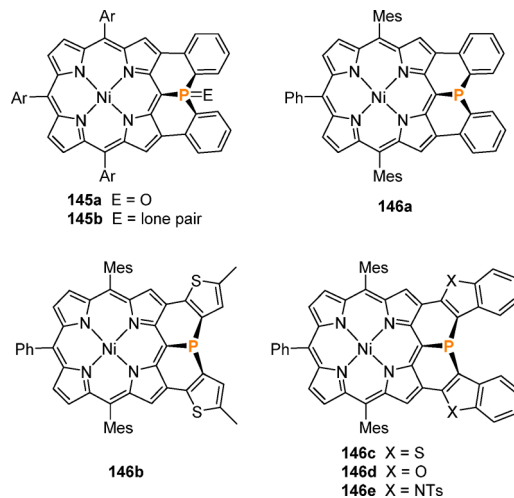


Figure 30. Structures of diphenylphosphine-fused porphyrin **145a** and its oxide derivative **145b** and a series of mesityl-substituted diarylphosphine-fused porphyrins **146a–e**. The later compounds were used to estimate inversion barriers of the P(III) center.

Ni(II) centers, thus an unusual pentacoordinate square pyramidal geometry about the Ni(II) center. This interaction crucially influences the magnetic property of the porphyrin derivatives, as compound **145b** in solution is diamagnetic with a low-spin Ni(II) center ($S = 0$) whereas in solid state is paramagnetic with a high-spin Ni(II) center ($S = 1$).

In order to elucidate the origin of the unusually planarized triarylphosphine moiety embedded in a porphyrin scaffold, Fujimoto and Osuka synthesized mesityl-substituted diphenylphosphine-fused Ni(II) porphyrin **146a** (Figure 30), in which the mesityl groups were utilized as markers in ^1H NMR spectroscopy to estimate the inversion barrier of the phosphorus center.³¹¹ In a related series, derivatives of dithienyl-, dibenzothienyl-, dibenzofuranyl-, and bis(*N*-tosylindolyl)-phosphines fused into the porphyrin framework were also prepared (**146b–e**; Figure 30). The inversion activation barriers of the P(III) centers (ΔG_{203}^\ddagger) in **146a–e** estimated by the help of VT ^1H NMR spectroscopy were in the range of 8.5 to 14.0 kcal mol $^{-1}$, thus demonstrating that the planar transition states are greatly stabilized. Note that these values were significantly smaller than those of classical triarylphosphines, which the inversion activation barriers ΔG_{403}^\ddagger are typically around 30 kcal mol $^{-1}$ to 35 kcal mol $^{-1}$.²⁸⁴ The authors stated that the effective conjugation of the lone pair of electrons on the phosphorus center through the Ni(II) porphyrin skeleton completes a 22π -aromatic circuit, which essentially stabilizes the planar transition state. This is an important finding to create highly planarized tricoordinate phosphine materials.

6. CONCLUSION AND PERSPECTIVES

Based on the research highlighted in this review, it should now be clear that structurally constrained arylated main-group compounds are versatile building blocks toward promising materials for next-generation organic devices. Depending on the central main group element, the structural and electronic properties were modulated, and thus a broad scope of practical applications could be covered.

Synthesis of fully- and quasi-planarized boron-embedded polycyclic π -electron systems were rather challenging and only a handful compared to those of nitrogen analogs have been

documented. Incorporation of a boron directly into the π -framework was found to add an electron-accepting character thus red-shifted absorption and emission. One notable feature of the planarized triarylboranes was their persistence toward heat, air, moisture, and some chemicals such as amines without the presence of sterically protecting substituents. This was particularly useful when applying them as charge carrier-transporting materials. Despite the remarkable stabilities, planarized triarylboranes retained a certain degree of Lewis acidity and underwent plane-to-bowl conversion, accordingly. This property was particular useful for gas and anion sensing as well as thin-film preparation. Also, atom-precise boron-doped and boron/nitrogen-substituted graphene nanoribbons were prepared by surface-assisted methods.

Fully- and partially planarized triarylamines are one of the most extensively researched classes of polycyclic π -systems, mainly because of the versatility of their synthetic and functionalization strategies. As electronically a natural complement to boron analogs, such compounds were readily employed as hole-transporting or hole-injection materials in OLEDs and perovskite solar cells. Furthermore, defect-free macrocycles, 1D polymers, and 2D covalent networks were successfully synthesized by on-surface reactions. The electronic gaps tend to drop upon increasing the dimensionality going from the monomers to planar 1D chains and 2D networks. Also, the π -conjugated framework played a crucial role to stabilize triaryamine radical cations by effectively delocalizing the unpaired electron within the entire molecule.

Meanwhile, annulation of heavier third-row elements such as silicon and phosphorus to the centroid of the π -framework typically led to the polycyclic systems with distorted conformations. In specific, structurally constrained arylated phosphorus compounds adopted either a bowl-shaped or a helical geometry depending on the connectivity of the three surrounding aryl groups. The bridging atoms and the axial substituent on the phosphorus atom affected the bowl geometry, which in turn modulated the self-assembly property. In addition, extensive delocalization of the lone pair of electrons on the phosphorus center leads to unusually planarized tricoordinate phosphorus materials.

In parallel with the rapid growth of graphene chemistry, the development of structurally constrained main-group polycyclic systems has exponentially grown especially over the past several decades. While possessing attractive structural and electronic properties, current research has not progressed enough to extrapolate the fundamental properties of much larger π -systems such as main-group-doped nanographenes. In particular, precise incorporation of heteroatoms into the π -conjugated framework as well as expansion of the π -system still remain a big challenge, and improvement of synthetic methodologies is a key factor for further development of this field. We strongly believe that the continuing efforts to rationalize the structure-properties relationship will provide deeper insights to design functional materials with tunable characteristics for organic π -systems.

AUTHOR INFORMATION

Corresponding Author

*E-mail: yamaguchi@chem.nagoya-u.ac.jp.

ORCID ®

Shigehiro Yamaguchi: 0000-0003-0072-8969

Notes

The authors declare no competing financial interest.

Biographies

Masato Hirai studied at Texas A&M University at College Station where he completed his Ph.D. degree under the supervision of Prof. François P. Gabbaï in 2016. In June of 2016, he joined the group of Prof. Shigehiro Yamaguchi at Nagoya University as a postdoctoral researcher. Since April of 2017, he has been working in the same group as a JSPS Research Fellowship for Young Scientists (PD) grantee. His research interests are centered around the development and exploration of unprecedented applications of structurally constrained triarylboranes.

Naoki Tanaka carried out his graduate studies at Tokyo Institute of Technology under the supervision of Prof. Takanori Fukushima and received his Ph.D. in 2018. Since April of 2018, he has been working in the group of Prof. Shigehiro Yamaguchi at Nagoya University as a JSPS research fellow (PD). His current research goal is to develop functional boron-based materials using structurally constrained triarylboranes.

Mika Sakai received her B.Sc. degree from Nagoya University in 2018. She is currently working towards her graduate degree under the guidance of Prof. Shigehiro Yamaguchi. Her research interests are focused on the novel synthesis of boron-based π -systems toward the applications in functional organic materials and supramolecular chemistry.

Shigehiro Yamaguchi received his B. Eng. degree in 1991 and M. Eng. degree in 1993 from Kyoto University. He then worked with Prof. Kohei Tamao at the Institute for Chemical Research, Kyoto University as an Assistant Professor from 1993 to 2003, during which he received his Dr. Eng. from Kyoto University in 1997 and was also a Visiting Scholar at the lab of Prof. Timothy M. Swager at Massachusetts Institute of Technology from 2000 to 2001. He relocated to Nagoya University as an Associate Professor in 2003 and was promoted to full professor in 2005. He has also held the post of Vice Director of the Institute of Transformative Bio-Molecules (ITbM) since 2014 and Director of the Research Center of Materials Science since 2017. His research interests revolve around the chemistry of π -conjugated main group systems with a broad scope of practical applications from material sciences to bioimaging.

ACKNOWLEDGMENTS

This work is partly supported by JSPS KAKENHI Grant 18H03909 and 18H05261. M.H. and N.T. are grateful to the Japan Society for the Promotion of Science (JSPS) for postdoctoral fellowships. ITbM is supported by the World Premier International Research Center (WPI) Initiative, Japan.

ABBREVIATIONS

1D	one-dimensional
2D	two-dimensional
3D	three dimensional
ABCN	1,1'-azobis(cyclohexanecarbonitrile)
α -NPD	2,2'-dimethyl-N,N'-bis[(1-naphthyl)-N,N'-diphenyl]-1,1'-biphenyl-4,4'-diamine
AFM	atomic force microscopy
Alq ₃	tris(8-hydroxyquinoline)aluminum(III)
AM	air mass (coefficient)
aq.	aqueous
azulene	bicyclo[5.3.0]decapentaene
Bpin	pinacolato boronate ester

<i>n</i> -Bu	<i>normal</i> -butyl	PCE	power conversion efficiency
<i>t</i> -Bu	<i>tert</i> -butyl	Pd/C	palladium on carbon
CBP	4,4'-di(9-carbazolyl)-2,2'-biphenyl	Ph	phenyl
CD	circular dichroism	PhtNSCl	phthalimidesulfenyl chlolate
CoCp ^{*2}	bis(pentamethylcyclopentadienyl)cobalt(II)	PHOLED	phosphorescent organic light-emitting diode
CPL	circularly polarized luminescence	PPA	polyphosphoric acid
CV	cyclic voltammetry	<i>i</i> Pr	isopropyl
dba	dibenzylideneacetone	py	pyridine
DCE	1,2-dichloroethane	rt	room temperature
DCV	2,2-dicyanovinyl	S ₁	lowest-energy excited singlet state
DDQ	2,3-dichloro-5,6-dicyano-1,4-benzoquinone	SOMO	singly occupied molecular orbital
DFT	density functional theory	spiro-OMeTAD	2,2',7,7'-tetrakis[N,N-bis(<i>p</i> -methoxyphenyl)-amino]-9,9'-spirobifluorene
DMAP	4-dimethylaminopyridine	STM	scanning tunneling microscopy
DMF	<i>N,N</i> -dimethylformamide	TAZ	3-(biphenyl-4-yl)-4-phenyl-5-(4- <i>tert</i> -butyl-phenyl)-1,2,4-triazole
DSC	differential scanning calorimetry	T ₁	lowest-energy excited triplet state
EBL	exciton blocking layer	TBA	tetrabutylammonium
ECD	electronic circular dichroism	TBP	2,4,6-tri <i>tert</i> -butylpyridine
e.g.	exempli gratia, for example (Latin)	TD DFT	time-dependent density functional theory
EPR	electron paramagnetic resonance	TEA	triethylamine
EQE	external quantum efficiency	T _g	glass transition temperature
Et	ethyl	THF	tetrahydrofuran
et al.	et alia, and others (Latin)	Tip	2,4,6-triisopropylphenyl
equiv	equivalents	TMS	trimethylsilyl
Fc	ferrocene	TOF	time-of-flight
Fc ⁺	ferrocenium	TPA	two-photon absorption
FDCD	fluorescence-detected circular dichroism	triflate	trifluoromethanesulfonate
FK209	tri(2-(1H-pyrazol-1-yl)-4- <i>tert</i> -butylpyridine)-cobalt(III) tris(bis(trifluoromethylsulfonyl)-imide)	UB3LYP	unrestricted 3-parameter hybrid Becke exchange/Lee-Yang-Parr correlation functional
fhwm	full width at half-maximum	UV-vis	ultraviolet-visible
<i>g</i> _{em}	emission dissymmetry ratio	VCD	vibrational circular dichroism
HOMO	highest occupied molecular orbital	vs	versus, against (Latin)
HPLC	high-performance liquid chromatography	VT	variable temperature
Hünig's base	<i>N,N</i> -diisopropylethylamine, <i>i</i> Pr ₂ NEt	w/	with
ICT	internal charge transfer	w/o	without
i.e.	id est, that is (Latin)	XRD	X-ray diffraction
IQE	internal quantum efficiency		
in situ	in the reaction mixture (Latin)		
Ir(ppy) ₃	iridium(III) <i>fac</i> -tris(2-phenylpyridine)		
LiTMP	lithium tetramethylpiperidine		
LUMO	lowest unoccupied molecular orbital		
Magic Blue	tris(4-bromophenyl)ammonium hexachloroantimonate		
MALDI	matrix-assisted laser desorption/ionization		
<i>m</i> -CBPA	<i>meta</i> -chloroperoxybenzoic acid		
MeCN	acetonitrile		
MeOH	methanol		
MePy	4-methylpyridine		
Mes	2,4,6-trimethylphenyl (mesityl) [not methylsulfonyl (mesyl)]		
<i>m/z</i>	mass-to-charge ratio (not <i>m/e</i>)		
NBO	natural bond order		
NBS	<i>N</i> -bromosuccinimide		
NICS	nucleus-independent chemical shifts		
NIR	near-infrared		
NMP	N-methyl-2-pyrrolidone		
NMR	nuclear magnetic resonance		
NPB	1,4-bis(1-naphthylphenyl)amino)biphenyl		
OFET	organic field-effect transistor		
OLED	organic light-emitting diode		
ORD	opticalrotatory dispersion		
PAH	polyaromatic hydrocarbon		
Palau'Chlor	2-chloro-1,3-bis(methoxycarbonyl)guanidine		

REFERENCES

- (1) Lam, J. W. Y.; Tang, B. Z. Functional Polyacetylenes. *Acc. Chem. Res.* **2005**, *38*, 745–754.
- (2) Cheng, Y.-J.; Yang, S.-H.; Hsu, C.-S. Synthesis of Conjugated Polymers for Organic Solar Cell Applications. *Chem. Rev.* **2009**, *109*, 5868–5923.
- (3) Grimsdale, A. C.; Leok Chan, K.; Martin, R. E.; Jokisz, P. G.; Holmes, A. B. Synthesis of Light-Emitting Conjugated Polymers for Applications in Electroluminescent Devices. *Chem. Rev.* **2009**, *109*, 897–1091.
- (4) Wu, W.; Liu, Y.; Zhu, D. π -Conjugated Molecules with Fused Rings for Organic Field-Effect Transistors: Design, Synthesis and Applications. *Chem. Soc. Rev.* **2010**, *39*, 1489–1502.
- (5) Watson, M. D.; Fechtenkötter, A.; Müllen, K. Big Is Beautiful—“Aromaticity” Revisited from the Viewpoint of Macromolecular and Supramolecular Benzene Chemistry. *Chem. Rev.* **2001**, *101*, 1267–1300.
- (6) Wang, C.; Dong, H.; Hu, W.; Liu, Y.; Zhu, D. Semiconducting π -Conjugated Systems in Field-Effect Transistors: A Material Odyssey of Organic Electronics. *Chem. Rev.* **2012**, *112*, 2208–2267.
- (7) Ye, Q.; Chi, C. Recent Highlights and Perspectives on Acene Based Molecules and Materials. *Chem. Mater.* **2014**, *26*, 4046–4056.
- (8) Zhang, L.; Cao, Y.; Colella, N. S.; Liang, Y.; Brédas, J.-L.; Houk, K. N.; Briseno, A. L. Unconventional, Chemically Stable, and Soluble Two-Dimensional Angular Polycyclic Aromatic Hydrocarbons: From

- Molecular Design to Device Applications. *Acc. Chem. Res.* **2015**, *48*, 500–509.
- (9) Facchetti, A. π -Conjugated Polymers for Organic Electronics and Photovoltaic Cell Applications. *Chem. Mater.* **2011**, *23*, 733–758.
- (10) Beaujuge, P. M.; Fréchet, J. M. J. Molecular Design and Ordering Effects in π -Functional Materials for Transistor and Solar Cell Applications. *J. Am. Chem. Soc.* **2011**, *133*, 20009–20029.
- (11) Mei, J.; Diao, Y.; Appleton, A. L.; Fang, L.; Bao, Z. Integrated Materials Design of Organic Semiconductors for Field-Effect Transistors. *J. Am. Chem. Soc.* **2013**, *135*, 6724–6746.
- (12) Feng, G.; Liu, B. Aggregation-Induced Emission (AIE) Dots: Emerging Theranostic Nanolights. *Acc. Chem. Res.* **2018**, *51*, 1404–1414.
- (13) Dawson, W. R.; Windsor, M. W. Fluorescence Yields of Aromatic Compounds. *J. Phys. Chem.* **1968**, *72*, 3251–3260.
- (14) Ferguson, J. Absorption Spectroscopy of Sandwich Dimers and Cyclophanes. *Chem. Rev.* **1986**, *86*, 957–982.
- (15) Acree, W. E.; Tucker, S. A.; Fetzer, J. C. Fluorescence Emission Properties of Polycyclic Aromatic Compounds in Review. *Polycyclic Aromat. Compd.* **1991**, *2*, 75–105.
- (16) Winnik, F. M. Photophysics of Preassociated Pyrenes in Aqueous Polymer Solutions and in Other Organized Media. *Chem. Rev.* **1993**, *93*, 587–614.
- (17) Martínez-Máñez, R.; Sancenón, F. Fluorogenic and Chromogenic Chemosensors and Reagents for Anions. *Chem. Rev.* **2003**, *103*, 4419–4476.
- (18) Okamoto, A.; Ichiba, T.; Saito, I. Pyrene-Labeled Oligodeoxynucleotide Probe for Detecting Base Insertion by Excimer Fluorescence Emission. *J. Am. Chem. Soc.* **2004**, *126*, 8364–8365.
- (19) Miao, W. Electrogenerated Chemiluminescence and Its Biorelated Applications. *Chem. Rev.* **2008**, *108*, 2506–2553.
- (20) Ramaiah, D.; Neelakandan, P. P.; Nair, A. K.; Avirah, R. R. Functional Cyclophanes: Promising Hosts for Optical Biomolecular Recognition. *Chem. Soc. Rev.* **2010**, *39*, 4158–4168.
- (21) Berezin, M. Y.; Achilefu, S. Fluorescence Lifetime Measurements and Biological Imaging. *Chem. Rev.* **2010**, *110*, 2641–2684.
- (22) Østergaard, M. E.; Hrdlicka, P. J. Pyrene-Functionalized Oligonucleotides and Locked Nucleic Acids (LNAs): Tools for Fundamental Research, Diagnostics, and Nanotechnology. *Chem. Soc. Rev.* **2011**, *40*, 5771–5788.
- (23) Figueira-Duarte, T. M.; Müllen, K. Pyrene-Based Materials for Organic Electronics. *Chem. Rev.* **2011**, *111*, 7260–7314.
- (24) Jeong, Y.; Yoon, J. Recent Progress on Fluorescent Chemosensors for Metal Ions. *Inorg. Chim. Acta* **2012**, *381*, 2–14.
- (25) Duhamel, J. New Insights in the Study of Pyrene Excimer Fluorescence to Characterize Macromolecules and their Supramolecular Assemblies in Solution. *Langmuir* **2012**, *28*, 6527–6538.
- (26) Babu, S. S.; Praveen, V. K.; Ajayaghosh, A. Functional π -Gelators and Their Applications. *Chem. Rev.* **2014**, *114*, 1973–2129.
- (27) Novoselov, K. S.; Geim, A. K.; Morozov, S. V.; Jiang, D.; Zhang, Y.; Dubonos, S. V.; Grigorieva, I. V.; Firsov, A. A. Electric Field Effect in Atomically Thin Carbon Films. *Science* **2004**, *306*, 666–669.
- (28) Geim, A. K.; Novoselov, K. S. The Rise of Graphene. *Nat. Mater.* **2007**, *6*, 183–191.
- (29) Nair, R. R.; Blake, P.; Grigorenko, A. N.; Novoselov, K. S.; Booth, T. J.; Stauber, T.; Peres, N. M. R.; Geim, A. K. Fine Structure Constant Defines Visual Transparency of Graphene. *Science* **2008**, *320*, 1308–1308.
- (30) Yang, X.; Dou, X.; Rouhanipour, A.; Zhi, L.; Räder, H. J.; Müllen, K. Two-Dimensional Graphene Nanoribbons. *J. Am. Chem. Soc.* **2008**, *130*, 4216–4217.
- (31) Jang, B. Z.; Zhamu, A. Processing of Nanographene Platelets (NGPs) and NGP Nanocomposites: A Review. *J. Mater. Sci.* **2008**, *43*, 5092–5101.
- (32) Jiao, L.; Zhang, L.; Wang, X.; Diankov, G.; Dai, H. Narrow Graphene Nanoribbons from Carbon Nanotubes. *Nature* **2009**, *458*, 877–880.
- (33) Geim, A. K. Graphene: Status and Prospects. *Science* **2009**, *324*, 1530–1534.
- (34) Bae, S.; Kim, H.; Lee, Y.; Xu, X.; Park, J.-S.; Zheng, Y.; Balakrishnan, J.; Lei, T.; Ri Kim, H.; Song, Y. I.; et al. Roll-to-Roll Production of 30-Inch Graphene Films for Transparent Electrodes. *Nat. Nanotechnol.* **2010**, *5*, 574–578.
- (35) Schwierz, F. Graphene Transistors. *Nat. Nanotechnol.* **2010**, *5*, 487–496.
- (36) Lin, Y.-M.; Dimitrakopoulos, C.; Jenkins, K. A.; Farmer, D. B.; Chiu, H.-Y.; Grill, A.; Avouris, P. 100-GHz Transistors from Wafer-Scale Epitaxial Graphene. *Science* **2010**, *327*, 662–662.
- (37) Pallecchi, E.; Ridene, M.; Kazazis, D.; Lafont, F.; Schopfer, F.; Poirier, W.; Goerbig, M. O.; Mailly, D.; Ouerghi, A. Insulating to Relativistic Quantum Hall Transition in Disordered Graphene. *Sci. Rep.* **2013**, *3*, 1791.
- (38) Pallecchi, E.; Lafont, F.; Cavaliere, V.; Schopfer, F.; Mailly, D.; Poirier, W.; Ouerghi, A. High Electron Mobility in Epitaxial Graphene on 4H-SiC(0001) via Post-Growth Annealing Under Hydrogen. *Sci. Rep.* **2015**, *4*, 4558.
- (39) Chen, L.; Hernandez, Y.; Feng, X.; Müllen, K. From Nanographene and Graphene Nanoribbons to Graphene Sheets: Chemical Synthesis. *Angew. Chem., Int. Ed.* **2012**, *51*, 7640–7654.
- (40) Narita, A.; Wang, X.-Y.; Feng, X.; Müllen, K. New Advances in Nanographene Chemistry. *Chem. Soc. Rev.* **2015**, *44*, 6616–6643.
- (41) Segawa, Y.; Ito, H.; Itami, K. Structurally Uniform and Atomically Precise Carbon Nanostructures. *Nat. Rev. Mater.* **2016**, *1*, 15002.
- (42) Ito, H.; Ozaki, K.; Itami, K. Annulative π -Extension (APEX): Rapid Access to Fused Arenes, Heteroarenes, and Nanographenes. *Angew. Chem., Int. Ed.* **2017**, *56*, 11144–11164.
- (43) Pun, S. H.; Miao, Q. Toward Negatively Curved Carbons. *Acc. Chem. Res.* **2018**, *51*, 1630–1642.
- (44) Son, Y.-W.; Cohen, M. L.; Louie, S. G. Half-Metallic Graphene Nanoribbons. *Nature* **2006**, *444*, 347–349.
- (45) Wu, J.; Pisula, W.; Müllen, K. Graphenes as Potential Material for Electronics. *Chem. Rev.* **2007**, *107*, 718–747.
- (46) Avouris, P.; Chen, Z.; Perebeinos, V. Carbon-based electronics. *Nat. Nanotechnol.* **2007**, *2*, 605–615.
- (47) Li, X.; Wang, X.; Zhang, L.; Lee, S.; Dai, H. Chemically Derived, Ultrasmooth Graphene Nanoribbon Semiconductors. *Science* **2008**, *319*, 1229–1232.
- (48) Wang, X.; Zhi, L.; Tsao, N.; Tomović, Ž.; Li, J.; Müllen, K. Transparent Carbon Films as Electrodes in Organic Solar Cells. *Angew. Chem., Int. Ed.* **2008**, *47*, 2990–2992.
- (49) Kosynkin, D. V.; Higginbotham, A. L.; Sinitskii, A.; Lomeda, J. R.; Dimiev, A.; Price, B. K.; Tour, J. M. Longitudinal Unzipping of Carbon Nanotubes to Form Graphene Nanoribbons. *Nature* **2009**, *458*, 872–876.
- (50) Dutta, S.; Pati, S. K. Novel Properties of Graphene Nanoribbons: A Review. *J. Mater. Chem.* **2010**, *20*, 8207–8223.
- (51) Cai, J.; Ruffieux, P.; Jaafar, R.; Bieri, M.; Braun, T.; Blankenburg, S.; Muoth, M.; Seitsonen, A. P.; Saleh, M.; Feng, X.; et al. Atomically Precise Bottom-up Fabrication of Graphene Nanoribbons. *Nature* **2010**, *466*, 470–473.
- (52) Pisula, W.; Feng, X.; Müllen, K. Charge-Carrier Transporting Graphene-Type Molecules. *Chem. Mater.* **2011**, *23*, 554–567.
- (53) Müllen, K. Evolution of Graphene Molecules: Structural and Functional Complexity as Driving Forces behind Nanoscience. *ACS Nano* **2014**, *8*, 6531–6541.
- (54) Wang, Y.; Yang, R.; Shi, Z.; Zhang, L.; Shi, D.; Wang, E.; Zhang, G. Super-Elastic Graphene Ripples for Flexible Strain Sensors. *ACS Nano* **2011**, *5*, 3645–3650.
- (55) Zhao, J.; Wang, G.; Yang, R.; Lu, X.; Cheng, M.; He, C.; Xie, G.; Meng, J.; Shi, D.; Zhang, G. Tunable Piezoresistivity of Nanographene Films for Strain Sensing. *ACS Nano* **2015**, *9*, 1622–1629.
- (56) Jameh-Bozorghi, S.; Soleymanabadi, H. Warped C₈₀H₃₀ Nanographene as a Chemical Sensor for CO Gas: DFT Studies. *Phys. Lett. A* **2017**, *381*, 646–651.

- (57) Li, X.; Yu, J.; Wageh, S.; Al-Ghamdi, A. A.; Xie, J. Graphene in Photocatalysis: A Review. *Small* **2016**, *12*, 6640–6696.
- (58) Sun, X.; Liu, Z.; Welsher, K.; Robinson, J. T.; Goodwin, A.; Zaric, S.; Dai, H. Nano-Graphene Oxide for Cellular Imaging and Drug Delivery. *Nano Res.* **2008**, *1*, 203–212.
- (59) Liu, Z.; Robinson, J. T.; Sun, X.; Dai, H. PEGylated Nanographene Oxide for Delivery of Water-Insoluble Cancer Drugs. *J. Am. Chem. Soc.* **2008**, *130*, 10876–10877.
- (60) Yang, K.; Zhang, S.; Zhang, G.; Sun, X.; Lee, S.-T.; Liu, Z. Graphene in Mice: Ultrahigh In Vivo Tumor Uptake and Efficient Photothermal Therapy. *Nano Lett.* **2010**, *10*, 3318–3323.
- (61) Yang, K.; Wan, J.; Zhang, S.; Tian, B.; Zhang, Y.; Liu, Z. The Influence of Surface Chemistry and Size of Nanoscale Graphene Oxide on Photothermal Therapy of Cancer Using Ultra-Low Laser Power. *Biomaterials* **2012**, *33*, 2206–2214.
- (62) Yang, K.; Feng, L.; Shi, X.; Liu, Z. Nano-Graphene in Biomedicine: Theranostic Applications. *Chem. Soc. Rev.* **2013**, *42*, 530–547.
- (63) Lin, H.-A.; Sato, Y.; Segawa, Y.; Nishihara, T.; Sugimoto, N.; Scott, L. T.; Higashiyama, T.; Itami, K. A Water-Soluble Warped Nanographene: Synthesis and Applications for Photoinduced Cell Death. *Angew. Chem., Int. Ed.* **2018**, *57*, 2874–2878.
- (64) Stepien, M.; Gońska, E.; Żyła, M.; Sprutta, N. Heterocyclic Nanographenes and Other Polycyclic Heteroaromatic Compounds: Synthetic Routes, Properties, and Applications. *Chem. Rev.* **2017**, *117*, 3479–3716.
- (65) Kushida, Y.; Nagano, T.; Hanaoka, K. Silicon-Substituted Xanthene Dyes and Their Applications in Bioimaging. *Analyst* **2015**, *140*, 685–695.
- (66) Parke, S. M.; Boone, M. P.; Rivard, E. Marriage of Heavy Main Group Elements with π -Conjugated Materials for Optoelectronic Applications. *Chem. Commun.* **2016**, *52*, 9485–9505.
- (67) Usachov, D.; Vilkov, O.; Grüneis, A.; Haberer, D.; Fedorov, A.; Adamchuk, V. K.; Preobrajenski, A. B.; Dudin, P.; Barinov, A.; Oehzelt, M.; et al. Nitrogen-Doped Graphene: Efficient Growth, Structure, and Electronic Properties. *Nano Lett.* **2011**, *11*, 5401–5407.
- (68) Wang, H.; Maiyalagan, T.; Wang, X. Review on Recent Progress in Nitrogen-Doped Graphene: Synthesis, Characterization, and Its Potential Applications. *ACS Catal.* **2012**, *2*, 781–794.
- (69) Sahoo, M.; Sreena, K. P.; Vinayan, B. P.; Ramaprabhu, S. Green Synthesis of Boron Doped Graphene and Its Application as High Performance Anode Material in Li Ion Battery. *Mater. Res. Bull.* **2015**, *61*, 383–390.
- (70) Thirumal, V.; Pandurangan, A.; Jayavel, R.; Ilangoan, R. Synthesis and Characterization of Boron Doped Graphene Nanosheets for Supercapacitor Applications. *Synth. Met.* **2016**, *220*, 524–532.
- (71) Agnoli, S.; Favaro, M. Doping Graphene with Boron: A Review of Synthesis Methods, Physicochemical Characterization, and Emerging Applications. *J. Mater. Chem. A* **2016**, *4*, 5002–5025.
- (72) Xu, H.; Ma, L.; Jin, Z. Nitrogen-doped graphene: Synthesis, characterizations and energy applications. *J. Energy Chem.* **2018**, *27*, 146–160.
- (73) Yu, X.; Han, P.; Wei, Z.; Huang, L.; Gu, Z.; Peng, S.; Ma, J.; Zheng, G. Boron-Doped Graphene for Electrocatalytic N_2 Reduction. *Joule* **2018**, *2*, 1610–1622.
- (74) Panchakarla, L. S.; Subrahmanyam, K. S.; Saha, S. K.; Govindaraj, A.; Krishnamurthy, H. R.; Waghmare, U. V.; Rao, C. N. R. Synthesis, Structure, and Properties of Boron- and Nitrogen-Doped Graphene. *Adv. Mater.* **2009**, *21*, 4726–4730.
- (75) Wu, Z.-S.; Ren, W.; Xu, L.; Li, F.; Cheng, H.-M. Doped Graphene Sheets As Anode Materials with Superhigh Rate and Large Capacity for Lithium Ion Batteries. *ACS Nano* **2011**, *5*, 5463–5471.
- (76) Wang, H.; Zhou, Y.; Wu, D.; Liao, L.; Zhao, S.; Peng, H.; Liu, Z. Synthesis of Boron-Doped Graphene Monolayers Using the Sole Solid Feedstock by Chemical Vapor Deposition. *Small* **2013**, *9*, 1316–1320.
- (77) Zhao, L.; Levendorf, M.; Goncher, S.; Schiros, T.; Pálová, L.; Zabet-Khosousi, A.; Rim, K. T.; Gutiérrez, C.; Nordlund, D.; Jaye, C.; et al. Local Atomic and Electronic Structure of Boron Chemical Doping in Monolayer Graphene. *Nano Lett.* **2013**, *13*, 4659–4665.
- (78) Xing, M.; Fang, W.; Yang, X.; Tian, B.; Zhang, J. Highly-Dispersed Boron-Doped Graphene Nanoribbons with Enhanced Conductibility and Photocatalysis. *Chem. Commun.* **2014**, *50*, 6637–6640.
- (79) Tang, Y.-B.; Yin, L.-C.; Yang, Y.; Bo, X.-H.; Cao, Y.-L.; Wang, H.-E.; Zhang, W.-J.; Bello, I.; Lee, S.-T.; Cheng, H.-M.; et al. Tunable Band Gaps and p-Type Transport Properties of Boron-Doped Graphenes by Controllable Ion Doping Using Reactive Microwave Plasma. *ACS Nano* **2012**, *6*, 1970–1978.
- (80) Bronner, C.; Strelmali, S.; Gille, M.; Brause, F.; Haase, A.; Hecht, S.; Tegeder, P. Aligning the Band Gap of Graphene Nanoribbons by Monomer Doping. *Angew. Chem., Int. Ed.* **2013**, *52*, 4422–4425.
- (81) Cai, J.; Pignedoli, C. A.; Talirz, L.; Ruffieux, P.; Söde, H.; Liang, L.; Meunier, V.; Berger, R.; Li, R.; Feng, X.; et al. Graphene Nanoribbon Heterojunctions. *Nat. Nanotechnol.* **2014**, *9*, 896–900.
- (82) Arai, S.; Hida, M. In *Adv. Heterocycl. Chem.*; Katritzky, A. R., Ed.; Academic Press: New York, 1992; Vol. 55, pp 261–358.
- (83) Power, P. P. Persistent and Stable Radicals of the Heavier Main Group Elements and Related Species. *Chem. Rev.* **2003**, *103*, 789–810.
- (84) Zeng, Z.; Shi, X.; Chi, C.; López Navarrete, J. T.; Casado, J.; Wu, J. Pro-Aromatic and Anti-Aromatic π -Conjugated Molecules: An Irresistible Wish to Be Diradicals. *Chem. Soc. Rev.* **2015**, *44*, 6578–6596.
- (85) Saito, M.; Shinokubo, H.; Sakurai, H. Figuration of Bowl-Shaped π -Conjugated Molecules: Properties and Functions. *Mater. Chem. Front.* **2018**, *2*, 635–661.
- (86) Entwistle, C. D.; Marder, T. B. Boron Chemistry Lights the Way: Optical Properties of Molecular and Polymeric Systems. *Angew. Chem., Int. Ed.* **2002**, *41*, 2927–2931.
- (87) Jäkle, F. Lewis Acidic Organoboron Polymers. *Coord. Chem. Rev.* **2006**, *250*, 1107–1121.
- (88) Yamaguchi, S.; Wakamiya, A. Boron as a Key Component for New π -Electron Materials. *Pure Appl. Chem.* **2006**, *78*, 1413–1424.
- (89) Hudson, Z. M.; Wang, S. Impact of Donor–Acceptor Geometry and Metal Chelation on Photophysical Properties and Applications of Triarylboranes. *Acc. Chem. Res.* **2009**, *42*, 1584–1596.
- (90) Wade, C. R.; Broomsgrove, A. E. J.; Aldridge, S.; Gabbaï, F. P. Fluoride Ion Complexation and Sensing Using Organoboron Compounds. *Chem. Rev.* **2010**, *110*, 3958–3984.
- (91) Jäkle, F. Advances in the Synthesis of Organoborane Polymers for Optical, Electronic, and Sensory Applications. *Chem. Rev.* **2010**, *110*, 3985–4022.
- (92) Lorbach, A.; Hübner, A.; Wagner, M. Aryl(hydro)boranes: Versatile Building Blocks for Boron-Doped π -Electron Materials. *Dalton Trans.* **2012**, *41*, 6048–6063.
- (93) Escande, A.; Ingleson, M. J. Fused Polycyclic Aromatics Incorporating Boron in the Core: Fundamentals and Applications. *Chem. Commun.* **2015**, *51*, 6257–6274.
- (94) Wakamiya, A.; Yamaguchi, S. Designs of Functional π -Electron Materials based on the Characteristic Features of Boron. *Bull. Chem. Soc. Jpn.* **2015**, *88*, 1357–1377.
- (95) Ji, L.; Griesbeck, S.; Marder, T. B. Recent Developments in and Perspectives on Three-Coordinate Boron Materials: A Bright Future. *Chem. Sci.* **2017**, *8*, 846–863.
- (96) Su, Y.; Kinjo, R. Boron-Containing Radical Species. *Coord. Chem. Rev.* **2017**, *352*, 346–378.
- (97) vonGrotthuss, E.; John, A.; Kaese, T.; Wagner, M. Doping Polycyclic Aromatics with Boron for Superior Performance in Materials Science and Catalysis. *Asian J. Org. Chem.* **2018**, *7*, 37–53.
- (98) Mercier, L. G.; Piers, W. E.; Parvez, M. Benzo- and Naphthoborepins: Blue-Emitting Boron Analogues of Higher Acenes. *Angew. Chem., Int. Ed.* **2009**, *48*, 6108–6111.

- (99) Yamaguchi, S.; Shirasaka, T.; Akiyama, S.; Tamao, K. Dibenzoborole-Containing π -Electron Systems: Remarkable Fluorescence Change Based on the “On/Off” Control of the $p\pi-p\pi^*$ Conjugation. *J. Am. Chem. Soc.* **2002**, *124*, 8816–8817.
- (100) Caruso, A.; Siegler, M. A.; Tovar, J. D. Synthesis of Functionalizable Boron-Containing π -Electron Materials that Incorporate Formally Aromatic Fused Borepin Rings. *Angew. Chem., Int. Ed.* **2010**, *49*, 4213–4217.
- (101) Emslie, D. J. H.; Piers, W. E.; Parvez, M. 2,2'-Diborabiphenyl: A Lewis Acid Analogue of 2,2'-Bipyridine. *Angew. Chem., Int. Ed.* **2003**, *42*, 1252–1255.
- (102) Jaska, C. A.; Emslie, D. J. H.; Bosdet, M. J. D.; Piers, W. E.; Sorenson, T. S.; Parvez, M. Triphenylene Analogues with B2N2C2 Cores: Synthesis, Structure, Redox Behavior, and Photophysical Properties. *J. Am. Chem. Soc.* **2006**, *128*, 10885–10896.
- (103) Jaska, C. A.; Piers, W. E.; McDonald, R.; Parvez, M. Synthesis, Characterization, and Fluorescence Behavior of Twisted and Planar B2N2-Quaterphenyl Analogues. *J. Org. Chem.* **2007**, *72*, 5234–5243.
- (104) Bosdet, M. J. D.; Piers, W. E.; Sorenson, T. S.; Parvez, M. 10a-Aza-10b-borapyrroles: Heterocyclic Analogs of Pyrene with Internalized BN Moieties. *Angew. Chem., Int. Ed.* **2007**, *46*, 4940–4943.
- (105) Bosdet, M. J. D.; Piers, W. E.; Sorenson, T. S.; Parvez, M. 5b,7b-Diaza-3b,9b-diborabenzo[ghi]perlyenes. *Can. J. Chem.* **2010**, *88*, 426–433.
- (106) Wang, X.-Y.; Lin, H.-R.; Lei, T.; Yang, D.-C.; Zhuang, F.-D.; Wang, J.-Y.; Yuan, S.-C.; Pei, J. Azaborine Compounds for Organic Field-Effect Transistors: Efficient Synthesis, Remarkable Stability, and BN Dipole Interactions. *Angew. Chem., Int. Ed.* **2013**, *52*, 3117–3120.
- (107) Wang, X.-Y.; Zhuang, F.-D.; Zhou, X.; Yang, D.-C.; Wang, J.-Y.; Pei, J. Influence of Alkyl Chain Length on the Solid-State Properties and Transistor Performance of BN-Substituted Tetrathienonaphthalenes. *J. Mater. Chem. C* **2014**, *2*, 8152–8161.
- (108) Wang, X.-Y.; Zhuang, F.-D.; Wang, R.-B.; Wang, X.-C.; Cao, X.-Y.; Wang, J.-Y.; Pei, J. A Straightforward Strategy toward Large BN-Embedded π -Systems: Synthesis, Structure, and Optoelectronic Properties of Extended BN Heterosuperbenzenes. *J. Am. Chem. Soc.* **2014**, *136*, 3764–3767.
- (109) Wang, X.-Y.; Zhuang, F.-D.; Wang, J.-Y.; Pei, J. Incorporation of Polycyclic Azaborine Compounds into Polythiophene-Type Conjugated Polymers for Organic Field-Effect Transistors. *Chem. Commun.* **2015**, *51*, 17532–17535.
- (110) Wang, X.-Y.; Wang, J.-Y.; Pei, J. BN Heterosuperbenzenes: Synthesis and Properties. *Chem. - Eur. J.* **2015**, *21*, 3528–3539.
- (111) Abbey, E. R.; Lamm, A. N.; Baggett, A. W.; Zakharov, L. N.; Liu, S.-Y. Protecting Group-Free Synthesis of 1,2-Azaborines: A Simple Approach to the Construction of BN-Benzoidoids. *J. Am. Chem. Soc.* **2013**, *135*, 12908–12913.
- (112) Krieg, M.; Reicherter, F.; Haiss, P.; Ströbele, M.; Eichele, K.; Treanor, M.-J.; Schaub, R.; Bettinger, H. F. Construction of an Internally B3N3-Doped Nanographene Molecule. *Angew. Chem., Int. Ed.* **2015**, *54*, 8284–8286.
- (113) Dosso, J.; Tasserou, J.; Fasano, F.; Marinelli, D.; Biot, N.; Fermi, A.; Bonifazi, D. Synthesis and Optoelectronic Properties of Hexa-peri-hexabenzoborazinocoronene. *Angew. Chem., Int. Ed.* **2017**, *56*, 4483–4487.
- (114) Hatakeyama, T.; Hashimoto, S.; Seki, S.; Nakamura, M. Synthesis of BN-Fused Polycyclic Aromatics via Tandem Intramolecular Electrophilic Arene Borylation. *J. Am. Chem. Soc.* **2011**, *133*, 18614–18617.
- (115) Hatakeyama, T.; Hashimoto, S.; Oba, T.; Nakamura, M. Azaboradibenzo[6]helicene: Carrier Inversion Induced by Helical Homochirality. *J. Am. Chem. Soc.* **2012**, *134*, 19600–19603.
- (116) Nakatsuka, S.; Yasuda, N.; Hatakeyama, T. Four-Step Synthesis of B2N2-Embedded Corannulene. *J. Am. Chem. Soc.* **2018**, *140*, 13562–13565.
- (117) Wadle, J. J.; McDermott, L. B.; Fort, E. H. Microwave Assisted Synthesis of 10b-Aza-10c-Borapyrrole. *Tetrahedron Lett.* **2014**, *55*, 445–447.
- (118) Jaye, J. A.; Gelinas, B. S.; McCormick, G. M.; Fort, E. H. Implications of the Final Ring Closure to 10b-Aza-10c-Borapyrrole for Aryl-Alkyne Ring-Closing Mechanisms. *Can. J. Chem.* **2017**, *95*, 357–362.
- (119) Li, C.; Liu, Y.; Sun, Z.; Zhang, J.; Liu, M.; Zhang, C.; Zhang, Q.; Wang, H.; Liu, X. Synthesis, Characterization, and Properties of Bis-BN Ullazines. *Org. Lett.* **2018**, *20*, 2806–2810.
- (120) Liu, Z.; Marder, T. B. B-N versus C-C: How Similar Are They? *Angew. Chem., Int. Ed.* **2008**, *47*, 242–244.
- (121) Bosdet, M. J. D.; Piers, W. E. B-N as a C-C Substitute in Aromatic Systems. *Can. J. Chem.* **2009**, *87*, 8–29.
- (122) Bonifazi, D.; Fasano, F.; Lorenzo-Garcia, M. M.; Marinelli, D.; Oubaha, H.; Tasserou, J. Boron–Nitrogen Doped Carbon Scaffolding: Organic Chemistry, Self-Assembly and Materials Applications of Borazine and its Derivatives. *Chem. Commun.* **2015**, *51*, 15222–15236.
- (123) Wang, J.-Y.; Pei, J. BN-Embedded Aromatics for Optoelectronic Applications. *Chin. Chem. Lett.* **2016**, *27*, 1139–1146.
- (124) Huang, J.; Li, Y. BN Embedded Polycyclic π -Conjugated Systems: Synthesis, Optoelectronic Properties, and Photovoltaic Applications. *Front. Chem.* **2018**, *6*. DOI: [10.3389/fchem.2018.00341](https://doi.org/10.3389/fchem.2018.00341)
- (125) Okada, K.; Inokawa, H.; Sugawa, T.; Oda, M. Synthesis and Conformational Analysis of a 2,2': 6',2": 6",6-Tris(ethano)-triarylborane. *J. Chem. Soc., Chem. Commun.* **1992**, *0*, 448–449.
- (126) Zhou, Z.; Wakamiya, A.; Kushida, T.; Yamaguchi, S. Planarized Triarylboranes: Stabilization by Structural Constraint and Their Plane-to-Bowl Conversion. *J. Am. Chem. Soc.* **2012**, *134*, 4529–4532.
- (127) Bieller, S.; Zhang, F.; Bolte, M.; Bats, J. W.; Lerner, H.-W.; Wagner, M. Bitopic Bis- and Tris(1-pyrazolyl)borate Ligands: Syntheses and Structural Characterization. *Organometallics* **2004**, *23*, 2107–2113.
- (128) Kirschner, S.; Mewes, J.-M.; Bolte, M.; Lerner, H.-W.; Dreuw, A.; Wagner, M. How Boron Doping Shapes the Optoelectronic Properties of Canonical and Phenylene-Containing Oligoacenes: A Combined Experimental and Theoretical Investigation. *Chem. - Eur. J.* **2017**, *23*, 5104–5116.
- (129) Chiu, C.-W.; Kim, Y.; Gabbaï, F. P. Lewis Acidity Enhancement of Triarylboranes via Peripheral Decoration with Cationic Groups. *J. Am. Chem. Soc.* **2009**, *131*, 60–61.
- (130) Kushida, T.; Camacho, C.; Shuto, A.; Irle, S.; Muramatsu, M.; Katayama, T.; Ito, S.; Nagasawa, Y.; Miyasaka, H.; Sakuda, E.; et al. Constraint-Induced Structural Deformation of Planarized Triphenylboranes in the Excited State. *Chem. Sci.* **2014**, *5*, 1296–1304.
- (131) Kushida, T.; Yamaguchi, S. A Radical Anion of Structurally Constrained Triphenylborane. *Organometallics* **2013**, *32*, 6654–6657.
- (132) Olmstead, M. M.; Power, P. P. First Structural Characterization of a Boron-Centered Radical: X-Ray Crystal Structure of $[Li(12\text{-Crown-}4)_2]^+ [Mes_3B]^{*-}$. *J. Am. Chem. Soc.* **1986**, *108*, 4235–4236.
- (133) Leffler, J. E.; Watts, G. B.; Tanigaki, T.; Dolan, E.; Miller, D. S. Triarylboron Anion Radicals and the Reductive Cleavage of Boron Compounds. *J. Am. Chem. Soc.* **1970**, *92*, 6825–6830.
- (134) Neugebauer, F. A.; Hellwinkel, D.; Aulmich, G. E.S.R. Study of 12,12c-Dihydro-4,4,8,8,12,12-Hexamethyl-4H, 8H-Dibenzo [cd,mn] Pyren-12c-yl, a Planar Triphenylmethyl. *Tetrahedron Lett.* **1978**, *19*, 4871–4874.
- (135) Kushida, T.; Zhou, Z.; Wakamiya, A.; Yamaguchi, S. Planarized B-Phenylborataanthracene Anions: Structural and Electronic Impacts of Coplanar Constraint. *Chem. Commun.* **2012**, *48*, 10715–10717.
- (136) Shuto, A.; Kushida, T.; Fukushima, T.; Kaji, H.; Yamaguchi, S. π -Extended Planarized Triphenylboranes with Thiophene Spacers. *Org. Lett.* **2013**, *15*, 6234–6237.
- (137) Tomokatsu, K.; Ayumi, S.; Masafumi, Y.; Takashi, K.; Shigehiro, Y. A Planarized Triphenylborane Mesogen: Discotic Liquid Crystals with Ambipolar Charge Carrier Transport Properties. *Angew. Chem., Int. Ed.* **2015**, *54*, 6922–6925.

- (138) Hertz, V. M.; Ando, N.; Hirai, M.; Bolte, M.; Lerner, H.-W.; Yamaguchi, S.; Wagner, M. Steric Shielding vs Structural Constraint in a Boron-Containing Polycyclic Aromatic Hydrocarbon. *Organometallics* **2017**, *36*, 2512–2519.
- (139) Hertz, V. M.; Bolte, M.; Lerner, H.-W.; Wagner, M. Boron-Containing Polycyclic Aromatic Hydrocarbons: Facile Synthesis of Stable, Redox-Active Luminophores. *Angew. Chem., Int. Ed.* **2015**, *54*, 8800–8804.
- (140) Hertz, V. M.; Massoth, J. G.; Bolte, M.; Lerner, H.-W.; Wagner, M. En Route to Stimuli-Responsive Boron-, Nitrogen-, and Sulfur-Doped Polycyclic Aromatic Hydrocarbons. *Chem. - Eur. J.* **2016**, *22*, 13181–13188.
- (141) Kushida, T.; Shirai, S.; Ando, N.; Okamoto, T.; Ishii, H.; Matsui, H.; Yamagishi, M.; Uemura, T.; Tsurumi, J.; Watanabe, S.; et al. Boron-Stabilized Planar Neutral π -Radicals with Well-Balanced Ambipolar Charge-Transport Properties. *J. Am. Chem. Soc.* **2017**, *139*, 14336–14339.
- (142) Hellwinkel, D.; Aulmich, G.; Melan, M. Polycyclen vom Triangulen-Typ, III1 Dreifach Ortho-verbrückte Triphenylmethan-Derivate. *Chem. Ber.* **1981**, *114*, 86–108.
- (143) Crossley, D. L.; Kahan, R. J.; Endres, S.; Warner, A. J.; Smith, R. A.; Cid, J.; Dunsford, J. J.; Jones, J. E.; Vitorica-Yrezabal, I.; Ingleson, M. J. A Modular Route to Boron Doped PAHs by Combining Borylative Cyclisation and Electrophilic C–H Borylation. *Chem. Sci.* **2017**, *8*, 7969–7977.
- (144) Warner, A. J.; Lawson, J. R.; Fasano, V.; Ingleson, M. J. Formation of C(sp²)-Boronate Esters by Borylative Cyclization of Alkynes Using BCl₃. *Angew. Chem., Int. Ed.* **2015**, *54*, 11245–11249.
- (145) Ando, N.; Kushida, T.; Yamaguchi, S. A Planarized B-Phenyldibenzoborepin: Impact of Structural Constraint on Its Electronic Properties and Lewis Acidity. *Chem. Commun.* **2018**, *54*, 5213–5216.
- (146) Messersmith, R. E.; Tovar, J. D. Assessment of the Aromaticity of Borepin Rings by Spectroscopic, Crystallographic and Computational Methods: A Historical Overview. *J. Phys. Org. Chem.* **2015**, *28*, 378–387.
- (147) Saito, S.; Matsuo, K.; Yamaguchi, S. Polycyclic π -Electron System with Boron at Its Center. *J. Am. Chem. Soc.* **2012**, *134*, 9130–9133.
- (148) Matsuo, K.; Saito, S.; Yamaguchi, S. Photodissociation of B–N Lewis Adducts: A Partially Fused Trinaphthylborane with Dual Fluorescence. *J. Am. Chem. Soc.* **2014**, *136*, 12580–12583.
- (149) Matsuo, K.; Saito, S.; Yamaguchi, S. A Soluble Dynamic Complex Strategy for the Solution Processed Fabrication of Organic Thin Film Transistors of a Boron Containing Polycyclic Aromatic Hydrocarbon. *Angew. Chem., Int. Ed.* **2016**, *55*, 11984–11988.
- (150) Schickedanz, K.; Trageser, T.; Bolte, M.; Lerner, H.-W.; Wagner, M. A Boron-Doped Helicene as a Highly Soluble, Benchtop-Stable Green Emitter. *Chem. Commun.* **2015**, *51*, 15808–15810.
- (151) Miyamoto, F.; Nakatsuka, S.; Yamada, K.; Nakayama, K.-i.; Hatakeyama, T. Synthesis of Boron-Doped Polycyclic Aromatic Hydrocarbons by Tandem Intramolecular Electrophilic Arene Borylation. *Org. Lett.* **2015**, *17*, 6158–6161.
- (152) Escande, A.; Crossley, D. L.; Cid, J.; Cade, I. A.; Vitorica-Yrezabal, I.; Ingleson, M. J. Inter- and intra-molecular C–H borylation for the formation of PAHs containing triarylborane and indole units. *Dalton Trans.* **2016**, *45*, 17160–17167.
- (153) Kitamoto, Y.; Suzuki, T.; Miyata, Y.; Kita, H.; Funaki, K.; Oi, S. The First Synthesis and X-Ray Crystallographic Analysis of an Oxygen-Bridged Planarized Triphenylborane. *Chem. Commun.* **2016**, *52*, 7098–7101.
- (154) Dileesh, S.; Gopidas, K. R. Photophysical and Electron Transfer Studies of a Stable Carbocation. *Chem. Phys. Lett.* **2000**, *330*, 397–402.
- (155) Reynisson, J.; Wilbrandt, R.; Brinck, V.; Laursen, B. W.; Nørgaard, K.; Harrit, N.; Brouwer, A. M. Photophysics of trioxatriangulenium ion. Electrophilic reactivity in the ground state and excited singlet state. *Photochem. Photobiol. Sci.* **2002**, *1*, 763–773.
- (156) Nakatsuka, S.; Gotoh, H.; Kinoshita, K.; Yasuda, N.; Hatakeyama, T. Divergent Synthesis of Heteroatom Centered 4,8,12 Triazatriangulenes. *Angew. Chem., Int. Ed.* **2017**, *56*, 5087–5090.
- (157) Hatakeyama, T.; Shiren, K.; Nakajima, K.; Nomura, S.; Nakatsuka, S.; Kinoshita, K.; Ni, J.; Ono, Y.; Ikuta, T. Ultrapure Blue Thermally Activated Delayed Fluorescence Molecules: Efficient HOMO–LUMO Separation by the Multiple Resonance Effect. *Adv. Mater.* **2016**, *28*, 2777–2781.
- (158) Liang, X.; Yan, Z.-P.; Han, H.-B.; Wu, Z.-G.; Zheng, Y.-X.; Meng, H.; Zuo, J.-L.; Huang, W. Peripheral Amplification of Multi-Resonance Induced Thermally Activated Delayed Fluorescence for Highly Efficient OLEDs. *Angew. Chem., Int. Ed.* **2018**, *57*, 11316–11320.
- (159) Hirai, H.; Nakajima, K.; Nakatsuka, S.; Shiren, K.; Ni, J.; Nomura, S.; Ikuta, T.; Hatakeyama, T. One-Step Borylation of 1,3-Diaryloxybenzenes Towards Efficient Materials for Organic Light-Emitting Diodes. *Angew. Chem., Int. Ed.* **2015**, *54*, 13581–13585.
- (160) Fujimoto, K.; Oh, J.; Yorimitsu, H.; Kim, D.; Osuka, A. Directly Diphenylborane-Fused Porphyrins. *Angew. Chem., Int. Ed.* **2016**, *55*, 3196–3199.
- (161) Fujimoto, K.; Yorimitsu, H.; Osuka, A. Porphyrinylboranes Synthesized via Porphyrinylolithiums. *Chem. - Eur. J.* **2015**, *21*, 11311–11314.
- (162) Berger, C.; Song, Z.; Li, X.; Wu, X.; Brown, N.; Naud, C.; Mayou, D.; Li, T.; Hass, J.; Marchenkov, A. N.; et al. Electronic Confinement and Coherence in Patterned Epitaxial Graphene. *Science* **2006**, *312*, 1191–1196.
- (163) Dou, C.; Saito, S.; Matsuo, K.; Hisaki, I.; Yamaguchi, S. A Boron-Containing PAH as a Substructure of Boron-Doped Graphene. *Angew. Chem., Int. Ed.* **2012**, *51*, 12206–12210.
- (164) Osumi, S.; Saito, S.; Dou, C.; Matsuo, K.; Kume, K.; Yoshikawa, H.; Awaga, K.; Yamaguchi, S. Boron-Doped Nanographene: Lewis Acidity, Redox Properties, and Battery Electrode Performance. *Chem. Sci.* **2016**, *7*, 219–227.
- (165) Dai, J.; Yuan, J.; Giannozzi, P. Gas Adsorption on Graphene Doped with B, N, Al, and S: A Theoretical Study. *Appl. Phys. Lett.* **2009**, *95*, 232105.
- (166) Matsui, K.; Oda, S.; Yoshiura, K.; Nakajima, K.; Yasuda, N.; Hatakeyama, T. One-Shot Multiple Borylation toward BN-Doped Nanographenes. *J. Am. Chem. Soc.* **2018**, *140*, 1195–1198.
- (167) Kawai, S.; Saito, S.; Osumi, S.; Yamaguchi, S.; Foster, A. S.; Spijker, P.; Meyer, E. Atomically Controlled Substitutional Boron-Doping of Graphene Nanoribbons. *Nat. Commun.* **2015**, *6*, 8098.
- (168) Cloke, R. R.; Marangoni, T.; Nguyen, G. D.; Joshi, T.; Rizzo, D. J.; Bronner, C.; Cao, T.; Louie, S. G.; Crommie, M. F.; Fischer, F. R. Site-Specific Substitutional Boron Doping of Semiconducting Armchair Graphene Nanoribbons. *J. Am. Chem. Soc.* **2015**, *137*, 8872–8875.
- (169) Carbonell-Sanromà, E.; Garcia-Lekue, A.; Corso, M.; Vasseur, G.; Brandimarte, P.; Lobo-Checa, J.; de Oteyza, D. G.; Li, J.; Kawai, S.; Saito, S.; et al. Electronic Properties of Substitutionally Boron-Doped Graphene Nanoribbons on a Au(111) Surface. *J. Phys. Chem. C* **2018**, *122*, 16092–16099.
- (170) Kawai, S.; Nakatsuka, S.; Hatakeyama, T.; Pawlak, R.; Meier, T.; Tracey, J.; Meyer, E.; Foster, A. S. Multiple Heteroatom Substitution to Graphene Nanoribbon. *Sci. Adv.* **2018**, *4*, No. eaar7181.
- (171) Shiota, Y. Photo- and Electroactive Amorphous Molecular Materials—Molecular Design, Syntheses, Reactions, Properties, and Applications. *J. Mater. Chem.* **2005**, *15*, 75–93.
- (172) Shiota, Y.; Kageyama, H. Charge Carrier Transporting Molecular Materials and Their Applications in Devices. *Chem. Rev.* **2007**, *107*, 953–1010.
- (173) Wang, J.; Liu, K.; Ma, L.; Zhan, X. Triarylamine: Versatile Platform for Organic, Dye-Sensitized, and Perovskite Solar Cells. *Chem. Rev.* **2016**, *116*, 14675–14725.

- (174) Yang, S.; Fu, W.; Zhang, Z.; Chen, H.; Li, C.-Z. Recent Advances in Perovskite Solar Cells: Efficiency, Stability and Lead-Free Perovskite. *J. Mater. Chem. A* **2017**, *5*, 11462–11482.
- (175) Sobolev, A. N.; Belsky, V. K.; Romm, I. P.; Chernikova, N. Y.; Guryanova, E. N. Structural Investigation of the Triaryl Derivatives of the Group V Elements. IX. Structure of Triphenylamine, $C_{18}H_{15}N$. *Acta Crystallogr., Sect. C: Cryst. Struct. Commun.* **1985**, *41*, 967–971.
- (176) Pan, J.-H.; Chiu, H.-L.; Chen, L.; Wang, B.-C. Theoretical Investigations of Triphenylamine Derivatives as Hole Transporting Materials in OLEDs: Correlation of the Hammett Parameter of the Substituent to Ionization Potential, and Reorganization Energy Level. *Comput. Mater. Sci.* **2006**, *38*, 105–112.
- (177) Cias, P.; Slugovc, C.; Gescheidt, G. Hole Transport in Triphenylamine Based OLED Devices: From Theoretical Modeling to Properties Prediction. *J. Phys. Chem. A* **2011**, *115*, 14519–14525.
- (178) Hammer, N.; Schaub, T. A.; Meinhardt, U.; Kivala, M. N-Heterotriangulenes: Fascinating Relatives of Triphenylamine. *Chem. Rec.* **2015**, *15*, 1119–1131.
- (179) Hellwinkel, D.; Schmidt, W. Modifizierte Tetrahelicen-Systeme, III. Zweifach ortho-verbrückte Triphenylamin-Derivate. *Chem. Ber.* **1980**, *113*, 358–384.
- (180) Hellwinkel, D.; Melan, M. Heteropolycyclen vom Triangulen Typ, I. 8.12 Dihydro 4H benzo[1.9]chinolizino[3.4.5.6.7 defg]acridin trion (4.8.12) und 5.9 Dihydro chino[3.2.1 de]acridin dion (5.9). *Chem. Ber.* **1971**, *104*, 1001–1016.
- (181) Field, J. E.; Venkataraman, D. Heterotriangulenes Structure and Properties. *Chem. Mater.* **2002**, *14*, 962–964.
- (182) Zhang, H.; Wang, S.; Li, Y.; Zhang, B.; Du, C.; Wan, X.; Chen, Y. Synthesis, Characterization, and Electroluminescent Properties of Star Shaped Donor–acceptor Dendrimers with Carbazole Dendrons as Peripheral Branches and Heterotriangulene as Central Core. *Tetrahedron* **2009**, *65*, 4455–4463.
- (183) Zhang, H.; Li, Y.; Wan, X.; Chen, Y. Two-Level Self-Assembly from Nanowires to Microrods Based on a Heterotriangulene Derivative. *Chem. Phys. Lett.* **2009**, *479*, 117–119.
- (184) Wan, X.; Zhang, H.; Li, Y.; Chen, Y. Self-Assembly Based on Heterotriangulene Derivatives: From Nanowires to Microrods. *New J. Chem.* **2010**, *34*, 661–666.
- (185) Kivala, M.; Pisula, W.; Wang, S.; Mavrinskiy, A.; Gisselbrecht, J. P.; Feng, X.; Müllen, K. Columnar Self Assembly in Electron Deficient Heterotriangulenes. *Chem. - Eur. J.* **2013**, *19*, 8117–8128.
- (186) Wang, S.; Kivala, M.; Lieberwirth, I.; Kirchhoff, K.; Feng, X.; Pisula, W.; Müllen, K. Dip-Coating-Induced Fiber Growth of a Soluble Heterotriangulene. *ChemPhysChem* **2011**, *12*, 1648–1651.
- (187) Inagi, S.; Kaihatsu, N.; Kurabayashi, S.; Fuchigami, T. Heterotriangulene as an Electron-transfer Mediator in Reduction of vic-Dibromide Compounds. *Chem. Lett.* **2013**, *42*, 846–848.
- (188) Haedler, A. T.; Beyer, S. R.; Hammer, N.; Hildner, R.; Kivala, M.; Köhler, J.; Schmidt, H.-W. Synthesis and Photophysical Properties of Multichromophoric Carbonyl-Bridged Triarylamines. *Chem. - Eur. J.* **2014**, *20*, 11708–11718.
- (189) Reger, D. L.; Debreczeni, A.; Reinecke, B.; Rassolov, V.; Smith, M. D.; Semeniuc, R. F. Highly Organized Structures and Unusual Magnetic Properties of Paddlewheel Copper(II) Carboxylate Dimers Containing the π - π Stacking, 1,8-Naphthalimide Synthon. *Inorg. Chem.* **2009**, *48*, 8911–8924.
- (190) Haedler, A. T.; Kreger, K.; Issac, A.; Wittmann, B.; Kivala, M.; Hammer, N.; Köhler, J.; Schmidt, H.-W.; Hildner, R. Long-Range Energy Transport in Single Supramolecular Nanofibres at Room Temperature. *Nature* **2015**, *523*, 196.
- (191) Haedler, A. T.; Meskers, S. C. J.; Zha, R. H.; Kivala, M.; Schmidt, H.-W.; Meijer, E. W. Pathway Complexity in the Enantioselective Self-Assembly of Functional Carbonyl-Bridged Triarylamine Trisamides. *J. Am. Chem. Soc.* **2016**, *138*, 10539–10545.
- (192) Chou, C.-M.; Saito, S.; Yamaguchi, S. Heterotriangulenes π -Expanded at Bridging Positions. *Org. Lett.* **2014**, *16*, 2868–2871.
- (193) Guldi, D. M.; Hungerbuehler, H.; Janata, E.; Asmus, K. D. Redox Processes and Alkylation Reactions of Fullerene C_{60} as Studied by Pulse Radiolysis. *J. Phys. Chem.* **1993**, *97*, 11258–11264.
- (194) Hammer, N.; Shubina, T. E.; Gisselbrecht, J.-P.; Hampel, F.; Kivala, M. Synthesis and Properties of Arylvinylidene-Bridged Triphenylamines. *J. Org. Chem.* **2015**, *80*, 2418–2424.
- (195) Jesberger, M.; Davis, T. P.; Barner, L. Applications of Lawesson's Reagent in Organic and Organometallic Syntheses. *Synthesis* **2003**, *2003*, 1929–1958.
- (196) Levy, A.; Biedermann, P. U.; Cohen, S.; Agranat, I. Stereochemistry of Selenium- and Tellurium-Bridged Heteromeric Bistricyclic Aromatic Enes. The Fluorenylidenechalcoxanthene Series. *J. Chem. Soc., Perkin Trans. 2* **2001**, 2329–2341.
- (197) Hellwinkel, D.; Melan, M. Heteropolycyclen vom Triangulen Typ, II. Zur Stereochemie verbrückter Triarylamine. *Chem. Ber.* **1974**, *107*, 616–626.
- (198) Fang, Z.; Zhang, X.; Hing Lai, Y.; Liu, B. Bridged Triphenylamine Based Molecules with Large Two-Photon Absorption Cross Sections in Organic and Aqueous Media. *Chem. Commun.* **2009**, 920–922.
- (199) Schlüter, F.; Rossel, F.; Kivala, M.; Enkelmann, V.; Gisselbrecht, J.-P.; Ruffieux, P.; Fasel, R.; Müllen, K. π -Conjugated Heterotriangulene Macrocycles by Solution and Surface-supported Synthesis Toward Honeycomb Networks. *J. Am. Chem. Soc.* **2013**, *135*, 4550–4557.
- (200) Fang, Z.; Webster, R. D.; Samoc, M.; Lai, Y.-H. Tuning Two-Photon Absorption Cross-Sections for Triphenylamine Derivatives. *RSC Adv.* **2013**, *3*, 17914–17917.
- (201) Fang, Z.; Teo, T.-L.; Cai, L.; Lai, Y.-H.; Samoc, A.; Samoc, M. Bridged Triphenylamine-Based Dendrimers: Tuning Enhanced Two-Photon Absorption Performance with Locked Molecular Planarity. *Org. Lett.* **2009**, *11*, 1–4.
- (202) Xu, C.; Zipfel, W.; Shear, J. B.; Williams, R. M.; Webb, W. W. Multiphoton Fluorescence Excitation: New Spectral Windows for Biological Nonlinear Microscopy. *Proc. Natl. Acad. Sci. U. S. A.* **1996**, *93*, 10763–10768.
- (203) Larson, D. R.; Zipfel, W. R.; Williams, R. M.; Clark, S. W.; Bruchez, M. P.; Wise, F. W.; Webb, W. W. Water-Soluble Quantum Dots for Multiphoton Fluorescence Imaging in Vivo. *Science* **2003**, *300*, 1434–1436.
- (204) Fang, Z.; Chellappan, V.; Webster, R. D.; Ke, L.; Zhang, T.; Liu, B.; Lai, Y.-H. Bridged-Triarylamine Starburst Oligomers as Hole Transporting Materials for Electroluminescent Devices. *J. Mater. Chem.* **2012**, *22*, 15397–15404.
- (205) Paek, S.; Cho, N.; Cho, S.; Lee, J. K.; Ko, J. Planar Star-Shaped Organic Semiconductor with Fused Triphenylamine Core for Solution-Processed Small-Molecule Organic Solar Cells and Field-Effect Transistors. *Org. Lett.* **2012**, *14*, 6326–6329.
- (206) Qin, P.; Paek, S.; Dar, M. I.; Pellet, N.; Ko, J.; Grätzel, M.; Nazeeruddin, M. K. Perovskite Solar Cells with 12.8% Efficiency by Using Conjugated Quinolizino Acridine Based Hole Transporting Material. *J. Am. Chem. Soc.* **2014**, *136*, 8516–8519.
- (207) Paek, S.; Choi, H.; Sim, J.; Song, K.; Lee, J. K.; Ko, J. Efficient Organic Solar Cells with Star-Shaped Small Molecules Comprising of Planar Donating Core and Accepting Edges. *J. Phys. Chem. C* **2014**, *118*, 27193–27200.
- (208) Lim, K.; Lee, S. Y.; Song, K.; Sharma, G. D.; Ko, J. Synthesis and Properties of Low Bandgap Star Molecules TPA-[DTS-PyBTTh₃]₃ and DMM-TPA[DTS-PyBTTh₃]₃ for Solution-processed Bulk Heterojunction Organic Solar Cells. *J. Mater. Chem. C* **2014**, *2*, 8412–8422.
- (209) Cho, N.; Paek, S.; Jeon, J.; Song, K.; Sharma, G. D.; Ko, J. Synthesis, Optical and Electrochemical Properties of Small Molecules DMM-TPA[DTS(FBTTh₃)₃] and TPA[DTS(FBTTh₃)₃], and Their Application as Donors for Bulk Heterojunction Solar Cells. *J. Mater. Chem. A* **2014**, *2*, 12368–12379.
- (210) Fantacci, S.; De Angelis, F.; Nazeeruddin, M. K.; Grätzel, M. Electronic and Optical Properties of the Spiro-MeOTAD Hole Conductor in Its Neutral and Oxidized Forms: A DFT/TDDFT Investigation. *J. Phys. Chem. C* **2011**, *115*, 23126–23133.
- (211) Choi, H.; Park, S.; Paek, S.; Ekanayake, P.; Nazeeruddin, M. K.; Ko, J. Efficient Star-Shaped Hole Transporting Materials with

- Diphenylethenyl Side Arms for an Efficient Perovskite Solar Cell. *J. Mater. Chem. A* **2014**, *2*, 19136–19140.
- (212) Choi, H.; Paek, S.; Lim, N.; Lee, Y. H.; Nazeeruddin, M. K.; Ko, J. Efficient Perovskite Solar Cells with 13.63% Efficiency Based on Planar Triphenylamine Hole Conductors. *Chem. - Eur. J.* **2014**, *20*, 10894–10899.
- (213) Choi, H.; Cho, J. W.; Kang, M.-S.; Ko, J. Stable and Efficient Hole Transporting Materials with a Dimethylfluorenylamino Moiety for Perovskite Solar Cells. *Chem. Commun.* **2015**, *51*, 9305–9308.
- (214) Choi, H.; Baik, C.; Kang, S. O.; Ko, J.; Kang, M.-S.; Nazeeruddin, M. K.; Grätzel, M. Highly Efficient and Thermally Stable Organic Sensitizers for Solvent-Free Dye-Sensitized Solar Cells. *Angew. Chem., Int. Ed.* **2008**, *47*, 327–330.
- (215) Kim, D.; Kim, C.; Choi, H.; Song, K.; Kang, M.-S.; Ko, J. A New Class of Organic Sensitizers with Fused Planar Triphenylamine for Nanocrystalline Dye Sensitized Solar Cells. *J. Photochem. Photobiol., A* **2011**, *219*, 122–131.
- (216) Do, K.; Kim, D.; Cho, N.; Paek, S.; Song, K.; Ko, J. New Type of Organic Sensitizers with a Planar Amine Unit for Efficient Dye-Sensitized Solar Cells. *Org. Lett.* **2012**, *14*, 222–225.
- (217) Cai, L.; Tsao, H. N.; Zhang, W.; Wang, L.; Xue, Z.; Grätzel, M.; Liu, B. Organic Sensitizers with Bridged Triphenylamine Donor Units for Efficient Dye-Sensitized Solar Cells. *Adv. Energy Mater.* **2013**, *3*, 200–205.
- (218) Makarov, N. S.; Mukhopadhyay, S.; Yesudas, K.; Brédas, J.-L.; Perry, J. W.; Pron, A.; Kivala, M.; Müllen, K. Impact of Electronic Coupling, Symmetry, and Planarization on One- and Two-Photon Properties of Triarylamines with One, Two, or Three Diarylboryl Acceptors. *J. Phys. Chem. A* **2012**, *116*, 3781–3793.
- (219) Meinhardt, U.; Lodermeyer, F.; Schaub, T. A.; Kunzmann, A.; Dral, P. O.; Sale, A. C.; Hampel, F.; Guldi, D. M.; Costa, R. D.; Kivala, M. N-Heterotriangulene Chromophores with 4-Pyridyl Anchors for Dye-Sensitized Solar Cells. *RSC Adv.* **2016**, *6*, 67372–67377.
- (220) Shores, M. P.; Sokol, J. J.; Long, J. R. Nickel(II)–Molybdenum(III)–Cyanide Clusters: Synthesis and Magnetic Behavior of Species Incorporating $[(\text{Me}_3\text{tacn})\text{Mo}(\text{CN})_3]$. *J. Am. Chem. Soc.* **2002**, *124*, 2279–2292.
- (221) Fendt, L.-A.; Stöhr, M.; Wintjes, N.; Enache, M.; Jung, T. A.; Diederich, F. Modification of Supramolecular Binding Motifs Induced By Substrate Registry: Formation of Self-Assembled Macrocycles and Chain-Like Patterns. *Chem. - Eur. J.* **2009**, *15*, 11139–11150.
- (222) Shchyrba, A.; Nguyen, M.-T.; Wäckerlin, C.; Martens, S.; Nowakowska, S.; Ivas, T.; Roose, J.; Nijs, T.; Boz, S.; Schär, M.; et al. Chirality Transfer in 1D Self-Assemblies: Influence of H-Bonding vs Metal Coordination between Dicyano[7]helicene Enantiomers. *J. Am. Chem. Soc.* **2013**, *135*, 15270–15273.
- (223) Müller, K.; Moreno López, J. C.; Gottardi, S.; Meinhardt, U.; Yildirim, H.; Kara, A.; Kivala, M.; Stöhr, M. Cyano Functionalized Triarylamines on Coinage Metal Surfaces: Interplay of Intermolecular and Molecule–Substrate Interactions. *Chem. - Eur. J.* **2016**, *22*, 581–589.
- (224) Schwartz, L. H.; Koukotas, C.; Kukkola, P.; Yu, C. S. 2,2'-Dicarbomethoxy-9,9'-Biphenyl. Synthesis, Conformational Stability, and Separation and Identification of the Conformers. *J. Org. Chem.* **1986**, *51*, 995–999.
- (225) Inomata, H.; Goushi, K.; Masuko, T.; Konno, T.; Imai, T.; Sasabe, H.; Brown, J. J.; Adachi, C. High-Efficiency Organic Electrophosphorescent Diodes Using 1,3,5-Triazine Electron Transport Materials. *Chem. Mater.* **2004**, *16*, 1285–1291.
- (226) Yang, X.; Müller, D. C.; Neher, D.; Meerholz, K. Highly Efficient Polymeric Electrophosphorescent Diodes. *Adv. Mater.* **2006**, *18*, 948–954.
- (227) Shih, P.-I.; Chiang, C.-L.; Dixit, A. K.; Chen, C.-K.; Yuan, M.-C.; Lee, R.-Y.; Chen, C.-T.; Diau, E. W.-G.; Shu, C.-F. Novel Carbazole/Fluorene Hybrids: Host Materials for Blue Phosphorescent OLEDs. *Org. Lett.* **2006**, *8*, 2799–2802.
- (228) Jiang, Z.; Chen, Y.; Yang, C.; Cao, Y.; Tao, Y.; Qin, J.; Ma, D. A Fully Diarylmethylene-Bridged Triphenylamine Derivative as Novel Host for Highly Efficient Green Phosphorescent OLEDs. *Org. Lett.* **2009**, *11*, 1503–1506.
- (229) Van Slyke, S. A.; Chen, C. H.; Tang, C. W. Organic Electroluminescent Devices with Improved Stability. *Appl. Phys. Lett.* **1996**, *69*, 2160–2162.
- (230) Adachi, C.; Baldo, M. A.; Forrest, S. R. High-Efficiency Organic Electrophosphorescent Devices with Tris(2-Phenylpyridine)-iridium Doped into Electron-Transporting Materials. *Appl. Phys. Lett.* **2000**, *77*, 904–906.
- (231) Jiang, Z.; Ye, T.; Yang, C.; Yang, D.; Zhu, M.; Zhong, C.; Qin, J.; Ma, D. Star-Shaped Oligotriarylamines with Planarized Triphenylamine Core: Solution-Processable, High-Tg Hole-Injecting and Hole-Transporting Materials for Organic Light-Emitting Devices. *Chem. Mater.* **2011**, *23*, 771–777.
- (232) Cui, L.; Yanhu, L.; Yingyue, Z.; Chuluo, Y.; Hongbin, W.; Jingui, Q.; Yong, C. Solution Processed, Undoped, Deep Blue Organic Light Emitting Diodes Based on Starburst Oligofluorenes with a Planar Triphenylamine Core. *Chem. - Eur. J.* **2012**, *18*, 6928–6934.
- (233) Hoke, E. T.; Slotcavage, D. J.; Dohner, E. R.; Bowring, A. R.; Karunadasa, H. I.; McGehee, M. D. Reversible Photo-Induced Trap Formation in Mixed-Halide Hybrid Perovskites for Photovoltaics. *Chem. Sci.* **2015**, *6*, 613–617.
- (234) Bouduban, M. E. F.; Burgos-Caminal, A.; Ossola, R.; Teuscher, J.; Moser, J.-E. Energy and Charge Transfer Cascade in Methylammonium Lead Bromide Perovskite Nanoparticle Aggregates. *Chem. Sci.* **2017**, *8*, 4371–4380.
- (235) Reddy, S. S.; Park, H.-Y.; Kwon, H.; Shin, J.; Kim, C.-S.; Song, M.; Jin, S.-H. An Efficient Amphiphilic-Type Triphenylamine-Based Organic Hole Transport Material for High-Performance and Ambient-Stable Dopant-Free Perovskite and Organic Solar Cells. *Chem. - Eur. J.* **2018**, *24*, 6426–6431.
- (236) Zhang, M.; Wang, G.; Zhao, D.; Huang, C.; Cao, H.; Chen, M. 3D Hole-Transporting Materials Based on Coplanar Quinolizino Acridine for Highly Efficient Perovskite Solar Cells. *Chem. Sci.* **2017**, *8*, 7807–7814.
- (237) Bieri, M.; Blankenburg, S.; Kivala, M.; Pignedoli, C. A.; Ruffieux, P.; Mullen, K.; Fasel, R. Surface-Supported 2D Heterotriangulene Polymers. *Chem. Commun.* **2011**, *47*, 10239–10241.
- (238) Kan, E.; Hu, W.; Xiao, C.; Lu, R.; Deng, K.; Yang, J.; Su, H. Half-Metallicity in Organic Single Porous Sheets. *J. Am. Chem. Soc.* **2012**, *134*, 5718–5721.
- (239) Schmolter, K.; Schlutter, F.; Kivala, M.; Baumgarten, M.; Winkler, S.; Trattnig, R.; Koch, N.; Klug, A.; List, E. J. W.; Mullen, K. A Heterotriangulene Polymer for Air-Stable Organic Field-Effect Transistors. *Polym. Chem.* **2013**, *4*, 5337–5344.
- (240) Steiner, C.; Gebhardt, J.; Ammon, M.; Yang, Z.; Heidenreich, A.; Hammer, N.; Görling, A.; Kivala, M.; Maier, S. Hierarchical On-Surface Synthesis and Electronic Structure of Carbonyl-Functionalized One- and Two-Dimensional Covalent Nanoarchitectures. *Nat. Commun.* **2017**, *8*, 14765.
- (241) Jiang, Z.; Chen, Y.; Fan, C.; Yang, C.; Wang, Q.; Tao, Y.; Zhang, Z.; Qin, J.; Ma, D. Bridged Triphenylamines as Novel Host Materials for Highly Efficient Blue and Green Phosphorescent OLEDs. *Chem. Commun.* **2009**, 3398–3400.
- (242) Fan, C.; Chen, Y.; Jiang, Z.; Yang, C.; Zhong, C.; Qin, J.; Ma, D. Diarylmethylene-Bridged Triphenylamine Derivatives Encapsulated with Fluorene: Very High Tg Host Materials for Efficient Blue and Green Phosphorescent OLEDs. *J. Mater. Chem.* **2010**, *20*, 3232–3237.
- (243) Field, J. E.; Hill, T. J.; Venkataraman, D. Bridged Triarylamines: A New Class of Heterohelicenes. *J. Org. Chem.* **2003**, *68*, 6071–6078.
- (244) Field, J. E.; Muller, G.; Riehl, J. P.; Venkataraman, D. Circularly Polarized Luminescence from Bridged Triarylamine Helices. *J. Am. Chem. Soc.* **2003**, *125*, 11808–11809.
- (245) Hassey, R.; Swain, E. J.; Hammer, N. I.; Venkataraman, D.; Barnes, M. D. Probing the Chiroptical Response of a Single Molecule. *Science* **2006**, *314*, 1437–1439.

- (246) Hassey, R.; McCarthy, K. D.; Swain, E.; Basak, D.; Venkataraman, D.; Barnes, M. D. Single-Molecule Chiroptical Spectroscopy: Fluorescence Excitation of Individual Helicene Molecules in Polymer-Supported Thin-Films. *Chirality* **2008**, *20*, 1039–1046.
- (247) Cyphersmith, A.; Surampudi, S.; Casey, M. J.; Jankowski, K.; Venkataraman, D.; Barnes, M. D. Chiroptical Dissymmetries in Fluorescence Excitation from Single Molecules of (M-2) Helicene Dimers. *J. Phys. Chem. A* **2012**, *116*, 5349–5352.
- (248) Kuratsu, M.; Kozaki, M.; Okada, K. Synthesis, Structure, and Electron-Donating Ability of 2,2':6',2"-Dioxatriphenylamine and Its Sulfur Analogue. *Chem. Lett.* **2004**, *33*, 1174–1175.
- (249) Wakamiya, A.; Nishimura, H.; Fukushima, T.; Suzuki, F.; Saeki, A.; Seki, S.; Osaka, I.; Sasamori, T.; Murata, M.; Murata, Y.; et al. On-Top π -Stacking of Quasiplanar Molecules in Hole-Transporting Materials: Inducing Anisotropic Carrier Mobility in Amorphous Films. *Angew. Chem., Int. Ed.* **2014**, *53*, 5800–5804.
- (250) Nishimura, H.; Fukushima, T.; Wakamiya, A.; Murata, Y.; Kaji, H. The Influence of Quasiplanar Structures of Partially Oxygen-Bridged Triphenylamine Dimers on the Properties of Their Bulk Films. *Bull. Chem. Soc. Jpn.* **2016**, *89*, 726–732.
- (251) Nishimura, H.; Ishida, N.; Shimazaki, A.; Wakamiya, A.; Saeki, A.; Scott, L. T.; Murata, Y. Hole-Transporting Materials with a Two-Dimensionally Expanded π -System around an Azulene Core for Efficient Perovskite Solar Cells. *J. Am. Chem. Soc.* **2015**, *137*, 15656–15659.
- (252) Jeon, N. J.; Noh, J. H.; Kim, Y. C.; Yang, W. S.; Ryu, S.; Seok, S. I. Solvent Engineering for High-Performance Inorganic–Organic Hybrid Perovskite Solar Cells. *Nat. Mater.* **2014**, *13*, 897.
- (253) Burschka, J.; Kessler, F.; Nazeeruddin, M. K.; Grätzel, M. Co(III) Complexes as p-Dopants in Solid-State Dye-Sensitized Solar Cells. *Chem. Mater.* **2013**, *25*, 2986–2990.
- (254) Nishimura, H.; Hasegawa, Y.; Wakamiya, A.; Murata, Y. Development of Transparent Organic Hole-transporting Materials Using Partially Oxygen-bridged Triphenylamine Skeletons. *Chem. Lett.* **2017**, *46*, 817–820.
- (255) Nishimura, H.; Tanaka, K.; Morisaki, Y.; Chujo, Y.; Wakamiya, A.; Murata, Y. Oxygen-Bridged Diphenylnaphthylamine as a Scaffold for Full-Color Circularly Polarized Luminescent Materials. *J. Org. Chem.* **2017**, *82*, 5242–5249.
- (256) Gilman, H.; Shirley, D. A.; Ess, P. R. V. The Metalation of Phenothiazine1. *J. Am. Chem. Soc.* **1944**, *66*, 625–627.
- (257) Lamanna, G.; Faggi, C.; Gasparrini, F.; Ciogli, A.; Villani, C.; Stephens, P. J.; Devlin, F. J.; Menichetti, S. Efficient Thia-Bridged Triarylamine Heterohelicenes: Synthesis, Resolution, and Absolute Configuration Determination. *Chem. - Eur. J.* **2008**, *14*, 5747–5750.
- (258) Islam, N.; Pandith, A. H. Chiro-Optic and Nonlinear Optical Studies of Bridged Triarylamine Heterohelicenes; A DFT Study. *J. Mol. Struct.* **2017**, *1142*, 1–10.
- (259) Lambert, C.; Nöll, G. The Class II/III Transition in Triarylamine Redox Systems. *J. Am. Chem. Soc.* **1999**, *121*, 8434–8442.
- (260) Zheng, S.; Barlow, S.; Risko, C.; Kinnibrugh, T. L.; Khrustalev, V. N.; Jones, S. C.; Antipin, M. Y.; Tucker, N. M.; Timofeeva, T. V.; Coropceanu, V.; et al. Isolation and Crystal Structures of Two Singlet Bis(Triarylamine) Dications with Nonquinoidal Geometries. *J. Am. Chem. Soc.* **2006**, *128*, 1812–1817.
- (261) Su, Y.; Wang, X.; Zheng, X.; Zhang, Z.; Song, Y.; Sui, Y.; Li, Y.; Wang, X. Tuning Ground States of Bis(Triarylamine) Dications: From a Closed-Shell Singlet to a Diradicaloid with an Excited Triplet State. *Angew. Chem., Int. Ed.* **2014**, *53*, 2857–2861.
- (262) Su, Y.; Wang, X.; Li, Y.; Song, Y.; Sui, Y.; Wang, X. Nitrogen Analogs of Thiele's Hydrocarbon. *Angew. Chem., Int. Ed.* **2015**, *54*, 1634–1637.
- (263) Tan, G.; Wang, X. Isolable Bis(Triarylamine) Dications: Analogs of Thiele's, Chichibabin's, and Müller's Hydrocarbons. *Acc. Chem. Res.* **2017**, *50*, 1997–2006.
- (264) Bamberger, S.; Hellwinkel, D.; Neugebauer, F. A. Über verbrückte Diaryl und Triarylamin Radikalkationen. *Chem. Ber.* **1975**, *108*, 2416–2421.
- (265) Zheng, X.; Wang, X.; Qiu, Y.; Li, Y.; Zhou, C.; Sui, Y.; Li, Y.; Ma, J.; Wang, X. One-Electron Oxidation of an Organic Molecule by $B(C_6F_5)_3$: Isolation and Structures of Stable Non-*para*-substituted Triarylamine Cation Radical and Bis(triarylamine) Dication Diradicaloid. *J. Am. Chem. Soc.* **2013**, *135*, 14912–14915.
- (266) Krossing, I. The Facile Preparation of Weakly Coordinating Anions: Structure and Characterisation of Silverpolyfluoroalkoxyaluminates $AgAl(OR^F)_4$: Calculation of the Alkoxide Ion Affinity. *Chem. - Eur. J.* **2001**, *7*, 490–502.
- (267) Kamada, K.; Fuku-En, S.-i.; Minamide, S.; Ohta, K.; Kishi, R.; Nakano, M.; Matsuzaki, H.; Okamoto, H.; Higashikawa, H.; Inoue, K.; et al. Impact of Diradical Character on Two-Photon Absorption: Bis(acridine) Dimers Synthesized from an Allenic Precursor. *J. Am. Chem. Soc.* **2013**, *135*, 232–241.
- (268) Kuratsu, M.; Kozaki, M.; Okada, K. 2,2':6',2":6",6-Trioxypyridophenylamine: Synthesis and Properties of the Radical Cation and Neutral Species. *Angew. Chem., Int. Ed.* **2005**, *44*, 4056–4058.
- (269) Kuratsu, M.; Suzuki, S.; Kozaki, M.; Shiomi, D.; Sato, K.; Takui, T.; Okada, K. Magnetic Interaction of Tri- and Di-oxypyridophenylamine Radical Cation $FeCl_4^-$ Salts. *Inorg. Chem.* **2007**, *46*, 10153–10157.
- (270) Kuratsu, M.; Suzuki, S.; Kozaki, M.; Shiomi, D.; Sato, K.; Takui, T.; Kanazawa, T.; Hosokoshi, Y.; Lan, X.-Z.; Miyazaki, Y.; et al. (Nitronyl Nitroxide)-Substituted Trioxypyridophenylamine Radical Cation Tetrachlorogallate Salt: A 2p-Electron-Based Weak Ferromagnet Composed of a Triplet Diradical Cation. *Chem. - Asian J.* **2012**, *7*, 1604–1609.
- (271) Shuichi, S.; Atsuki, N.; Masato, K.; Masatoshi, K.; Rika, T.; Daisuke, S.; Kenji, S.; Kazuo, T.; Kazunobu, S.; Takeji, T.; et al. Trinitroxide Trioxypyridophenylamine: Spin State Conversion from Triradical Doublet to Diradical Cation Triplet by Oxidative Modulation of a π Conjugated System. *Angew. Chem., Int. Ed.* **2012**, *51*, 3193–3197.
- (272) Itoh, T.; Matsuda, K.; Iwamura, H.; Hori, K. Tris[*p*-(*N*-oxyl-*N*-*tert*-butylamino)phenyl]amine, -methyl, and -borane Have Doublet, Triplet, and Doublet Ground States, Respectively. *J. Am. Chem. Soc.* **2000**, *122*, 2567–2576.
- (273) Suzuki, S.; Tanaka, N.; Kozaki, M.; Shiomi, D.; Sato, K.; Takui, T.; Okada, K. Synthesis and Magnetic Properties of Trioxypyridophenylamine Dimers in their Di(radical cationic) States. *Chem. - Eur. J.* **2017**, *23*, 16014–16025.
- (274) Menichetti, S.; Cecchi, S.; Procacci, P.; Innocenti, M.; Bucelli, L.; Franco, L.; Viglianisi, C. Thia-Bridged Triarylamine Heterohelicene Radical Cations as Redox-Driven Molecular Switches. *Chem. Commun.* **2015**, *51*, 11452–11454.
- (275) Gliemann, B. D.; Petrovic, A. G.; Zolnhofer, E. M.; Dral, P. O.; Hampel, F.; Breitenbruch, G.; Schulze, P.; Raghavan, V.; Meyer, K.; Polavarapu, P. L.; et al. Configurationally Stable Chiral Dithia-Bridged Hetero[4]helicene Radical Cation: Electronic Structure and Absolute Configuration. *Chem. - Asian J.* **2017**, *12*, 31–35.
- (276) Li, L.-L.; Diau, E. W.-G. Porphyrin-sensitized Solar Cells. *Chem. Soc. Rev.* **2013**, *42*, 291–304.
- (277) Fukui, N.; Cha, W.-Y.; Lee, S.; Tokujii, S.; Kim, D.; Yorimitsu, H.; Osuka, A. Oxidative Fusion Reactions of *meso*-(Diarylaminoo)porphyrins. *Angew. Chem., Int. Ed.* **2013**, *52*, 9728–9732.
- (278) Fukui, N.; Yorimitsu, H.; Osuka, A. *meso* β -Oligohaloporphyrins as Useful Synthetic Intermediates of Diphenylamine-Fused Porphyrin and *meso*-to-*meso* β -to- β Doubly Butadiyne-Bridged Diporphyrin. *Angew. Chem., Int. Ed.* **2015**, *54*, 6311–6314.
- (279) Fukui, N.; Yorimitsu, H.; Osuka, A. *meso*-*meso*-Linked Diarylamine-Fused Porphyrin Dimers. *Chem. - Eur. J.* **2016**, *22*, 18476–18483.
- (280) Fukui, N.; Cha, W.; Shimizu, D.; Oh, J.; Furukawa, K.; Yorimitsu, H.; Kim, D.; Osuka, A. Highly Planar Diarylamine-Fused Porphyrins and Their Remarkably Stable Radical Cations. *Chem. Sci.* **2017**, *8*, 189–199.

- (281) Rodriguez, R. A.; Pan, C.-M.; Yabe, Y.; Kawamata, Y.; Eastgate, M. D.; Baran, P. S. Palau'chlor: A Practical and Reactive Chlorinating Reagent. *J. Am. Chem. Soc.* **2014**, *136*, 6908–6911.
- (282) Kato, K.; Kim, J. O.; Yorimitsu, H.; Kim, D.; Osuka, A. Triphenylsilane-fused Porphyrins. *Chem. - Asian J.* **2016**, *11*, 1738–1746.
- (283) Cordero, B.; Gómez, V.; Platero-Prats, A. E.; Revés, M.; Echeverría, J.; Cremades, E.; Barragán, F.; Alvarez, S. Covalent radii revisited. *Dalton Trans.* **2008**, 2832–2838.
- (284) Baechler, R. D.; Mislow, K. Effect of Structure on the Rate of Pyramidal Inversion of Acyclic Phosphines. *J. Am. Chem. Soc.* **1970**, *92*, 3090–3093.
- (285) Alabugin, I. V.; Bresch, S.; Manoharan, M. Hybridization Trends for Main Group Elements and Expanding the Bent's Rule Beyond Carbon: More than Electronegativity. *J. Phys. Chem. A* **2014**, *118*, 3663–3677.
- (286) Baumgartner, T.; Réau, R. Organophosphorus π -Conjugated Materials. *Chem. Rev.* **2006**, *106*, 4681–4727.
- (287) Shameem, M. A.; Orthaber, A. Organophosphorus Compounds in Organic Electronics. *Chem. - Eur. J.* **2016**, *22*, 10718–10735.
- (288) Baumgartner, T. Insights on the Design and Electron-Acceptor Properties of Conjugated Organophosphorus Materials. *Acc. Chem. Res.* **2014**, *47*, 1613–1622.
- (289) Regulska, E.; Romero-Nieto, C. Highlights on π -Systems Based on Six-Membered Phosphorus Heterocycles. *Dalton Trans.* **2018**, *47*, 10344–10359.
- (290) Hellwinkel, D.; Wiel, A.; Sattler, G.; Nuber, B. Ring Closure and Ring Expansion Reactions in Bridged Triarylphosphanes and Triarylsarnes with o-Isopropenyl Substituents. Novel Candidates for Turnstile Geometry. *Angew. Chem., Int. Ed. Engl.* **1990**, *29*, 689–692.
- (291) Sobolev, A. N.; Belsky, V. K.; Chernikova, N. Y.; Akhmadulina, F. Y. Structure Analysis of Triaryl Derivatives of the Group v Elements: VIII. the Crystal and Molecular Structure of Triphenylarsine, $C_{18}H_{15}As$. *J. Organomet. Chem.* **1983**, *244*, 129–136.
- (292) Schaub, T. A.; Zolnhofer, E. M.; Halter, D. P.; Shubina, T. E.; Hampel, F.; Meyer, K.; Kivala, M. A Stable Crystalline Triarylphosphine Oxide Radical Anion. *Angew. Chem., Int. Ed.* **2016**, *55*, 13597–13601.
- (293) Schaub, T. A.; Sure, R.; Hampel, F.; Grimme, S.; Kivala, M. Quantum Chemical Dissection of the Shortest $P = O \cdots I$ Halogen Bond: The Decisive Role of Crystal Packing Effects. *Chem. - Eur. J.* **2017**, *23*, 5687–5691.
- (294) Krebs, F. C.; Larsen, P. S.; Larsen, J.; Jacobsen, C. S.; Boutton, C.; Thorup, N. Synthesis, Structure, and Properties of 4,8,12-Trioxa-12c-phospha-4,8,12,12c-tetrahydrodibenzo[cd,mn]pyrene, a Molecular Pyroelectric. *J. Am. Chem. Soc.* **1997**, *119*, 1208–1216.
- (295) Madsen, G. K. H.; Krebs, F. C.; Lebech, B.; Larsen, F. K. Evaluation of the Solid State Dipole Moment and Pyroelectric Coefficient of Phosphangulene by Multipolar Modeling of X-ray Structure Factors. *Chem. - Eur. J.* **2000**, *6*, 1797–1804.
- (296) Lin, R.; Braun, K. F.; Tang, H.; Quaade, U. J.; Krebs, F. C.; Meyer, G.; Joachim, C.; Rieder, K. H.; Stokbro, K. Imaging and Manipulation of a Polar Molecule on Ag(111). *Surf. Sci.* **2001**, *477*, 198–208.
- (297) Yamamura, M.; Saito, T.; Nabeshima, T. Phosphorus-Containing Chiral Molecule for Fullerene Recognition Based on Concave/Convex Interaction. *J. Am. Chem. Soc.* **2014**, *136*, 14299–14306.
- (298) Yamamura, M.; Sukegawa, K.; Nabeshima, T. Tuning the Depth of Bowl-Shaped Phosphine Hosts: Capsule and Pseudo-Cage Architectures in Host-Guest Complexes with C_{60} Fullerene. *Chem. Commun.* **2015**, *51*, 12080–12083.
- (299) Yamamura, M.; Sukegawa, K.; Okada, D.; Yamamoto, Y.; Nabeshima, T. Chiroptical Switching Caused by Crystalline/Liquid Crystalline Phase Transition of a Chiral Bowl-Shaped Molecule. *Chem. Commun.* **2016**, *52*, 4585–4588.
- (300) Yamamura, M.; Nabeshima, T. Relationship between the Bowl-Shaped Geometry of Phosphangulene and an Axial Group on the Phosphorus Atom. *Bull. Chem. Soc. Jpn.* **2016**, *89*, 42–49.
- (301) Yamamura, M.; Hasegawa, T.; Nabeshima, T. Synthesis of Phosphorus-Centered and Chalcogen-Bridged Concave Molecules: Modulation of Bowl Geometries and Packing Structures by Changing Bridging Atoms. *Org. Lett.* **2016**, *18*, 816–819.
- (302) Suzuki, S.; Kira, S.; Kozaki, M.; Yamamura, M.; Hasegawa, T.; Nabeshima, T.; Okada, K. An Efficient Synthetic Method for Organometallic Radicals: Structures and Properties of gold(I)-(Nitronyl Nitroxide)-2-Ide Complexes. *Dalton Trans.* **2017**, *46*, 2653–2659.
- (303) Gotoh, H.; Nakatsuka, S.; Kondo, Y.; Sasada, Y.; Hatakeyama, T. Triangulene-based Efficient Exciton Blocking Material for Organic Light-emitting Diodes. *Chem. Lett.* **2018**, *47*, 920–922.
- (304) Chen, C. H.; Doney, J. J.; Fox, J. L.; Luss, H. R. 1,1,6,6-Tetramethyldibenzo[b,e]phosphajulolidine. *J. Org. Chem.* **1985**, *50*, 2914–2917.
- (305) Gray, M.; Chapell, B. J.; Taylor, N. J.; Snieckus, V. Carbanion-Mediated Heterocyclizations: Regiospecific, General Route to Dibenzo-[b,e]phosphinones by Synthetic Anionic Equivalents of Friedel–Crafts Reactions and Remote Fries Rearrangement. *Angew. Chem., Int. Ed. Engl.* **1996**, *35*, 1558–1560.
- (306) Hatakeyama, T.; Hashimoto, S.; Nakamura, M. Tandem Phospha-Friedel–Crafts Reaction toward Curved π -Conjugated Frameworks with a Phosphorus Ring Junction. *Org. Lett.* **2011**, *13*, 2130–2133.
- (307) Hashimoto, S.; Nakatsuka, S.; Nakamura, M.; Hatakeyama, T. Construction of a Highly Distorted Benzene Ring in a Double Helicene. *Angew. Chem., Int. Ed.* **2014**, *53*, 14074–14076.
- (308) Kawai, H.; Suzuki, T.; Ohkita, M.; Tsuji, T. A Kinetically Stabilized [1.1]Paracyclophane: Isolation and X-Ray Structural Analysis. *Angew. Chem., Int. Ed.* **1998**, *37*, 817–819.
- (309) Yamamura, M.; Hongo, D.; Nabeshima, T. Twofold Fused Concave Hosts Containing Two Phosphorus Atoms: Modules for the Sandwich-Type Encapsulation of Fullerenes in Variable Cavities. *Chem. Sci.* **2015**, *6*, 6373–6378.
- (310) Fujimoto, K.; Kasuga, Y.; Fukui, N.; Osuka, A. Diphenylphosphine-Oxide-Fused and Diphenylphosphine-Fused Porphyrins: Synthesis, Tunable Electronic Properties, and Formation of Cofacial Dimers. *Chem. - Eur. J.* **2017**, *23*, 6741–6745.
- (311) Fujimoto, K.; Osuka, A. Effective Stabilization of a Planar phosphorus(III) Center Embedded in a Porphyrin-Based Fused Aromatic Skeleton. *Chem. Sci.* **2017**, *8*, 8231–8239.